April 2014

Physical Simulation of Tornado-Like Vortices

Maryam Refan
The University of Western Ontario

Supervisor
Horia Hangan
The University of Western Ontario

Graduate Program in Mechanical and Materials Engineering

A thesis submitted in partial fulfillment of the requirements for the degree in Doctor of Philosophy

PHYSICAL SIMULATION OF TORNADO-LIKE VORTICES

(Thesis format: Integrated Article)

by

Maryam Refan

Graduate Program in Engineering Science
Department of Mechanical and Materials Engineering

A thesis submitted in partial fulfillment
of the requirements for the degree of
Doctor of Philosophy

The School of Graduate and Postdoctoral Studies
The University of Western Ontario
London, Ontario, Canada

Abstract

Scaling ratios of simulations are essential to research the effect of tornadic winds on buildings and structures, in both experimental and numerical studies. In order to determine the proper scaling, access to wind fields of simulated and full-scale tornadoes is needed. For the first time here Doppler radar tornado velocity fields are analyzed and compared to experimental tornado-like vortices data in order to establish the scaling necessary to simulate tornadoes in a physical laboratory setting.

A prototype three-dimensional wind testing chamber capable of simulating tornadoes, named Model WindEEE Dome (MWD), was designed and built. Tornado-like vortices were simulated and investigated for swirl ratios ranging from 0.12 to 1.29. Flow visualization captured a laminar single-celled core at very low swirl ratios, a vortex breakdown bubble formation and then the drowned vortex jump at moderate swirl ratios, and a two-celled turbulent vortex at high swirl ratios. The surface static pressure of simulated tornadoes was measured and the mean velocity field of the tornado-like vortices was characterized using Particle Image Velocimetry method. It was shown that for radial Reynolds numbers greater than 6.7×10^4, the core radius and the swirl ratio corresponding the transition from laminar to turbulent are nearly independent of the radial Reynolds number. Local peaks in the axial profile of the tangential velocities near the surface, together with the very large surface pressure deficits, observed in the experimental data, are distinctive characteristics of tornado-like vortices and may be responsible for structural damages in tornadic winds.

Nine volumes of single-Doppler radar data obtained from five tornado events were analyzed using the Ground-Based Velocity Track Display method and a unique dataset of three-dimensional axisymmetric tornado flow fields was created. This full-scale dataset contains various vortex structures spanning from a weak single-celled vortex to a very strong two-celled vortex and wind fields with the overall maximum tangential velocities ranging from 36.3 m/s to 62 m/s. The structure of the vortex was discussed in detail for each volume of data. The swirl ratio of the full-scale data was calculated and related to the forensic EF-Scale (Enhanced Fujita Scale) for each volume. It was observed that swirl ratio increases as the tornado vortex intensifies which is consistent with laboratory results.

Lastly, experimentally simulated tornado-like vortices were compared to the field tornadoes. The length and velocity scaling ratios of the simulation and the swirl ratio of the full-scale tornadoes were identified. It is concluded that the MWD apparatus can generate tornado-like vortices equivalent to EF0 to low-end EF3 rated tornadoes in nature. Also, an average length scale of 1550 is determined for simulating mid-range EF1 to low-end EF3 rated tornadoes with fully turbulent flow characteristics.

Keywords

Tornado-like vortex, physical simulation, swirl ratio, Particle Image Velocimetry, full-scale data, Fujita scale, Ground-Based Velocity Track Display, similarity analysis, scaling ratio

Co-Authorship Statement

Chapter Four will be submitted for publication under the co-authorship of Refan, M. and Hangan, H.

Chapter Five will be submitted for publication under the co-authorship of Refan, M., Kosiba, K., Wurman, J. and Hangan, H.

Chapter Six is a journal article submitted to and currently under revision by the Journal of Wind Engineering and Industrial Aerodynamics. It is co-authored by Refan, M., Hangan, H. and Wurman, J.

Acknowledgments

My first and sincere appreciation goes to Dr. Horia Hangan, my supervisor for all I have learned from him and for his continuous help and support in all stages of this research. I would also like to thank him for being an open person to ideas, and for helping me to shape my interest and ideas. His attitude to research inspired me to start this PhD program.

I gratefully acknowledge the National Science and Engineering Research Council (NSERC) for the financial support of this project.

I would like to thank Adrian Costache and Gerry Dafoe for their invaluable help and advice on experiments. I also wish to express my deep gratitude to Paul Robinson for his advice and insight on radar data analysis and for all I learned from him. In addition, I would like to thank Dr. Kamran Siddiqui for his invaluable advice on PIV measurements.

I have furthermore to thank my friends and colleagues Ashkan Rasouli, Ahmed Elatar and Dan Parvu for their assistance throughout my experiments and equipment installations and Sarah Macdonald, Adam Kirchhefer and Djordje Romanic for their practical suggestions and comments and, for their support.

I am eternally grateful to many people for their support; my parents Kobra Mehrabi and Akbar Refan, my husband Behzad Ghafouri and my brother Masih Refan.

Dedication

This dissertation work is dedicated to Kobra, Akbar, Behzad and Masih who supported and motivated me every step of the way.

Table of Contents

List of Tables

List of Figures

List of Appendices

List of Nomenclature

a	Aspect ratio
C_{max}	Terminal fall speed of dominant particles in the flow, m/s
C_p	Pressure coefficient
$C_{p,i}$	Pressure coefficient at i^{th} tap
D	Depth, m
e	Maximum allowed error
g	Gravitational acceleration, m/s^2
H	Height, m
h	Inflow height, m
L	Length, m
n	Sample size
P	Static pressure, Pa
p_0	Reference static pressure, Pa
p_∞	Far field static pressure, Pa
p_i	Static pressure of i^{th} tap, Pa
p_q	Reference stagnation pressure, Pa
Q	Volumetric flow rate per unit axial length, m^2/s
Q'	Volumetric flow rate, m^3/s
R	Seeding particle radius, m

Re_r	Radial Reynolds number
r	Radial distance, m
r_0	Updraft radius, m
r_c	Core radius, m
$r_{c,max}$	The core radius corresponding the overall maximum tangential velocity, m
S	Swirl ratio
t	Time, s
t_p	Response time of the seeding particles, s
V	Wind speed, m/s
V_1	Wind speed averaged over 1 s, m/s
V_{3600}	Wind speed averaged over 3600 s, m/s
V_∞	Wind tunnel free stream velocity, m/s
V_{ax}	Average axial velocity at the updraft hole, m/s
V_D	Doppler velocity, m/s
V_m	Average maximum core velocity, m/s
V_{tan}	Tangential velocity, m/s
$V_{tan,max}$	Overall maximum tangential velocity, m/s
V_{trans}	Translational velocity, m/s
V_{rad}	Radial velocity, m/s
$V_{rad,bias}$	Bias in the radial velocity due to the centrifuging of debris, m/s

z	Height above the ground surface, m
Z_{max}	The height corresponding the maximum tangential velocity, m
z_{max}	The height corresponding the overall maximum tangential velocity, m
z_{min}	Lowest height scanned by the Doppler radar, m

Greek Symbols

α	A constant representing the strength of the suction
Γ	Maximum vortex strength, m^2/s
Γ_{max}	Maximum vortex strength, m^2/s
Δx	Grid size in x direction in a Cartesian coordinate system, m
ΔP	Pressure deficit, Pa
Δt	Time interval between two consecutive image, s
Δy	Grid size in y direction in a Cartesian coordinate system, m
Δz	Grid size in z direction in a Cartesian coordinate system, m
θ	Vane angle, $^\circ$
θ_M	The direction of the mean wind flow, $^\circ$
λ_l	Length scale ratio
λ_v	Velocity scale ratio
μ	Dynamic viscosity of fluid, kg/s.m
v	Kinematic viscosity, m^2/s
v_t	Terminal velocity of hydrometeors and debris, m/s

$v_{t,p}$	Seeding particle terminal velocity, m/s
ρ_f	Fluid density, kg/m^3
ρ_p	Seeding particle density, kg/m^3
σ_x	Standard deviation of the tangential velocity fluctuations, m/s
φ	The elevation angle of the radar beam, $^\circ$

Subscripts

D	Doppler radar data
i	Tap number
S	Simulation

Chapter 1

1 Introduction

1.1 General introduction

Tornadoes are rotating columns of rising air that create a low pressure area close to the ground and draw air in radially. They are very complex flows due to their unsteady, three-dimensional and turbulent nature. On average, tornadoes are 150 m wide and travel on the ground for 8.0 km [1] with a translational speed of 9 m/s to 18 m/s [2].

The intensity of a tornado is measured by Fujita Scale (F-Scale) which was introduced by Tetsuya Theodore Fujita in 1971. This is a forensic scale for which each damage level is associated with a wind speed (V) calculated as $V=6.3(F+2)^{3/2}$ [3]. This relationship has been derived by smoothly connecting the Beaufort scale and the Mach number scale (see Appendix A for detail). The Beaufort scale is an empirical measure that relates wind speed to observed conditions at sea or on land and Mach number is the ratio of the speed of an object moving through a fluid to the speed of sound. A damage survey is usually performed after the tornado has passed a development. Then, using the damage markers (see Appendix B), the severity of the event is scaled between 0 (weakest) and 5 (strongest).

In 2006, the National Weather Service of the United States introduced the Enhanced Fujita Scale (EF-Scale) as an improved version of the original F-Scale. This new scale became operational in US on February 2007, and was very recently adopted by Environment Canada in April 2013. The EF-Scale employs a larger number of structures as damage indicators than the F-scale, including residential housings, office towers and trees, and therefore wind speeds are more accurately related to wind damage. The estimated wind speeds (3 sec gusts) associated with each level of Fujita and Enhanced Fujita scale are shown in Table 1-1.

Table 1-1: Estimated wind speed for each category of tornado intensity.

Fujita Scale	Wind Speed (km/h), 3s gusts	Enhanced Fujita Scale	Wind Speed (km/h), 3s gusts
F0	64–116	EF0	105–137
F1	117–180	EF1	138-178
F2	181–253	EF2	179-218
F3	254–332	EF3	219-266
F4	333–418	EF4	267-322
F5	419–512	EF5	>322

1.2 Motivation and objectives

Tornadoes are a serious threat to vast regions of North America, Bangladesh, South Africa, parts of Argentina, as well as portions of Europe (England mainly), Australia and New Zealand, and far eastern Asia. Over the last 15 year, the United States have experienced an average of more than 1200 tornadoes per year which resulted in 1378 fatalities and $24.5 billion damage. Although major tornadoes happen every year, the return period of a disaster in tornado prone areas is 5000 years. This return period is well beyond what buildings are designed for. As a result, the main focus in regions susceptible to tornadoes has been on preserving human lives with *safe rooms* rather than designing tornado-resistant residential dwellings. Also, the performance of essential buildings such as hospitals during and after the event is of high importance from the recovery point of view. The recent study performed by the National Institute of Standards and Technology (NIST) on the impacts of the May 22, 2011 tornado that struck Joplin, MO has revealed

the inefficiency of essential buildings and safe rooms in tornado-prone regions. This 2-year technical investigation showed that safe areas (tornado shelters and safe rooms) did not adequately protect occupants, and essential buildings did not remain operational. The conclusion of this study is strongly supported by another recent NIST report in which the impacts of the May 20, 2013 tornado in the Newcastle-Moore area (Oklahoma) are provided. These reports highlight the need for a better understanding of tornado flows and the damage associated with them.

Tornado flow studies started in 1882 with simple one-dimensional analytical models which represented the flow using only the tangential velocity component; the Rankine Vortex model. This early work was followed by more thorough analytical models such as the Burgers-Rott vortex [4, 5]. As the knowledge of tornado vortex dynamics broadened and as the measurement techniques and technology advanced, experimental and numerical simulations of tornado-like vortices widely increased. Experimental simulations of tornado-like flows started by reproducing the observed features of tornado vortices. These features include: 1) a columnar vortex that touches the ground, 2) updraft at the center of the vortex with a surface pressure drop, 3) spiraling flow with radial convergence to the vortex core, and 4) turbulent flow regime [2]. In laboratory simulations, the effects of buoyancy are neglected and therefore the vortex is purely momentum driven. In 1969, Ying and Chang [2] designed and built a tornado simulator that fulfilled the above mentioned features. Later, the Ward-type Tornado Vortex Chamber (TVC) was introduced [6] which was an improved version of the Ying and Chang apparatus. Ward's simulator provided more realistic boundary conditions for the vortex. Hereafter, substantial effort has been made to better represent the tornado flow structure and boundary conditions in the lab [7-11] and to better characterize the flow characteristics [10, 12-18]. This was followed by numerical simulations of tornado-like vortices [19-22]. Numerical simulations can be divided into two general categories: thunderstorm scale simulations which are meteorological models and tornado scale simulations which are essentially engineering models. Thunderstorm scale models reproduce the supercell storm and can be used to study tornadogenesis. On the other hand, the tornado scale models focus on the interaction between the tornado vortex and

the ground surface. So far, numerical simulations of tornadic flows with engineering applications have been mainly limited to simulating laboratory models or simple axisymmetric flows.

Collecting full-scale velocity data from tornadoes has been always challenging for researchers. Technological developments of Doppler radars and the introduction of Doppler on Wheels (DOW) in 1995 [23, 24] are important recent developments enabling scientists to obtain full-scale data from a safe distance. However, these measurements mainly focus on tornadogenesis. In addition, the Doppler radar data are mostly collected from heights on the order of tens of meters above the surface [25-31], which is significantly higher than the majority of buildings of interest. Obtaining surface pressure data from real tornadoes is an even more difficult task and only on very rare events have measurements been successfully collected [32].

Despite the significant number of analytical, experimental and numerical studies and advances in measurement methods, investigation of the wind loading effects on structures and buildings has been very limited. This is attributed to an unidentified relationship (i.e. geometric and velocity scales) between simulated and real tornadoes. Once this relationship is identified, modelling structures and buildings and testing them in tornado simulators to measure the wind loading is possible.

Mishra *et al.* [33] placed a 1:3500 scaled cubical building model (edge length of 30 mm) in the path of a simulated single-celled vortex and measured the surface static pressures. They observed a clear difference between the pressure distribution over the building in tornadic winds compared to atmospheric boundary layer flows. Mishra *et al.* estimated the geometric scale of their simulation by comparing the core radius of the simulated vortex with that of the May 1998 Manchester, SD tornado both obtained from surface static pressure measurements. Although the 1:3500 geometric scale resulted in a good agreement between the surface pressure profiles of the simulated and the full-scale tornado, there is no evidence of a match between radial profiles of tangential velocities.

A single-story, gable roof building was modeled in the Iowa State University (ISU) tornado simulator and the tornado wind-induced loads were measured by Haan *et al.* [34]. Using the length scale of 1:100, the model building was 91 mm×91 mm×66 mm (L×D×H). As explained in [11], the geometric scale was estimated based on the building model scale with no clear relation between the simulated vortex and real tornado characteristics.

In order to conclude that a simulated tornado-like vortex is a valid representation of a tornado flow in nature, it is important that the geometric, kinematic and dynamic similitudes are analyzed. The difficulty with the case of tornadic flows originates in the definition of the main non-dimensional number governing tornado-like flows, i.e. the swirl ratio (S). This important parameter is defined based on the geometry and boundaries of a simulator and is location dependent. Therefore, it is nearly impossible (or very subjective) to calculate the swirl ratio for a real tornado as there is no clear definition of inlet/outlet boundary conditions in a field tornado. An alternative approach was suggested by Hangan and Kim [35] in which they compared simulated velocity data at various swirl ratios with that of a Doppler radar full-scale data from the F4 rated tornado of Spencer, SD on May 30, 1998. Hangan and Kim [35] showed that a simulated tornado-like vortex with S=2 best represents the Spencer tornado. Although their results were promising, this approach has not yet been validated, mainly due to the shortage of full-scale velocity data from tornadoes of various structures and intensities.

Establishing a relationship between simulated and real tornadoes is the main focus of this study. In order to achieve this, a complete set of experimental and full-scale data from tornadoes of various intensities and characteristics is required. A prototype three-dimensional wind testing chamber capable of simulating tornadoes, called Model WindEEE Dome (MWD), was designed and built. Tornado-like vortices of various structures and intensities were simulated in MWD. Afterwards, flow visualization methods, surface static pressure tests and Particle Image Velocimetry (PIV) method were implemented to characterize the tornado-like vortex both qualitatively and quantitatively. Subsequently, full-scale Doppler radar data from various tornado events, provided by the

Centre for Severe Weather Research (CSWR) in Boulder Colorado, were analyzed using a mathematical method called the Ground-based Velocity Track Display (GBVTD). The outcome of these analyses is identification of the three-dimensional axisymmetric flow structure of each volume of real tornado data. Also, these analyses provide the opportunity to examine the swirl ratio of the field data as well as to create a database of full-scale tornado velocities which has been lacking for a long time.

Finally, results of the experimental simulations of tornado-like flows, performed in MWD are compared with the GBVTD-retrieved full-scale data. Based on these comparisons, geometric and velocity scale ratios of the simulated tornadoes and, the swirl ratio of the full-scale tornadoes are identified. This finding provides the opportunity to correctly simulate tornado-like vortices and study the wind load effects on properly scaled buildings and structures.

1.3 Thesis layout

This thesis is written in the "integrated article" format as specified by the Faculty of Graduate Studies at Western University.

Chapter One provides a general introduction to tornadoes and the motivation behind this study. In the next chapter, the tornadogenesis is briefly discussed. The main focus of Chapter Two is the parameters that govern the tornado flow and the dynamic structure of the vortex. Various tornado simulators, including the recently developed Model WindEEE Dome at Western University, are also introduced in this chapter. Measurement techniques implemented for the purpose of this work, as well as test plans are discussed in detail in Chapter Three. Chapter Four is based on a technical article prepared for the Journal of Fluids and Structures. In this work, the tornado-like vortices generated in the Model WindEEE Dome are characterized using flow visualization methods, surface pressure measurements and Particle Image Velocimetry (PIV) technique. In Chapter Five, the process of creating a dataset of full-scale tornado velocity fields is explained. Single-Doppler radar measurements from five tornado events are obtained and analyzed using the Ground-Based Velocity Track Display (GBVTD) method. This chapter is also based

on a technical article which will be submitted to the Journal of Applied Meteorology and Climatology. Chapter Six presents similarity analysis performed using the experimental and full-scale data obtained in Chapters Four and Five, respectively. Chapter Six is a technical article, currently under revision by the Journal of Wind Engineering and Industrial Aerodynamics. The final chapter summarizes the findings and remarks from previous chapters, presents the original contributions of this work to science and provides recommendations for future works.

References

[1] Lyons, W.A., 1997, "The Handy Weather Answer Book (2nd Ed.),"Visible Ink press, Detroit, Michigan, pp. 175-200.

[2] Ying, S. J., and Chang, C. C., 1970, "Exploratory Model Study of Tornado-Like Vortex Dynamics," Journal of the Atmospheric Sciences, **27**(1) pp. 3-14.

[3] Abbott, P.L., 2002, "Natural Disasters," McGraw-Hill, pp. 422.

[4] Burgers, J. M., 1948, "A Mathematical Model Illustrating the Theory of Turbulence," Adv. Appl. Mech., **1**pp. 197-199.

[5] Rott, N., 1958, "On the Viscous Core of a Line Vortex," Z. Angew Math. Mech., **9**pp. 543-553.

[6] Ward, N. B., 1972, "The Exploration of Certain Features of Tornado Dynamics using a Laboratory Model," Journal of Atmospheric Sciences, **29**pp. 1194.

[7] Mitsuta, Y., and Monji, N., 1984, "Development of a Laboratory Simulator for Small Scale Atmospheric Vortices," Natural Disaster Science, **6**pp. 43-54.

[8] Lund, D. E., and Snow, J. T., 1993, "Laser Doppler Velocimetry Measurements in Tornado Like Vortices," Geophysical Monograp, **79**pp. 297.

[9] Wang, J., James, D. L., Letchford, C. W., 2001, "Development of a prototype tornado simulator for the assessment of fluid-structure interaction," Proceedings of the 1st Americas Conference on Wind Engineering, 4-6 June, Clemson Uni., SC.

[10] Mishra, A. R., Jamesa, D. L., and Letchford, C. W., 2008, "Physical Simulation of a Single-Celled Tornado-Like Vortex, Part A: Flow Field Characterization," J. Wind Eng. Ind. Aerodyn., **96**pp. 1243.

[11] Haan Jr, F. L., Sarkar, P. P., and Gallus, W. A., 2008, "Design, Construction and Performance of a Large Tornado Simulator for Wind Engineering Applications," Engineering Structures, **30**pp. 1146.

[12] Jischke, M. C., and Parang, M., 1974, "Properties of Simulated Tornado-Like Vortices," J. Atmos. Sci., **31**pp. 506.

[13] Jischke, M. C., and Light, B. D., 1983, "Laboratory Simulation of Tornadic Wind Loads on a Rectangular Model Structure," Journal of Wind Engineering and Industrial Aerodynamics, **13**(1–3) pp. 371-382.

[14] Monji, N., Wang, Y., and Mitsuta, Y., 1988, "A Laboratory Experiment on the Effect of Surface Roughness on the Small Scale Atmospheric Vortices," Disaster Prevention Research Institute Annals, **31**pp. 177.

[15] Bienkiewicz, B., and Dudhia, P., 1993, "Physical modeling of tornado-like flow and tornado effects on building loading," Anonymous Proceedings of the Seventh US National Conference on Wind Engineering, **1,** pp. 95.

[16] Cleland, J. D., 2001, "Laboratory Measurements of Velocity Profiles in Simulated Tornado-Like Vortices," The J. of Undergraduate Research in Phys., **18**pp. 51.

[17] Hashemi Tari, P., Gurka, R., and Hangan, H., 2010, "Experimental Investigation of a Tornado-Like Vortex Dynamics with Swirl Ratio: The Mean and Turbulent Flow Fields," J. Wind Eng. Ind. Aerodyn., **98**pp. 936-944.

[18] Zhang, W., and Sarkar, P. P., 2012, "Near-Ground Tornado-Like Vortex Structure Resolved by Particle Image Velocimetry (PIV)," Exp. Fluids, **52**pp. 479-493.

[19] Lewellen, W. S., Lewellen, D. C., and Sykes, R. I., 1997, "Large-Eddy Simulation of a Tornado's Interaction with the Surface," Journal of Atmospheric Sciences, **54**pp. 581.

[20] Lewellen, D.,C., Lewellen, W.,S., and Xia, J., 2000, "The Influence of a Local Swirl Ratio on Tornado Intensification Near the Surface," Journal of the Atmospheric Sciences, **57**(4) pp. 527-544.

[21] Kuai, L., Haan, F. L., Gallus, W. A., 2008, "CFD Simulations of the Flow Field of a Laboratory-Simulated Tornado for Parameter Sensitivity Studies and Comparison with Field Measurements," Wind and Structures, **11**(2) pp. 1-22.

[22] Natarajan, D., and Hangan, H., 2012, "Large Eddy Simulations of Translation and Surface Roughness Effects on Tornado-Like Vortices," Journal of Wind Engineering and Industrial Aerodynamics, .

[23] Wurman, J., Randall, M., and Zahrai, A., 1997, "Design and Deployment of a Portable, Pencil-Beam, Pulsed, 3-Cm Doppler Radar," J. Atmos. Oceanic Technol, **14**pp. 1531-1539.

[24] Wurman, J., 2001, "The DOW mobile multiple-Doppler network," Preprints, 30th Conf. on Radar Meteorology, Anonymous Amer. Meteor. Soc., Munich, Germany, pp. 95-97.

[25] Wurman, J., and Gill, S., 2000, "Fine-Scale Radar Observations of the Dimmitt, Texas (2 June 1995) Tornado," Monthly Weather Review, February.

[26] Alexander, C. R., and Wurman, J., 2005, "The 30 may 1998 Spencer, South Dakota, Storm. Part I: The Structural Evolution and Environment of the Tornadoes," Monthly Weather Review, **133**(1) pp. 72-97.

[27] Wurman, J., and Alexander, C. R., 2005, "The 30 may 1998 Spencer, South Dakota, Storm. Part II: Comparison of Observed Damage and Radar-Derived Winds in the Tornadoes," Monthly Weather Review, **133**(1) pp. 97-119.

[28] Lee, W. C., and Wurman, J., 2005, "Diagnosed Three-Dimensional Axisymmetric Structure of the Mulhall Tornado on 3 may 1999," American Meteorological Society, **62**pp. 2373-2393.

[29] Kosiba, K., and Wurman, J., 2010, "The Three-Dimensional Axisymmetric Wind Field Structure of the Spencer, South Dakota, 1998 Tornado," Journal of Atmospheric Sciences, **67**pp. 3074-3083.

[30] Wakimoto, R. M., Atkins, N. T., and Wurman, J., 2011, "The LaGrange Tornado during VORTEX2. Part1: Photogrammetric Analysis of the Tornado Combined with Single-Doppler Radar Data," Monthly Weather Review, **139**pp. 2233-2258.

[31] Wakimoto, R. M., Stauffer, P., Lee, W. C., 2012, "Finescale Structure of the LaGrange, Wyoming Tornado during VORTEX2: GBVTD and Photogrammetric Analyses," Monthly Weather Review, **140**pp. 3397-3418.

[32] Lee, J., and Samaras, T., 2004, "Pressure measurements at the ground in an F-4 tornado," Proceedings of the 22nd Conference on Severe Local Storms, Anonymous Hyannis, MA.

[33] Mishra, A. R., James, D. L., and Letchford, C. W., 2008, "Physical Simulation of a Single-Celled Tornado-Like Vortex, Part B: Wind Loading on a Cubical Model," Journal of Wind Engineering and Industrial Aerodynamics, **96**(8) pp. 1258-1273.

[34] Haan, F., Balaramudu, V., and Sarkar, P., 2010, "Tornado-Induced Wind Loads on a Low-Rise Building," Journal of Structural Engineering, **136**(1) pp. 106-116.

[35] Hangan, H., and Kim, J., 2008, "Swirl Ratio Effects on Tornado Vortices in Relation to the Fujita Scale," Wind and Structures, **11**(4) pp. 291.

Chapter 2

2 Tornado simulations

2.1 Tornado formation and structure

Most tornadoes develop within supercell thunderstorms. Supercells are intense weather systems that mainly form where cold dry air meets warm moist tropical air. An environment with significant variation of wind speed with height at the ground is a necessity for supercell thunderstorms to initiate. Supercell thunderstorms rotate around a vertical axis as a result of *tilting*. The vertical wind shear at the surface induces horizontal vorticity which is tilted into a vertical vorticity by the warm air that is drawn into the thunderstorm updraft. The rotating updraft is called *mesocyclone* (a small-scale cyclone) and is part of the storm circulation. The energy that drives this type of thunderstorms, and therefore the energy in tornadoes, comes primarily from the redistribution of energy within the air masses that form the storm and the latent heat that is released when condensation of water vapor takes place in the updrafts [1]. The total amount of energy of an average thunderstorm is about $4x10^8$ kg of water (10^{15} J). Although the source of the supercell rotation and the structure of the mesocyclone are well understood, tornadogenesis within mesocyclones is debatable. Nevertheless, it is agreed by all scientists that *vortex stretching* plays an important role in the tornadogenesis. The vertical vorticity is usually intensified further by vortex stretching and, an area of low pressure is generated at the axis which sucks the air inwards. If the rotating updraft is sustained, a tornado vortex may form. Figure 2-1demonstrates five flow regions in a typical tornado introduced by Lewellen [2]. These regions are as follows:

- Outer flow (Ia): this region is above the boundary layer and extends at least 1km outward from the vortex core. The spinning air in the outer region approaches the axis while rising. The rotational speed of the flow increases as it gets closer to the axis.
- Core (Ib): this region surrounds the axis of the vortex and becomes wider as moving downstream (upward). The vortex core extends outward to the radius of

maximum tangential velocity and varies, in size, from tens to hundreds of meters. Upward or downward axial velocities are observed in the core region, depending on the vortex structure.

- Corner flow (III): the transition from inflow to core flow occurs in this region. The low pressure zone at the vortex center results in a radially converging flow which is then tilted upwards in the corner flow region and translates axially. Lewellen [2] has argued that maximum tangential velocities occur in the upper part of the corner region.
- Inflow (II): this region is dominated by the boundary layer flow. The rotational flow interaction with surface reduces the tangential velocity. On the other hand, the pressure does not vary significantly across the boundary layer. Therefore, the imbalance between the centrifugal force and the radial pressure force draws a significant flow towards the axis in the boundary layer.
- Upper flow (IV): this region is embedded in the parent storm.

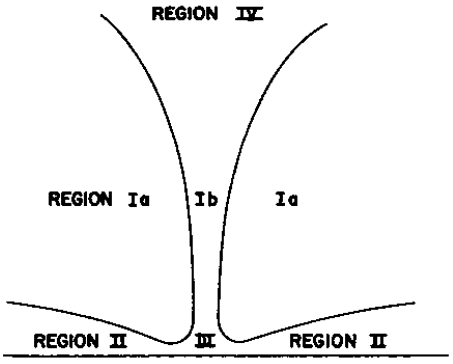

Figure 2-1: Schematic drawing of various zones in a tornado presented by Davies-Jones *et al.* [3] - image adapted from Lewellen [2].

2.2 Analytical models

The combined Rankine vortex model represents the air flow around a tornado with only the tangential velocity component (V_{tan}). This model divides the vortex into two parts: the inner part of the vortex which is in solid body rotation and the outer part of the vortex in

which the tangential velocity is a decreasing function of radius. The combined Rankine vortex model results in the definition of *core radius* (r_c) which is the radius where the maximum tangential velocity occurs. Eq. (2.1) shows the mathematical representation of combined Rankine vortex model.

$$V_{tan}(r) = \frac{V_{tan,max}\mathrm{r}}{r_c}, \quad (r \leq r_c) \tag{2.1}$$

$$V_{tan}(r) = \frac{V_{tan,max}r_c}{\mathrm{r}}, \quad (r > r_c)$$

where $V_{tan,max}$ is the tangential velocity at r_c and r is the radial coordinate with r=0 being at the center of the vortex core. The modified Rankine vortex is another mathematical model in which the tangential velocity is defined as

$$V_{tan}(r) = \frac{r\Gamma_\infty}{\pi\left(r^2 + r_c^2\right)} \tag{2.2}$$

where $\Gamma_\infty = 2\pi r_c V_{tan,max}$ is the maximum vortex strength. The non-dimensional tangential velocity for a combined and modified Rankine vortex as a function of non-dimensional radius is demonstrated in Figure 2-2. As shown, the transition from the inner core of the vortex to the outer core flow is better represented by the modified Rankine vortex.

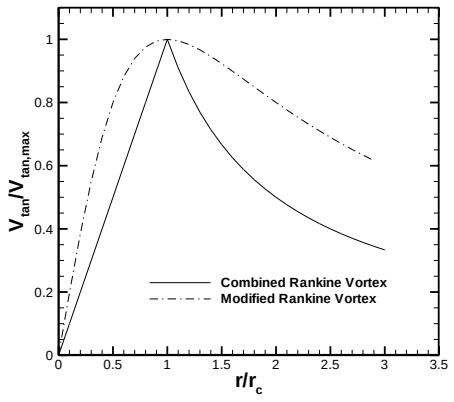

Figure 2-2: Tangential velocity vs. radius for combined and modified Rankine vortex models.

The pressure field can be calculated by using the Bernoulli equation

$$P(r) - P(\infty) = \frac{-\rho\Gamma_{\infty}^{2}}{2\pi^{2}\left(r^{2} + r_{c}^{2}\right)} \tag{2.3}$$

where ρ is the fluid density and $P(r)$ and $P(\infty)$ are static pressure at radius r and the atmospheric static pressure, respectively.

The Burgers-Rott vortex model is obtained as an exact solution of the Navier-Stokes equations with the following assumptions

- Axisymmetric geometry
- Constant density and viscosity
- Steady flow
- Radial and tangential velocity only a function of radius
- Axial velocity only a function of height

By assuming circulation strength of $\Gamma \equiv rV_{tan}$ for the vortex, a radial velocity of $V_{rad} = -\alpha r$ and an axial velocity of $V_{ax} = 2\alpha z$, where α is a constant representing the strength of the suction, the Navier-Stokes equations in the tangential direction can be written as

$$-\alpha r\frac{d\Gamma}{dr} = \nu r\frac{d}{dr}\left(\frac{1}{r}\frac{d\Gamma}{dr}\right) \tag{2.4}$$

where ν is the kinematic viscosity of fluid. After solving for Γ and using the relation between circulation and the tangential velocity, the tangential velocity is determined:

$$V_{tan}(r) = \frac{\Gamma}{2\pi r}\left(1 - exp\left(-\frac{\alpha r^{2}}{2\nu}\right)\right) \tag{2.5}$$

The pressure distribution estimated by this model is as follows

$$P(r,z) = P(\infty) + \rho\int_{0}^{r}\frac{\nu^{2}}{r}dr - \rho\frac{\alpha^{2}}{2}(r^{2} + 4z^{2}) \tag{2.6}$$

Unlike the Rankine vortex, the Burgers-Rott vortex has radial and axial velocity components as well. Although there is partially a mechanism for making a Burgers-Rott vortex in the atmosphere, this model has fundamental disadvantages; the axial velocity is only a function of height and the vertical pressure gradient is increasing by height without bound.

Recently, Xu and Hangan [4] have modeled the tornado-like vortex by using a free narrow jet solution combined with a modified Rankine vortex. While the modified Rankine vortex can describe the swirl motion of the tornado vortex, the upward free jet can represent the two-dimensional, radial and axial, motions. Therefore this model provides three velocity components for the tornado-like vortices

$$V_{rad}(r,z) = \left(\frac{1}{r} + \frac{2r}{z^2}\right) e^{-(\frac{r}{z})^2} - \frac{1}{r} \tag{2.7}$$

$$V_{ax}(r,z) = \frac{2}{z} e^{-(\frac{r}{z})^2} \tag{2.8}$$

$$V_{tan}(r,z) = 2(V_{tan,0}/2V_{rad,0})(r_c^2(z)+1)\frac{r}{r_c^2(z)+r^2} \tag{2.9}$$

where *0* denotes the inflow boundary.

2.3 Experimental models

2.3.1 Governing parameters

In order to accurately simulate a tornado-like vortex, it is important to define the parameters that control the flow dynamics. Lewellen [5] introduced three important tornado flow parameters: a geometric parameter, the aspect ratio; a kinematic parameter, the swirl ratio; and a dynamic parameter, the radial Reynolds number.

Aspect ratio, a, is defined as the ratio between the inflow height (h) and the updraft radius (r_0) which is less than one for a real tornado [6]. Swirl ratio, S, is defined as

$$S = \frac{r_o \Gamma}{2Qh} \tag{2.10}$$

where Γ is the circulation and Q is the volumetric flow rate per unit axial length. S is the ratio between the angular momentum to the radial momentum of the flow. It is an important controlling parameter which characterizes the vortex breakdown and the transition to multiple vortices [7, 8]. The radial Reynolds number is defined as

$$Re_r = \frac{Q}{2\pi\nu} \tag{2.11}$$

2.3.2 Tornado simulators

2.3.2.1 Ward-type tornado vortex simulator

Ying and Chang [9] developed a simulator based on the basic structure of a tornado; a vertical updraft and an inflow from a thin layer near the ground. Ward [10] improved the simulator that was first designed and built by Ying and Chang and introduced the Ward-type simulator, Tornado Vortex Chamber (TVC). He limited the inflow to a layer close to the surface and used a fine-mesh flow straightener right before the exhaust to remove the vertical vorticity from the rising flow. The TVC designed and built by Ward is shown in Figure 2-3. He presented three regions in the simulator [6]: *confluence*, *convergence* and *convection* zones.

The lowest part of the simulator includes the annular confluence region that surrounds the central convergence zone. A rotating mesh wire surrounding the confluence region provides the background angular momentum. At this point, the initial vorticity and then circulation are supplied to the radial inflow. In the convergence region, the radial gradient of the vertical velocity tilts the radial component of the inflow vorticity upward. The axial velocity gradient in the vortex core stretches the vertical vorticity and therefore, a column of swirling air forms at the center line and stretches toward the convection zone [6]. The *lid* that separates the convergence region from the convective region represents the stable layer of air which prevents any convection from outside the central updraft region of the storm. The baffle that is used as the upper boundary condition of the

convection region, removes any horizontal motion in the flow while leaving the axial flow unaffected. The main disadvantage of TVCs is the limited access to the chamber. The vortex chamber configuration does not allow for optical measurements as well as for translating the vortex.

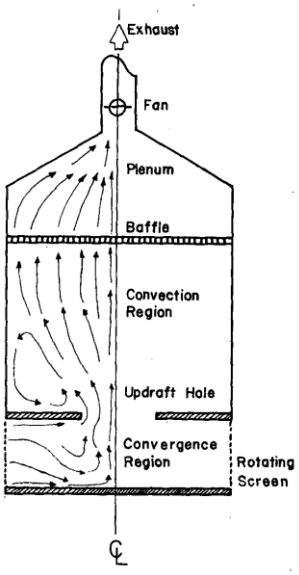

Figure 2-3: Schematic of the major components of the Ward-type TVC – image from [6].

2.3.2.2 Purdue tornado simulator

The Purdue TVC design concept is based on Ward's TVC (see Figure 2-4).Compared to the Ward's simulator, the Purdue simulator has the advantage of a more independent control over the three flow parameters, i.e., aspect ratio, swirl ratio and radial Reynolds number. The inflow depth and the updraft radius are adjustable in this apparatus which allows for varying the aspect ratio [6]. The radial Reynolds number is determined through flow rate measurements at the exhaust and the swirl ratio is calculated using the inflow angle measured far from the axis (at the confluence region). Although the tornado-like vortex generated in this simulator was very stable, which facilitated the measurement

process, an unwanted circulating cell was observed in the upper chamber. Church *et al.* [11] attributed this cell to the sharp edge of the updraft hole.

2.3.2.3 Texas Tech tornado simulator

A Ward-type simulator was assembled at Texas Tech University (TTU) in 2001 [12]. This simulator was later modified by Mishra *et al.* [13] with an intention to perform experiments towards wind engineering, rather than the atmospheric science applications. Figure 2-5 displays the TTU vortex simulator II. In this simulator, updraft and circulation were provided by means of a blower at the top of the convection chamber and 16 slotted jets at the inflow, respectively. Mishra *et al.* used slotted jets instead of vanes/rotating screens to enable independent control of the circulation. Also, this configuration provided an easy access to the chamber for measurement purposes. The updraft radius is fixed at 0.19 m and the inflow height is variable between 0.06 m and 0.19 m. A vortex blower at the base of the simulator is used to regulate the flow from each slotted jet and therefore, adjust the swirl ratio.

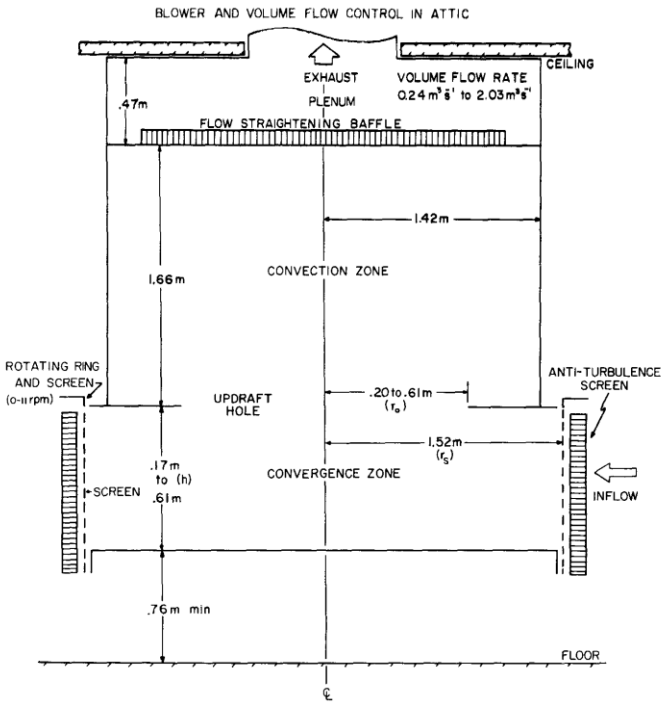

Figure 2-4: Schematic of the Purdue TVC – image from [6].

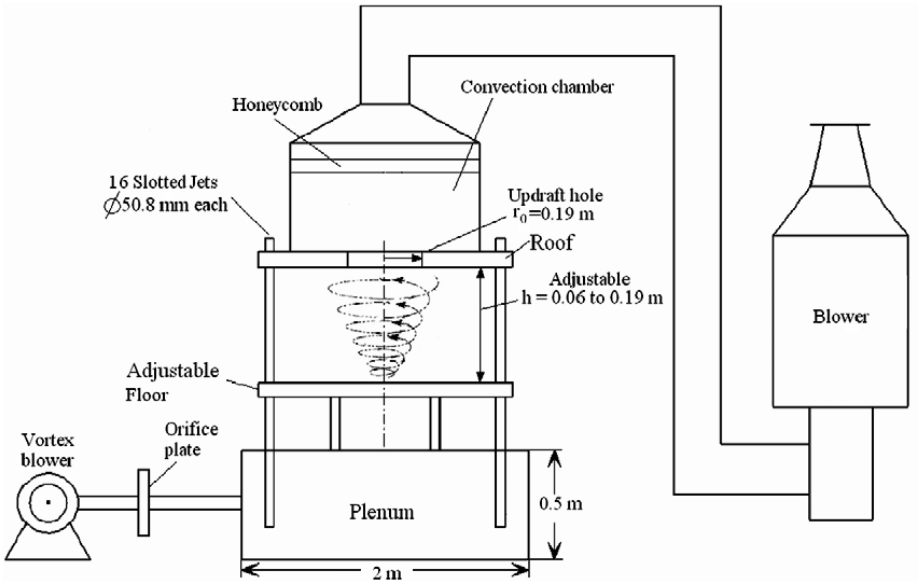

Figure 2-5: Schematic drawing of the second generation vortex simulator at Texas Tech University – image from [13].

2.3.2.4 Iowa State University (ISU) tornado simulator

This simulator is designed and constructed to meet two important requirements: first, to accommodate models of reasonable size for measuring loads on structures and buildings and second, to be able to translate along the ground plane for a realistic simulation of a natural tornado. The maximum translational speed of this simulator is 0.61 m/s.

Figure 2-6 demonstrates the schematic diagram of the ISU simulator. The simulator consists of a circular duct that is suspended from an overhead crane so that it allows translation along a 10.36 m long ground plane [14]. The updraft is provided by means of a fan located in the center of the duct. The flow from the updraft is directed downward while rotated by means of vanes in an annular duct surrounding the inner region. This technique is called *rotating forced downdraft* (see Figure 2-6). The transition from a laminar core to a turbulent core that was clearly observed in Ward-type simulators, is not observed in the ISU simulator which can be due to the instability of the vortex.

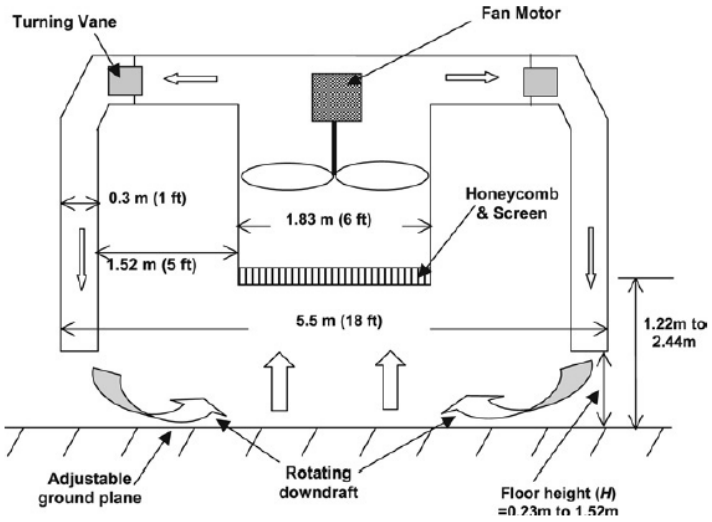

Figure 2-6: Schematic illustration of the ISU tornado simulator – image from [14].

2.3.2.5 Model WindEEE Dome

Western University initiated a project in 2008 to design, construct, and operate the Wind Engineering, Energy and Environment (WindEEE) Dome. The WindEEE facility is capable of simulating various wind systems such as tornadoes, downbursts and gust fronts. The design process consisted of the conceptual design involving Computational Fluid Dynamics (CFD) simulations for selected modes of operations and the design of a 1/11 scaled physical model (the Model WindEEE Dome). Extensive CFD simulations were performed by Natarajan [15] in which he demonstrated the feasibility of five operational scenarios for WindEEE (see Figure 2-7); uniform straight flows, shear flows, boundary layer flows, downburst-like flows with translation and tornado-like flows with translation. The Model WindEEE Dome (MWD) was designed and built to validate the CFD results, to make improvements/modifications to the flow circuit and to implement the control system for the dome and to investigate the performance of the facility before finalizing the full-scale facility design. MWD is also a research tool to determine new operational scenarios for WindEEE.

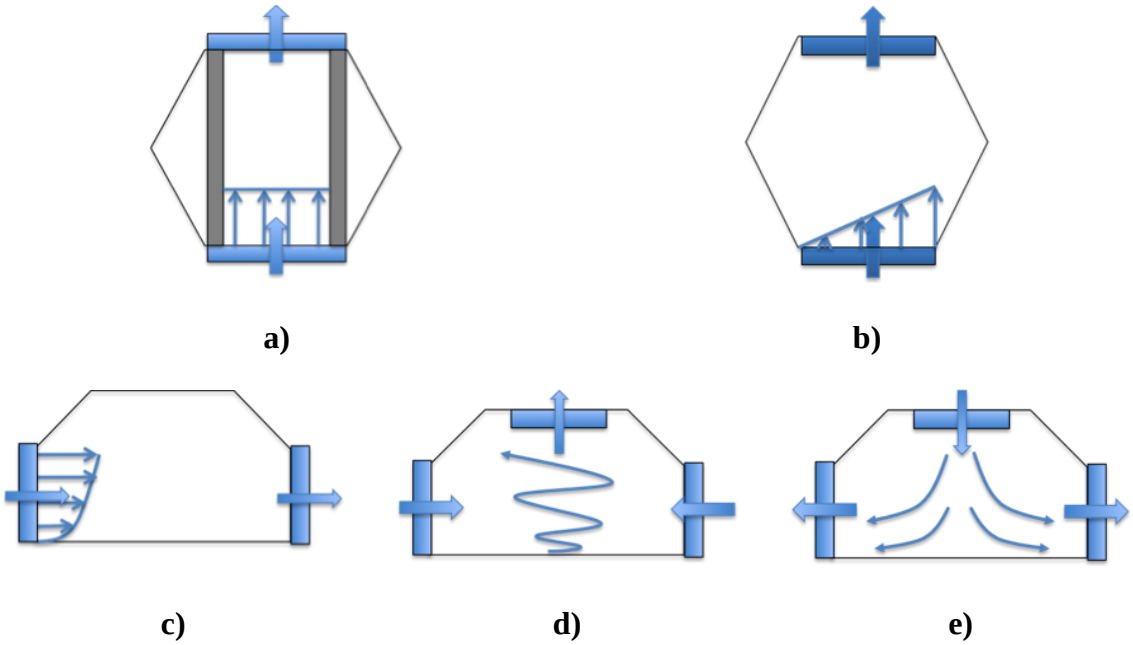

Figure 2-7: Five operational scenarios for WindEEE Dome include a) uniform straight flows, b) shear flows, c) boundary layer flows, d) tornado flows with translation and e) downburst flows with translation.

The MWD is a closed loop, three-dimensional wind testing facility consisting of two hexagonal chambers; one at the top with 18 fans and one at the bottom with 100 fans (Figure 2-8a and Figure 2-8b, respectively). Each fan can be controlled individually and the upper fans are reversible. Figure 2-8c shows 7 cm high adjustable vanes that are installed in front of all lower fans to produce the desired swirl. The lower chamber is connected to the upper chamber through a bell-mouth which is 0.4 m wide (see Figure 2-8d). The updraft hole can be varied in diameter between 0.14 m and 0.4 m. Using a single axis traverser system called *guillotine*, the bell-mouth and therefore the tornado/downburst can be translated at a maximum speed of 0.25 m/s. A matrix of 4 rows×15 fans (as shown in Figure 2-8e) at one of the peripheral walls along with two porous curtains can form a versatile multi-fan wind tunnel. Horizontally or vertically sheared flows can be produced by adjusting each fan on the wall of fans. Figure 2-8e displays the heat exchangers used in the return circuit in order to control the air flow temperature. A single air temperature sensor, located just upstream of the 60 fan wall,

sends a signal to the heat exchangers pump as needed. Figure 2-8f shows the simulator after completion. The chamber floor is 1.3 m above the ground to provide access to the test chamber from underneath. The test chamber has a diagonal of 2.76 m long while the return circuit is 3.52 m long in diagonal.

There are two possible configurations for generating tornado-like vortices inside the dome: a) using top fans to provide updraft and periphery vanes at a given angle to generate swirl and, b) running top fans and periphery fans as a source of suction and inflow, respectively while using vanes to control the swirl.

The MWD construction was started in spring 2010. The engineering design was provided by AIOLOS and the construction was mainly done by the University Machine Shop (UMS) and the University Electronics Shop (UES). During the construction of the model, some modifications were suggested to AIOLOS which improved the design of MWD and applied to the full-scale facility design. Some of these modifications are as follow

- Using rpm sensors to measure the rotation speed of each fan
- Replacing the wooden panels surrounding the model with transparent panels to enable visual inspection of fans and water leakage from heat exchangers
- Changing heat exchanger tubes to withstand higher water temperature flow
- Using water trays to collect possible drain from heat exchangers

The commissioning started in Dec 2010 with a series of validation experiments. The test program involved flow visualizations for tornado-like and downburst-like flows and surface static pressure measurements with pitot and pitot-static tubes for horizontal flows. Flow visualizations were performed by Refan [16] with a special attention to tornado-like flows and the uniformity tests were carried out by AIOLOS engineers [17]. The commissioning tests demonstrated the basic functionality of the MWD for all flow cases. The fans were able to operate successfully and be controlled in various modes, the vanes and the guillotine operated as designed and the cooling system was functional. The tornado and downburst modes were successfully demonstrated using flow visualization methods.

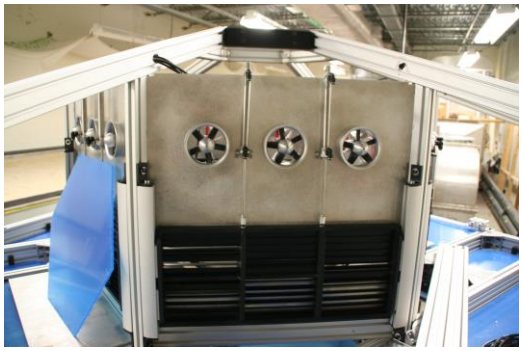

a)

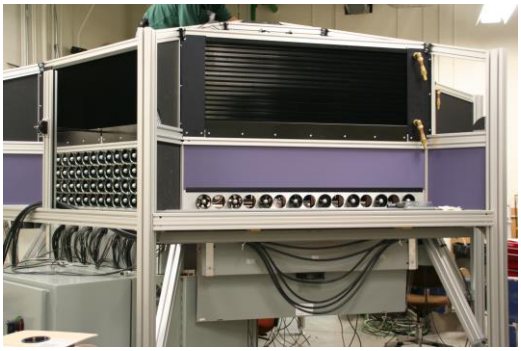

b)

c)

d)

e)

f)

Figure 2-8: Model WindEEE Dome components: a) upper plenum with 18 fans, b) lower chamber with 100 fans, c) directional vanes at the periphery, d) bell-mouth, e) wall of 60 fans with heat exchangers on the top, f) relatively large scale of the simulator after completion.

2.3.3 Vortex evolution

The swirl ratio effect on tornado-like vortices has been investigated widely using tornado simulators. A summary of observational studies documenting the vortex evolution with variations in swirl ratio is provided here. These flow visualizations are mainly performed by Ward [10], Church *et al.* [6] and Snow [18, 19]. To better visualize the vertical structure of tornado-like flows, idealized axial velocity profiles of the vortex at various swirl ratios as proposed by Church *et al.* [6], Snow [18, 19] and Davies-Jones [20] are also presented here.

For no-swirl setting (see Figure 2-9) a stagnation zone forms at the surface near the central axis where the inflow separates from the surface. The flow is axisymmetric and irrotational at this point. At very low swirls, $0<S<0.1$, a stagnation zone at the surface along the axis continues to be present and prevents any angular momentum reaching the centerline. As such, a swirling flow forms in the convection region of the simulator at mid-heights rather than on the surface. As the angular momentum increases, the core travels down towards the surface and the inflow boundary layer is forced to reattach to the surface (see Figure 2-10). As a result, a ring-shaped separation-reattachment region is observed on the surface [21].

The evolution of the vortex structure in a moderate swirl range ($0.1<S<0.5$) can be divided into two categories. At the lower end of this range, $0.1<S<0.2$, the flow is mainly characterized by a thin boundary layer that is growing towards the centerline. The horizontal inflow turns into a vertical flow with a rotational core and a very slow increase in the vortex core size with height is observed. As the swirl ratio increases, an abrupt expansion of the vortex core is observed aloft which is due to the *vortex breakdown bubble* formation. This phenomenon was first recorded in the Purdue University TVC [22]. The term *laminar* is used in TVC's to characterize the vortex state before the breakdown. Once the vortex breaks down, the flow becomes highly turbulent. As explained by Hall [23, 24], a key feature of quasi-cylindrical vortices is to develop an adverse axial pressure gradient which is related to the radial expansion of the turbulent core aloft. As a result, the updraft decelerates at the centerline and maximum vertical

velocities relocate to an annular ring surrounding the vortex breakdown bubble. Figure 2-11a illustrates the vortex breakdown captured in a TVC simulator at S≈0.3. An important characteristic of the vortex breakdown is formation of a free stagnation point at the border of the subcritical and the supercritical flow. This stagnation point is very unstable and as a result, the breakdown point oscillates around a mean position [6].

The presence of vortex breakdowns in actual tornadoes has been confirmed by Paulry and Snow [25] and Lugt [26]. A schematic drawing of the vortex with breakdown bubble is presented in Figure 2-11b. As the axial velocity decelerates at the centerline, a free stagnation point forms above the vortex breakdown bubble. Downstream of this stagnation point, vertical velocities are very small. In some cases, even downflow is observed (see Figure 2-11c).

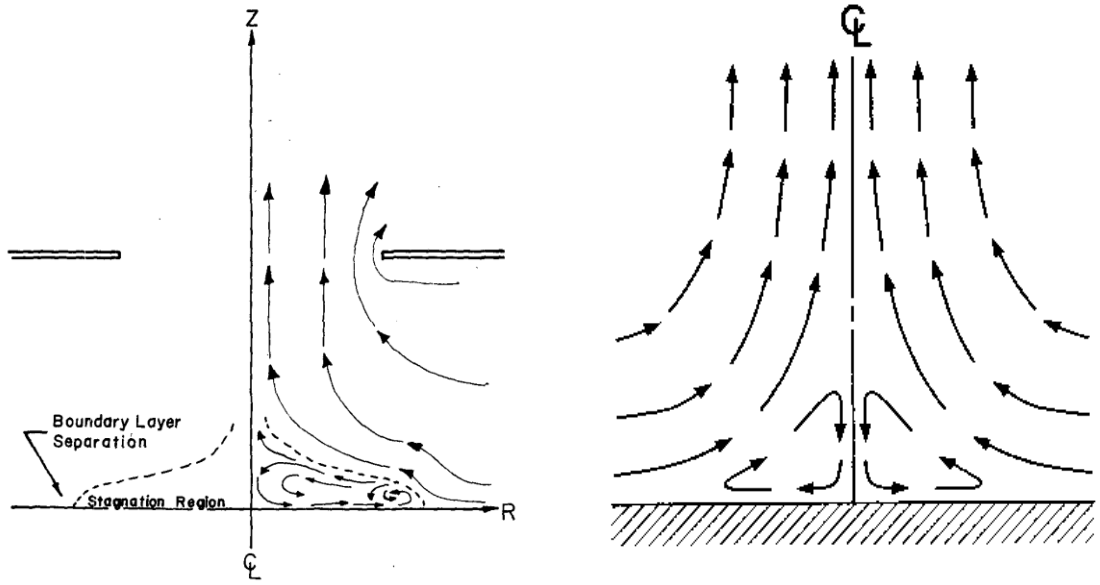

a) **b)**

Figure 2-9: Schematic drawing of the flow in the convergence region for no swirl presented by a) Church *et al.* [6] and b) Davies-Jones [20].

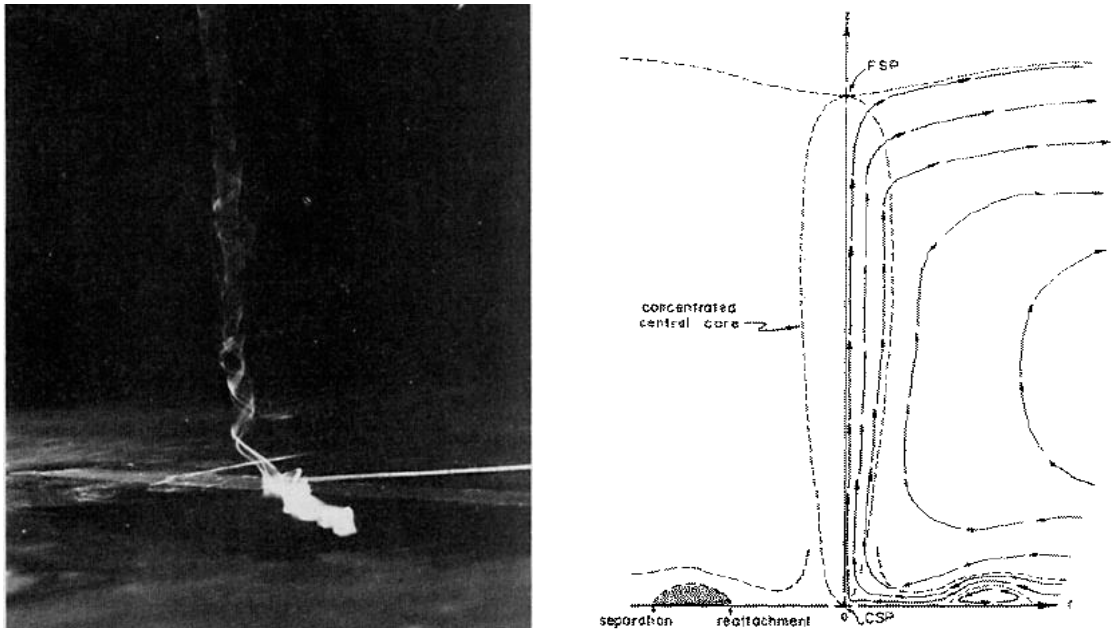

a) **b)**

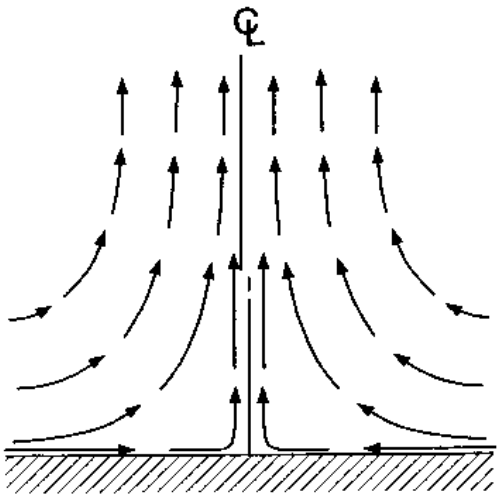

c)

Figure 2-10: a) laminar core of a simulated vortex [6] and schematic drawing of the flow structure showing the separation-reattachment regions proposed by b) Snow [18] and c) Davies-Jones [20].

By further increasing the swirl ratio, the vortex breakdown bubble moves upstream (towards the surface) while developing downward flow and eventually, it touches the surface (at $S \approx 0.45$ in TVCs). At this point, highest vertical accelerations and pressure deficits are experienced in the surface layer [27] and the boundary layer inflow is squeezed into a very thin layer at the touch-down region (see Figure 2-12). Maxworthy [22] named this condition a *drowned vortex jump* which is associated with the strongest tangential velocities near the ground.

Once the drowned vortex jump occurs, the vortex core expands radially while the downdraft intensifies. At this point, the central downflow is surrounded by two intertwining spiral vortices. Further increase in the swirl ratio, forces the two intertwining vortices to separate and form two separate tornado-like vortices (see Figure 2-13a and Figure 2-13b) that rotate around their own axis while spinning around the centerline [27]. This configuration is observed at $S \approx 1$ in TVCs. For $S > 1$, multiple vortices, with a maximum of six sub-vortex, are formed in TVCs (see Figure 2-13c). This multi-celled configuration is common in nature as shown by Fujita [28].

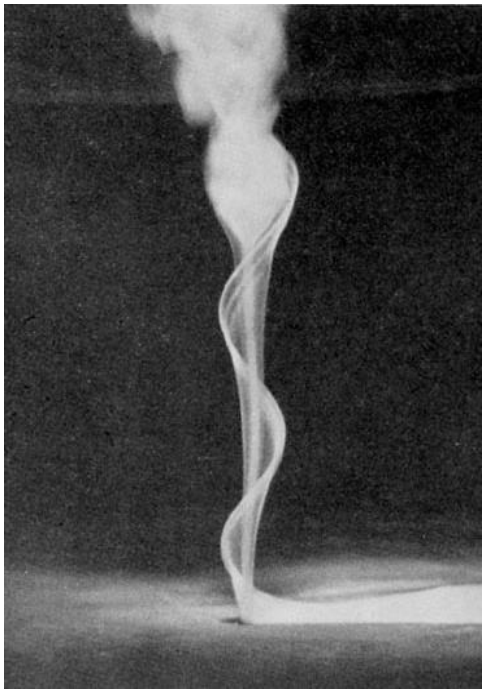

a)

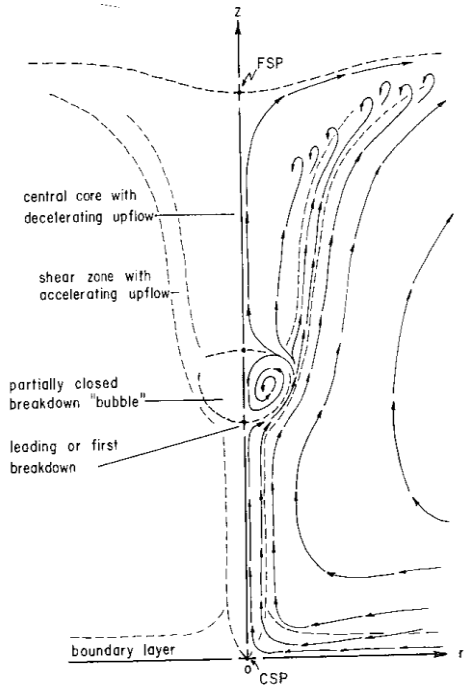

b)

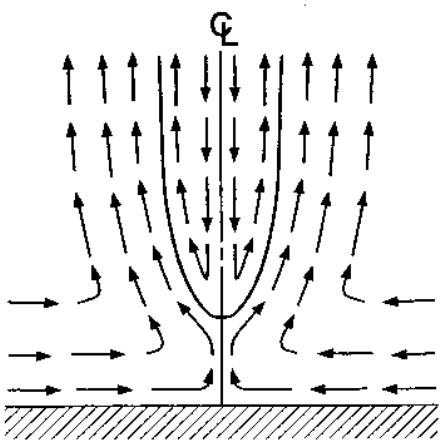

c)

Figure 2-11: a) smoke-traced flow with breakdown aloft [10] and drawing of a vortex configuration at breakdown stage proposed by b) Snow [19] and c) Davies-Jones [20].

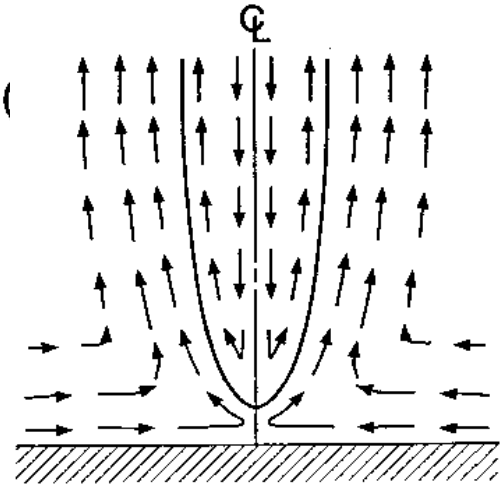

Figure 2-12: vertical structure of the vortex at the drowned vortex jump stage, Davies-Jones [20].

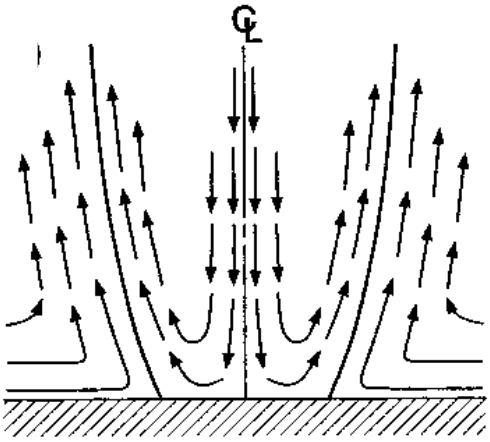

a)

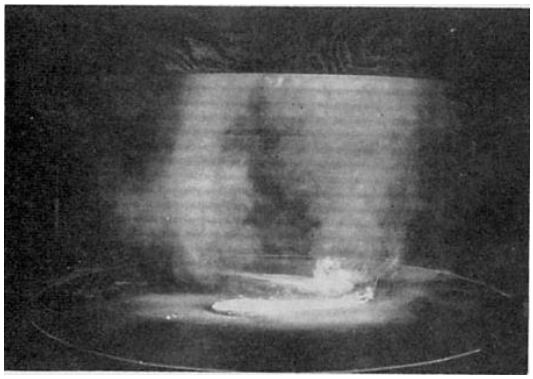

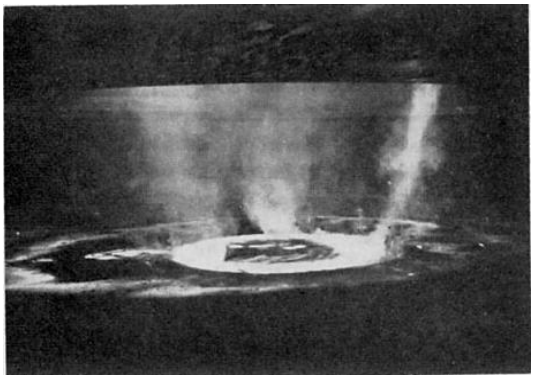

b) **c)**

Figure 2-13: a) Vertical structure of a two-celled vortex – image from [20] and a family of b) two- and c) three-celled vortices simulated in TVCs – image from [10].

2.3.4 Real tornado versus simulated vortex

Typical characteristics of tornadoes in nature are compared with those of laboratory simulated vortices and listed in Table 2-1.

The aspect ratio of real tornadoes is estimated to be less than unity which is achievable in simulators. However, as seen in Table 2-1, the radial Reynolds number of a real tornado is many orders of magnitude larger compared to the generated ones. Therefore, it can be concluded that dynamic scaling requirements are not satisfied. However, Ward [10],

Jischke and Parang [21], Davies-Jones [7] and Church *et al.* [6] found that for a given geometry, if the radial Reynolds number is large enough to ensure turbulent flow, vortex characteristics are independent of the radial Reynolds number (see Figure 2-14). They concluded that the core radius and the transition from a single vortex to multiple vortices are mainly controlled by the swirl ratio and therefore, the primary dynamic similarity variable is the swirl ratio.

Table 2-1: Dimensionless groups and translation speed for a real tornado and simulated tornado-like vortices.

	Likely atmospheric range [6]	Purdue Tornado Simulator [6]	TTU vortex simulator II [29]	ISU [14]	MWD
a	0.2-1	0.2-3	0.31-1.0	0.25-1.68	0.35-1.0
S	0.05-2	0.01-27.5	0.15-1.54	0.08-1.14	0.1-1.3
Re_r	10^9-10^{11}	4.1×10^3-1.2×10^5	4.3×10^4-2.1×10^5	Not Provided	8.4×10^4
V_{tran} (m/s)	10-18	Not applicable	Not applicable	0.61	0.25

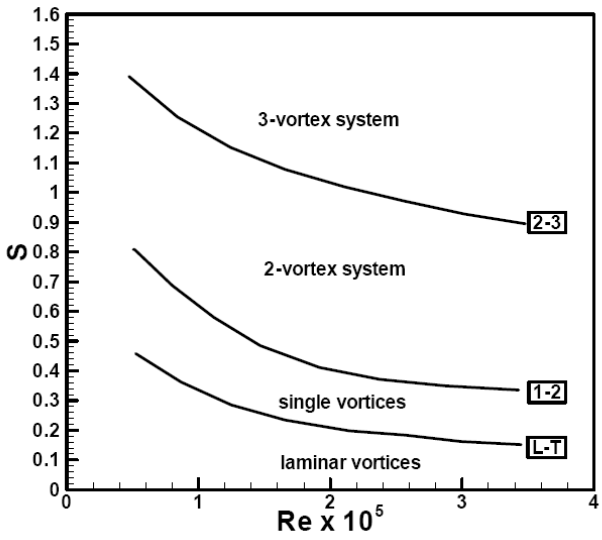

Figure 2-14: Critical (transition) swirl ratio as a function of radial Reynolds number; L-T → laminar to turbulent, 1-2 → Single-celled to two-celled vortices, 2-3 → two-celled vortices to three-celled vortices – image from [6].

References

[1] Braham, R. R., 1952, "The Water and Energy Budget of the Thunderstorm and their Relation to Thunderstorm Development," Journal of Meteorology, **9**(4) pp. 227-242.

[2] Lewellen, W. S., 1976, "Theoretical models of the tornado vortex," Proceeding of symposium of tornadoes, R. E. Peterson, ed. Texas Technical University, Lubbock, pp. 107-143.

[3] Davies-Jones, R. R., Trapp, J., and Bluestein, H. B., 2001, "Tornadoes and Tornadic Storms," Meteorological Monographs, (50) pp. 167.

[4] Xu, Z., and Hangan, H., 2009, "An Inviscid Solution for Modeling of Tornado-Like Vortices," ASME Journal of Mechanics, **76**.

[5] Lewellen, W. S., 1962, "A Solution of Three Dimensional Vortex Flows with Strong Circulation," Journal of Fluid Mechanics, **14**pp. 420.

[6] Church, C. R., Snow, J. T., Baker, G. L., 1979, "Characteristics of Tornado-Like Vortices as a Function of Swirl Ratio: A Laboratory Investigation," Journal of Atmospheric Sciences, **36**pp. 1175.

[7] Davies-Jones, R. P., 1973, "The Dependence of Core Radius on Swirl Ratio in a Tornado Simulator," Journal of Atmospheric Sciences, **30**pp. 1427.

[8] Rotunno, R. A., 1979, "A Study in Tornado-Like Vortex Dynamics," Journal of Atmospheric Sciences, **36**pp. 140.

[9] Ying, S. J., and Chang, C. C., 1970, "Exploratory Model Study of Tornado-Like Vortex Dynamics," Journal of the Atmospheric Sciences, **27**(1) pp. 3-14.

[10] Ward, N. B., 1972, "The Exploration of Certain Features of Tornado Dynamics using a Laboratory Model," Journal of Atmospheric Sciences, **29**pp. 1194.

[11] Church, C. R., Snow, J. T., and Agee, E. M., 1977, "Tornado Vortex Simulation at Purdue University," Bulletin of the American Meteorological Society, **58**pp. 900-908.

[12] Wang, J., James, D. L., Letchford, C. W., 2001, "Development of a prototype tornado simulator for the assessment of fluid-structure interaction," Proceedings of the 1st Americas Conference on Wind Engineering, 4-6 June, Clemson Uni., SC.

[13] Mishra, A. R., Jamesa, D. L., and Letchford, C. W., 2008, "Physical Simulation of a Single-Celled Tornado-Like Vortex, Part A: Flow Field Characterization," J. Wind Eng. Ind. Aerodyn., **96**pp. 1243.

[14] Haan Jr, F. L., Sarkar, P. P., and Gallus, W. A., 2008, "Design, Construction and Performance of a Large Tornado Simulator for Wind Engineering Applications," Engineering Structures, **30**pp. 1146.

[15] Natarajan, D., 2011, "Numerical Simulation of Tornado-Like Vortices," PhD Thesis, the University of Western Ontario.

[16] Refan, M., 2011, "WindEEE (Wind Engineering, Energy and Environment) Dome; Prototype design and validation," WindEEE Research Institute, Western University, London, ON.

[17] Aiolos Engineering Corporation, 2011, "Model WindEEE Dome preliminary commissioning report," 4183R336 rev 0, London, ON.

[18] Snow, J. T., Chang, C. R., and Barnhart, B. J., 1979, "An Investigation of the Surface pressure Fields Beneath Simulated Tornado Cyclones," J. Atmos. Sci., **37**pp. 1013-1026.

[19] Snow, J. T., 1982, "A Review of Recent Advances in Tornado Vortex Dynamics," Rev. Geophys., **20**pp. 953.

[20] Davies-Jones, R.P., 1986, "Tornado dynamics. Thunderstorms morphology and dynamics," 2d ed. E. Kessler, Ed., University of Oklahoma Press, pp. 197-236.

[21] Jischke, M. C., and Parang, M., 1974, "Properties of Simulated Tornado-Like Vortices," J. Atmos. Sci., **31**pp. 506.

[22] Maxworthy, T., 1972, "On the Structure of Concentrated Columnar Vortices," Actro. Acta., **17**pp. 363-374.

[23] Hall, M. G., 1966, "The Structure of Concentrated Vortex Cores," Prog. Aeronaut Sci., **7**pp. 53-110.

[24] Hall, M. G., 1972, "Vortex Breakdown," Annual Review of Fluid Mechanics, **4**(1) pp. 195-218.

[25] Pauley, R. L., and Snow, J. T., 1989, "On the Kinematics and Dynamics of the 18 July 1986 Minneaopolis Tornado," Mon.Wea.Rev., **116**pp. 2731-2736.

[26] Lugt, H. J., 1989, "Vortex Breakdown in Atmospheric Columnar Vortices," Bull. Amer. Meteor. Soc., **70**pp. 1526-1537.

[27] Church, C. R., and Snow, J. T., 1993, "Laboratory Models of Tornadoes," Geophysical Monograph, **79**.

[28] Fujita, T. T., 1976, "Graphic Examples of Tornadoes," Bull.Amer.Meteor.Soc., **57**pp. 401-412.

[29] Wang, H., 2002, "Fluid-Structure Interaction of a Tornado-Like Vortex with Low-Rise Structures," PhD Thesis, Texas Tech University.

Chapter 3

3 Experimental techniques and procedure

The tornado-like vortex flow fields generated in Model WindEEE Dome were investigated, at various swirl ratios, using flow visualizations, surface pressure measurements and Particle Image Velocimetry (PIV). All experiments were performed for a fixed aspect ratio of 0.35 and different vane angles (swirl ratios).

3.1 Flow visualization

The flow visualizations were performed for 8 different vane angles (θ=5˚, 10˚, 15˚, 20˚, 25˚, 30˚, 35˚ and 40˚) and at Re_r=6.7×10^4. Note that dependency of the flow characteristics on the radial Reynolds number will be discussed in more details in Chapter 4. Dry ice and helium bubbles were used to obtain qualitative information on the tornado-like vortex.

As a first approach, a bucket of dry ice mixed with water was located at the center of the simulator, under the surface level. As soon as the smoke entered the chamber, the simulator was turned on and the flow was visualized with the smoke. Alternatively, a helium bubble generator manufactured by Sage Action Inc. was used for visualization. This generator produces neutrally buoyant, helium-filled bubbles of controlled size for visualizing complex airflow patterns. These bubbles can be used to trace airflow patterns at speeds ranging from 0 to 60 m/s. Since these bubbles follow the flow streamlines exactly, they rarely collide with any objects in the air stream. The bubbles are also extremely durable. Therefore, they best match the requirements for visualizing tornado-like vortices in a test chamber like MWD.

Figure 3-1 shows the helium bubble console and different parts in the *Mini Vortex Filter*. The Plug-In Head consists of a concentric arrangement of two stainless steel hypodermic tubes, one inside the other, attached in a cantilever fashion to a cylindrical manifold base or body. Within the Head, helium passes through the inner hypodermic tube and Bubble Film Solution (BFS) through the annulus between the inner tube and the outer tube to

form the helium-filled bubbles at the tip. A much larger, concentric jet of air blows the bubbles continuously off the tip. The air and helium pressure settings of 40 psi and 20 psi were used, respectively to generate bubbles of 3.175 mm in diameter. Two plastic tubes were utilized to transfer the helium bubbles from the outlet tubes to the simulator. The bubbles were fed into the chamber from one side far from the center of the simulator in order to minimize any disturbance in the flow.

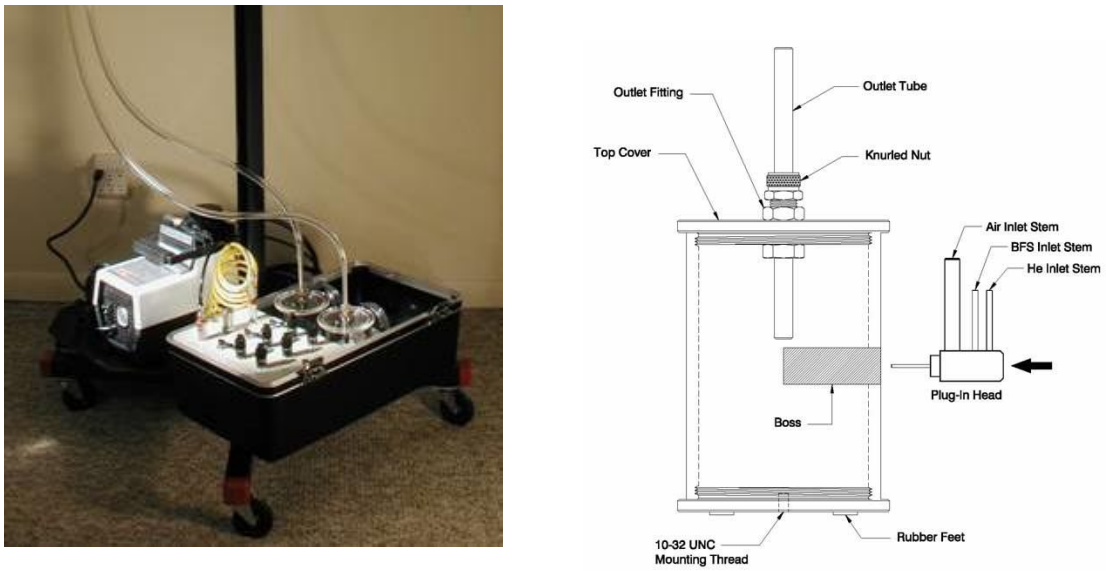

a) **b)**

Figure 3-1: a) Helium bubble generator console and b) Mini vortex filter.

3.2 Surface pressure tests

The surface static pressure distribution of tornado-like vortices and its variation with the swirl ratio provides useful insights into the vortex dynamics mostly in the near surface region where the flow velocity measurements are difficult.

3.2.1 Experimental setup

A pressure measurement system, provided by the Boundary Layer Wind Tunnel Laboratory (BLWTL), and a floor panel with several pressure taps were used to measure

the surface static pressure deficit. Figure 3-2 shows the center floor panel of the simulator with 413 static pressure taps distributed on concentric circles (with a maximum diameter of 56 cm) around the simulator centerline. Each tap was connected to a pressure scanner port using PVC tubing 1.34 mm in diameter (see Figure 3-3a). Thirty two pressure scanners (ESP, model: 16TL, 16 ports/transducers each) were used to convert pressures to proportional voltages measured by a custom system designed and built by BLWTL.

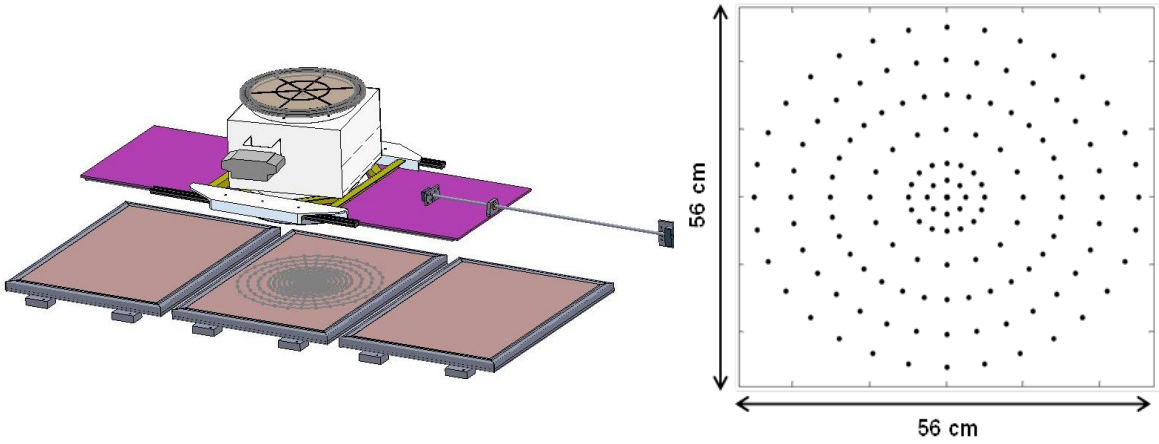

a) **b)**

Figure 3-2: a) Center floor panel position in the chamber and b) pressure taps distribution over the surface.

The BLWTL pressure system handles scanner control, A/D conversion and data recording using a PC-based architecture integrated with hardware multiplexing, counter/timer as well as high speed data acquisition boards/extensions. The pressure system also includes two stand-alone high-accuracy transducers used to provide reference measurements. These transducers are usually connected to pitot-static tubes mounted in the center of the wind tunnel to determine the reference velocity. The pressure system and the processing software were developed specifically for straight-flow wind tunnel applications. As a result, the output of the processing software is based on pressure coefficients (C_p) defined as

$$C_{p,i} = \frac{p_i - p_0}{p_q - p_0} = \frac{p_i - p_0}{\frac{1}{2}\rho V_\infty^2} \tag{3.1}$$

where p_i is the static pressure measured at i^{th} tap, p_0 is the reference static pressure or the *zero line*, p_q is the reference stagnation pressure and $1/2\rho V_\infty^2$ is the reference dynamic pressure where V_∞ is the wind tunnel free stream velocity.

3.2.2 Experimental procedure and data processing

Pressure measurements were taken for 8 different vane angles ranging from 5˚ to 40˚, with 5˚ increments and at a volumetric flow rate of 0.462 m^3/s. Pressure signals were sampled at a frequency of 400 Hz and were recorded for a period of 60 s. The completed setup for pressure measurements, including various components involved, are illustrated in Figure 3-3b.

Prior to the data recording, a *bag test* was performed to check for malfunctioning pressure scanners, leaking or blocked connections/tubes. Figure 3-3c demonstrates the setup for this test. While, the ground plate was completely sealed under a plastic bag, high pressure air was exerted inside the bag on the pressure taps to produce a constant pressure higher than ambient pressure. The feedback from each pressure tap was investigated and, blocked/leaking connections and malfunctioning scanners were identified and repaired.

As mentioned, the pressure data processing program developed at the BLWTL uses the wind tunnel free stream velocity as a reference to calculate the pressure coefficient at each tap. Since such a reference dynamic pressure does not exist in current experiments, a pressure bottle (see Figure 3-3d) was used to determine an equivalent to the reference velocity. The reference pressure (p_q) was created based on the height of water trapped inside its tube while the zero line (p_0) was kept at an atmospheric pressure.

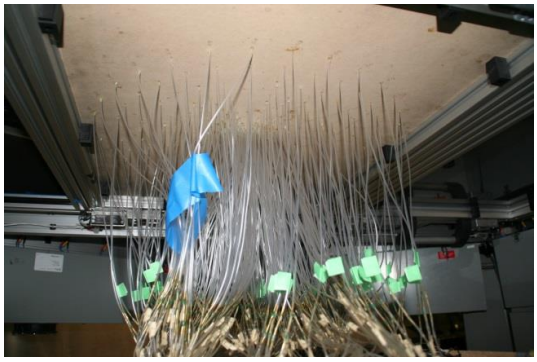

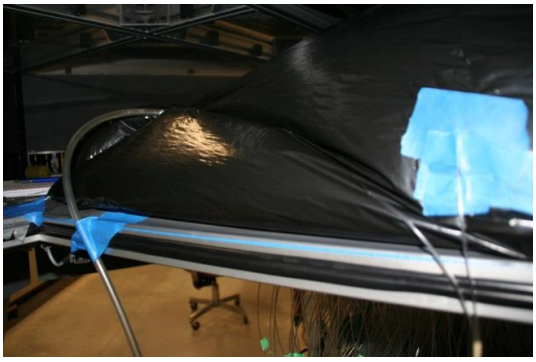

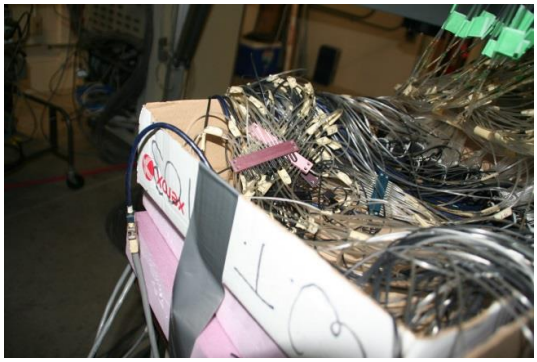

a)

c)

b)

d)

Figure 3-3: Static pressure test setup: a) pressure tubes and scanners arrangement, b) pressure bottle, c) pressure system, Barocel and simulator controllers an d) bag test.

The calibration was performed by applying atmospheric pressure to the transducers while the simulator was off. The logged voltage outputs determined the zero offset of the

measurements. Afterwards, the reference pressure (p_q) was sent to the transducers and to a Barocel (a stand-alone pressure transducer). The resulting voltage outputs were recorded and used to calculate the pressure coefficients using Eq. (3.1) and then the pressure deficit (ΔP) as follows

$$\Delta \mathrm{P} = (p_i - p_0) = C_{p,i}\left(p_q\right)_{Barocel} \tag{3.2}$$

where ΔP is the pressure difference between the i^{th} tap and environment. In the post processing of the data, the surface pressure deficit values were normalized by a dynamic pressure calculated using the average axial velocity through the updraft.

The uncertainty analysis was performed for surface pressure measurements (see Appendix C) and a maximum error of 1.17% was estimated.

3.3 Particle Image Velocimetry

Particle Image Velocimetry (PIV) is a non-intrusive method which measures the velocity field in a plane. In this technique, the displacement of small tracer particles that are carried by the fluid is determined in a short time interval (Δt). The tracer particles are chosen to be sufficiently small to follow the fluid motion accurately and to avoid any alteration in the fluid properties or flow characteristics. The particles are illuminated by a thin light sheet generated by a double-head pulsed laser system, and the light scattered by particles is recorded onto two subsequent image frames by a digital imaging device. A PIV system was implemented to measure the mean velocity field of the simulated tornado-like vortices at various swirl ratios and at different heights above the surface.

3.3.1 PIV system

A pulsed Nd:YAG laser generator with a wavelength of 532 nm was used as a source of illumination. The laser can be run at pulse repetition rates of up to 30 Hz with 120 mJ/pulse output energy. A CCD camera (VA-4M32, Vieworks) with a spatial resolution of 2336 × 1752 pixels was used to capture images. Using a calibration board, the field of view of the camera was set to 23.4 cm by 17.5 cm and pixel to meter conversion ratio was determined. The light sheet with uniform thickness of 2 mm was created using only a

cylindrical lens. Since this thickness is small enough to avoid the out of plane motion errors, no spherical lens was used for these experiments.

The camera was connected to an image acquisition system (CORE-DVR, IO industries) that acquires 8-bit images. A four-channel digital pulse/delay generator (555-4C, Berkeley Nucleonics Corporation) was used to control the timing of the laser light pulses and synchronize them with camera frames. For each experimental run, images were acquired at a rate of 30 Hz resulting in 15 vector maps per second.

The LaVision Aerosol Generator was utilized to seed the tornado chamber with Di-Ethyl-Hexyl-Sebacate (C26H50O4) particles with an average diameter of 1 μm. To examine the ability of seeding particles to follow the fluid motion, their response time is compared with the lowest possible time-scale for fluid motion known as Kolmogorov time scale. The response time (t_p) of a particle is defined as

$$t_p = \frac{v_{t,p}}{g} \tag{3.3}$$

where

$$v_{t,p} = \frac{2}{9}\frac{(\rho_p - \rho_f)}{\mu} g R^2 \tag{3.4}$$

$v_{t,p}$ is the particle terminal velocity, g is the gravitational acceleration (9.81 m/s^2), ρ_p is the particle density, ρ_f is the fluid density, μ is the dynamic viscosity and R is the particle radius. The density of the Di-Ethyl-Hexyl-Sebacate is 912 kg/m^3. The working fluid is air with dynamic viscosity of 1.98×10^{-5} kg/ms and density of 1.1839 kg/m^3 at 25˚C. By substituting these values in Eqs. (3.3) and (3.4), terminal velocity of 2.5×10^{-5} m/s with a response time of 2.55×10^{-6} s is obtained for the seeding particles. The Kolmogorov scales of the simulated flow can be estimated if the dissipation rate (ε) is known. Since the size of the largest eddies in the flow are limited by the updraft size, the dissipation rate can be calculated using the updraft diameter and the axial velocity fluctuations at the updraft. Based on this approach, Kolmogorov time scale is approximated between 3.06×10^{-4} s and 1.2×10^{-2} s, depending on the swirl ratio. Since the response time of the seeding particles

is 2 to 4 orders of magnitude smaller than the Kolmogorov time scale of the simulated tornado flow, it can be concluded that these particles are sufficiently small to follow the fluid flow accurately [1, 2].

To perform statistical analysis of the flow properties, sample size of PIV recordings needs to be determined. The sample size with 95% confidence interval, can be calculated based on the equation given by Hamburg [3]

$$n = \left(\frac{3\sigma_x}{e}\right)^2 \tag{3.5}$$

where n is the sample size, σ_x is the standard deviation and e is the maximum allowed error (e= ±0.08 m/s) with 99.7% probability. The azimuthally averaged velocity value at a certain radial position (z/r_0=0.35) in the outer region of the vortex flow for S=0.57 was considered to calculate an appropriate sample size. The average of tangential velocity in horizontal plane measurements was 8.74 m/s with the standard deviation of 0.82 m/s. After substituting all the values in the equation, the sample size found to be n=946, i.e. statistical analyses converge for measurement of 946 or higher vector maps. Herein, 4000 images were acquired for each experimental run, resulting in 2000 vector maps.

3.3.2 Experiment plan

The horizontal velocity field (radial and tangential components) measurements were performed for two different speeds of the top fan (resulting in Re_r=6.7×10^4 and 8.4×10^4) and for 8 different vane angles (θ=5˚, 10˚, 15˚, 20˚, 25˚, 30˚, 35˚ and 40˚). These measurements were carried out at the center of the simulator and at 8 different heights above the surface (z=3.5, 4, 4.5, 5, 7, 8, 13.5 and 15 cm). As mentioned before, the swirl ratio in MWD can be set by varying the angle of vanes at the periphery while the flow rate (and consequently the Radial Reynolds number) can be adjusted by changing the top fans speed.

Since the tornado-like vortex was unsteady, capturing the vertical velocity field and performing statistical analysis was not possible. In addition, due to the limited field of

view, it was not possible to cover the whole height of the vortex in one image. As a result, the vertical velocity field was only measured at the updraft region to calculate the flow rate. In a separate test, the rotational speed of the fans was monitored for various swirl ratios and at a constant top fan speed. It was observed that, even for high swirls, the fan performance was not affected by the vane angle and the flow rate was constant. As a result, the vertical velocity field was only measured for the smallest swirl ratio (θ=5˚) to determine the flow rate inside the simulator. The smallest *S* was chosen for this purpose because the most uniform axial velocity profile at the updraft is expected for this swirl ratio.

As shown in Figure 3-4, the laser unit was mounted on a tripod and located outside the chamber. The laser beam was shot through one of the middle fan openings at the periphery of the simulator and was converted to a horizontal (or vertical, depending on the measurement plane) laser sheet using the cylindrical lens located inside the chamber.

Figure 3-5a displays the cylindrical lens with its mount on a base plate. This configuration was used for lower heights. As the laser beam height increased, the optic was also moved using a post with an adjustable height (see Figure 3-5b). The main challenge of directing the laser beam towards the cylindrical lens was reflections from the metallic surface of the vanes at lower elevations and the glass at higher elevations. To prevent these reflections from entering the chamber, a thick black plastic sheet with a very small hole at the center was installed right before the cylindrical lens.

For the case of horizontal plane measurements, the camera was mounted on a traverse system and was positioned on the ground facing upwards (see Figure 3-6). It was ensured that the camera is covering the center of the simulator for all cases. Figure 3-7 shows the complete experiment setup for the horizontal plane measurements.

Figure 3-8 shows the camera setup for the vertical velocity measurements. In this case, the camera was inside the chamber with its axis parallel to the ground and was fixed at a certain elevation and distance from the laser sheet.

A calibration board with uniform grid spacing was used to focus the camera at the plane of measurement, to set the field of view to 23.4 cm by 17.5 cm as well as to calculate the pixel to meter conversion ratio (see Figure 3-9).

Figure 3-4: The laser setup.

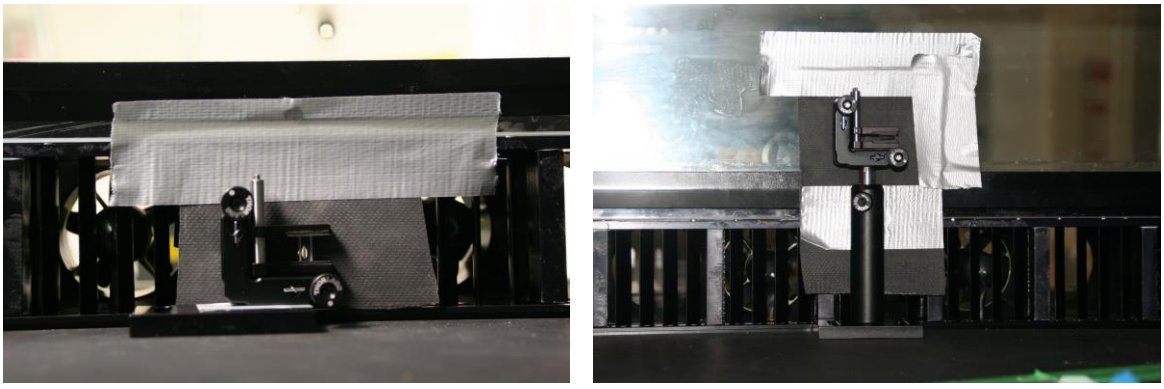

a) **b)**

Figure 3-5: The cylindrical lens configuration inside the chamber at a) lower and b) higher elevations.

Figure 3-6: Camera setup for horizontal plane measurements.

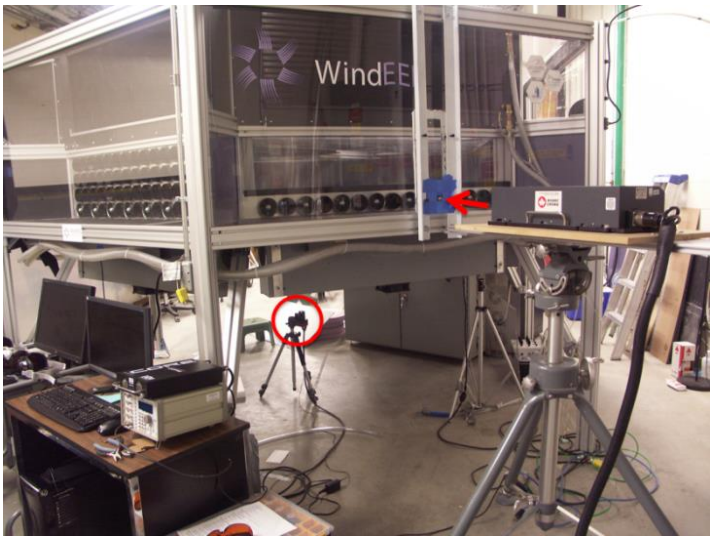

Figure 3-7: PIV setup for horizontal velocity field measurements in MWD.

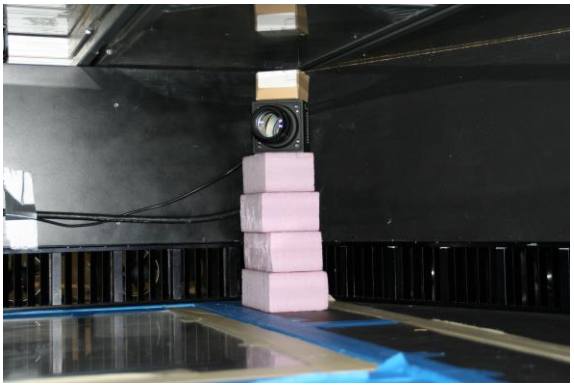

Figure 3-8: Camera setup for vertical plane measurements.

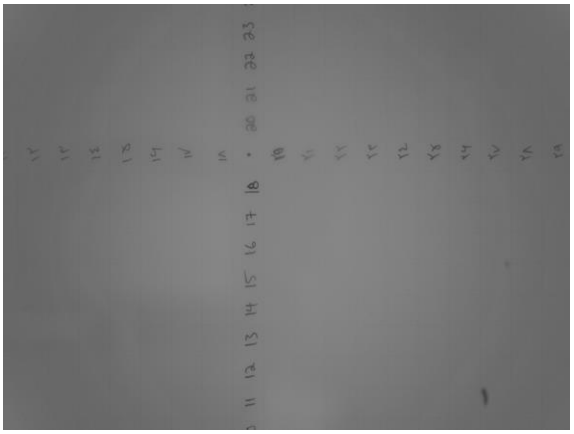

Figure 3-9: Image of the calibration plate used to set the field of view and lens focus and, calculate pixel to meter conversion ratio.

The seed generator was placed outside of the simulator and the seeding particles were guided into the chamber using a plastic tube (Figure 3-10a and Figure 3-10b). The tube was connected to the seed generator outlet at one end and was taped to the simulator ground plate, away from the center of the vortex, at the other end. Depending on the flow speed inside the chamber, the flow rate of the seeding particles was adjusted.

a) **b)**

Figure 3-10: a) seed generator and b) seeder output directed into the chamber.

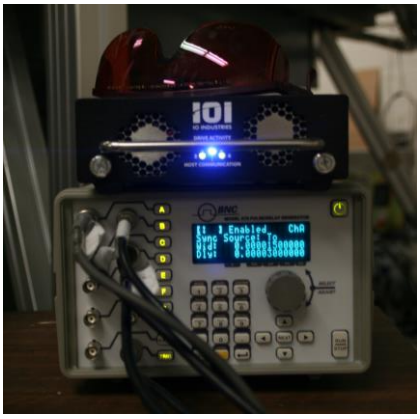

Figure 3-11: Frame grabber (top) and pulse/delay generator (bottom).

The time interval between the two laser pulses was selected based on the mean velocity of the flow and was set using the pulse/delay generator shown in Figure 3-11. These time intervals varied between 100 μs and 550 μs depending on the swirl ratio and the height at which measurements were performed. The adjustments were made to have a particle displacement of 16 pixels or less [4] and peak to noise ratio of 1.5 or higher in all experimental runs. Once all the adjustments and calibrations were performed, 4000 images were captured for each experimental run.

3.3.3 Image processing and data post-processing

Figure 3-12 shows an image pair captured in a horizontal plane 3.5 cm above the ground and for vanes angle of 10˚. The bright strip in these images is due to the reflection inside the chamber. The captured images were processed using the TSI software to extract vector maps. Cross-correlations were performed between interrogation windows (64 by 64 pixels) in the first image and search regions (128 by 128 pixels) in the second image. Using a 50% overlap of interrogation windows, the nominal resolution of the velocity field is increased to 32 by 32 pixels. Spurious vectors were identified and removed using global and local filtering and then replaced by local median vectors. The total number of spurious vectors in each map did not exceed 1% of the total vectors. In the next step, MATLAB (R2008b) was used to analyze the data. Pixel displacements were converted to velocities (m/s) using the calibration ratio (m/pixel) and time interval values (μs). Figure 3-13 displays instantaneous velocity field obtained from the horizontal plane measurement 3.5 cm above the ground and for three vane angles. It is observed that as the vane angle (and consequently the swirl ratio) increases, the vortex core expands. Also, a two-celled vortex is observed at θ=30˚ which implies that the drowned vortex jump has occurred and the flow regime is fully turbulent. This conclusion is further investigated and confirmed through flow visualizations and surface static pressure measurements [5].

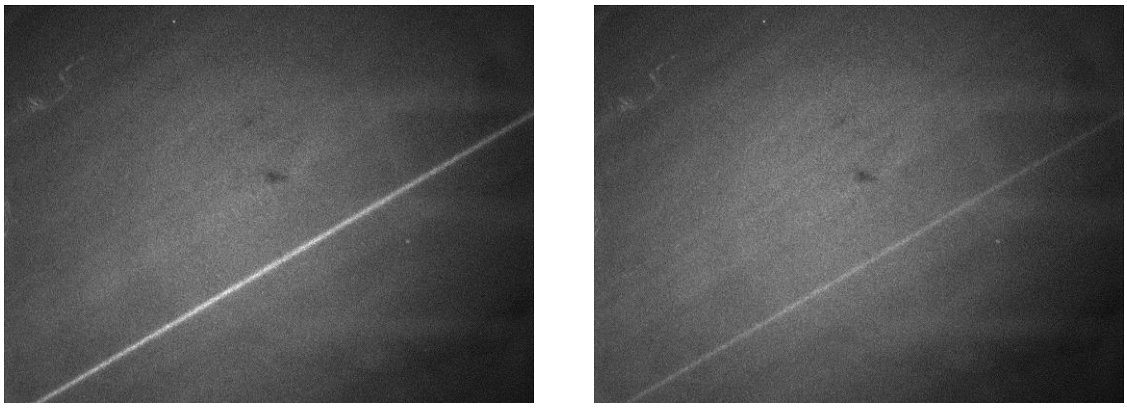

a) **b)**

Figure 3-12: Sample of an image pair captured for θ=10˚ and at z=3.5 cm.

In order to compute the time and azimuthally averaged velocities, the center of the vortex was located in each vector map. In these calculations, it was assumed that the vortex is axisymmetric and therefore there is no velocity variation with azimuth. Assuming that the vortex center is always at the geometric center of the simulator, radial and tangential velocities were averaged over time and azimuth.

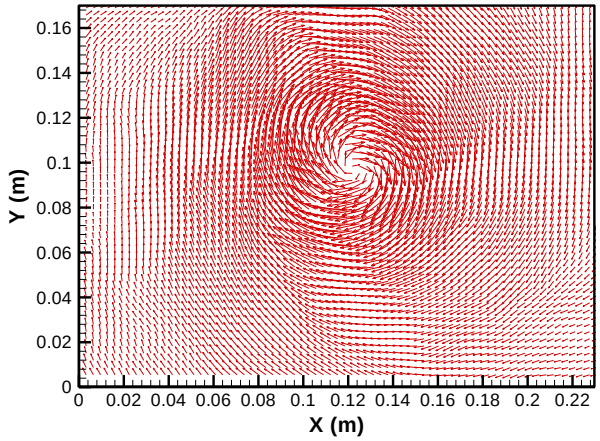

a)

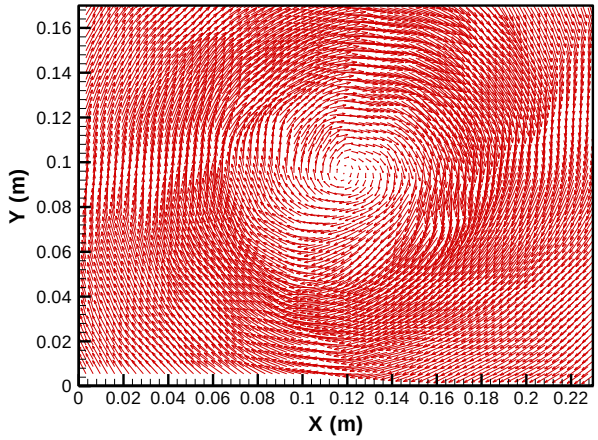

b)

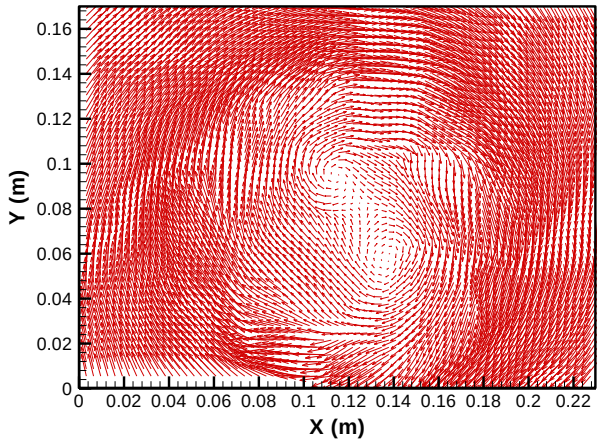

c)

Figure 3-13: Instantaneous horizontal velocity vector maps obtained from PIV measurements at z=3.5 cm for a) θ=10°, b) θ=20° and c) θ=30°.

Detecting the center of the vortex was one of the most challenging parts of the data analysis. There are several methods for identifying the core of a vortex (line-based) as well as the region of a vortex (region-based). In general, the region-based algorithms are easier to apply and computationally less expensive when compared to the line-based methods. In this work a novel approach, proposed by Jiang *et al.* [6] in 2002, was implemented. This point-based algorithm is based on the concept from Sperner's lemma [7]. This method was selected for vortex detection due to its simplicity and efficiency compared to other existing methods. The following steps explain the vortex detection process applied to each vector maps:

1. Direction ranges: equally spaced direction ranges were defined for each vector. Figure 3-14 displays three (A, B, C) and four (A, B, C and D) equally-spaced direction ranges defined for two-dimensional cases.

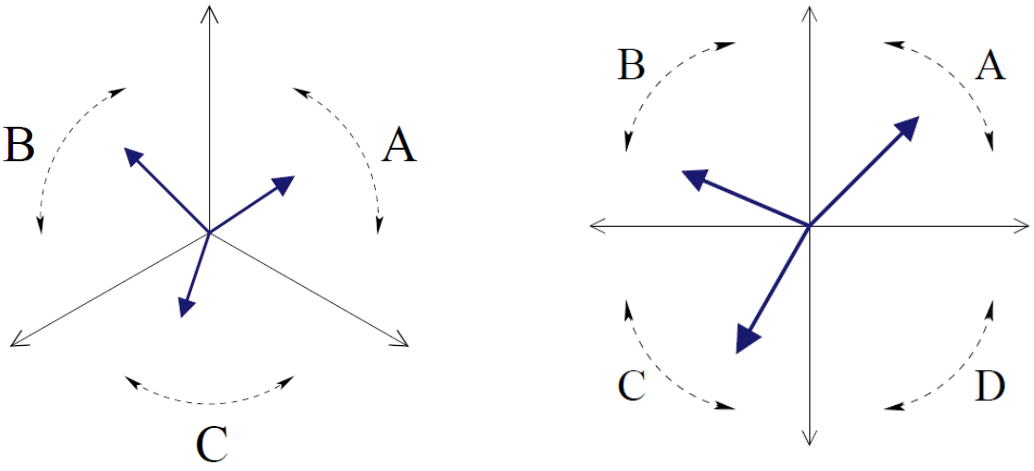

a) **b)**

Figure 3-14: a) three and b) four equally-spaced direction ranges – image from [6].

2. Labeling: using the direction ranges, vectors were labeled based on the direction they point at. This method states that if a fully labeled triangular cell (square cell in case of using four direction ranges) exists, then the direction spanning property is satisfied. The direction spanning property means each vector at the vertex of a cell point is in a unique direction range. Therefore, a grid point which its neighbors satisfy the direction-spanning property is within the core region [6]. Figure 3-15 shows vectors in a 2D grid labeled using three and four direction ranges. It is seen that, for this sample of the vector map, the four direction ranges perform more accurately in detecting the vortex core region. Considering the complexity of the flow in the current work, labeling was done using four direction ranges.
3. Checking grid points: Once labeling was complete, the immediate neighbors of each grid point were checked for direction spanning property. If satisfied, that grid point was identified as being within the core region.

The accuracy of the algorithm was evaluated through visual investigations of vortex center in several vector fields. Note that for two-celled vortex structures, the center of the vortex with stronger circulation was selected as the center of the parent vortex.

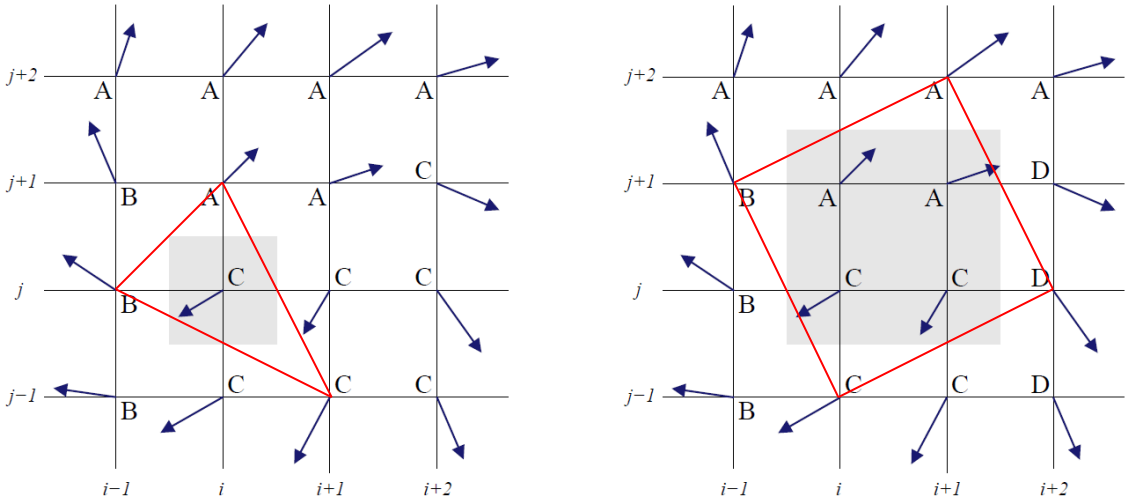

a) **b)**

Figure 3-15: Core region detection for a 2D vortex using a) three and b) four direction ranges – image from [6].

The guidelines provided by Cowen and Monismith [8] and Prasad [9] were followed to determine the uncertainties in velocity measurements using PIV. A maximum error of 7.2% is estimated for velocity measurements in horizontal planes. The uncertainty analysis details can be found in Appendix D.

References

[1] Snyder, W. H., and LumIey, J. L., 1971, "Some Measurements of Particle Velocity Autocorrelation Functions in a Turbulent Flow," J. Fluid Mech., **48**pp. 41-71.

[2] Loth, E., 2000, "Numerical Approaches for Motion of Dispersed Particles, Droplets, and Bubbles," Progress in Energy and Combustion Science, **26**pp. 161-223.

[3] Hamburg, M., 1970, "Statistical analysis for decision making," Harcourt, Brace and World, .

[4] Adrian, R. J., 1991, "Particle-Imaging Techniques for Experimental Fluid Mechanics," Annual Review of Fluid Mechanics, **23**(1) pp. 261-304.

[5] Refan, M., and Hangan, H., 2013, "The Flow Field Characteristics in the Model WindEEE Dome," Unpublished Results.

[6] Jiang, M., Machiraju, R., and Thompson, D., 2002, "A novel approach to vortex core region detection," Joint EUROGRAPHICS - IEEE TCVG Symposium on Visualization, D. Ebert, P. Brunet and I. Navazo, eds. The Eurographics Association, pp. 217-225.

[7] Cohen, D. I. A., 1967, "On the Sperner Lemma," J. Combinatorial Theory, **2**pp. 585-587.

[8] Cowen, E. A., Monismith, S. G., Cowen, E. A., 1997, "A Hybrid Digital Particle Tracking Velocimetry Technique," Experiments in Fluids, **22**(3) pp. 199-211.

[9] Prasad, A. K., Adrian, R. J., Landreth, C. C., 1992, "Effect of Resolution on the Speed and Accuracy of Particle Image Velocimetry Interrogation," Experiments in Fluids, **13**(2-3) pp. 105-116.

Chapter 4

4 Qualitative and quantitative characterization of tornado-like flow fields in a new model scale wind dome

4.1 Introduction

Tornadoes and downbursts are the main manifestations of non-synoptic, local high intensity wind systems (or simply thunderstorm winds).These wind storms are responsible for approx. 65% of the total wind damage to buildings and structures in continental North America. Every year tornadoes kill hundreds of people and leave behind billions of dollars' worth of damage. Characterizing the three-dimensional and transient wind field of tornadoes and then, designing safer homes/structures to resist tornado wind loads have been challenging. Full-scale measurements of tornadic flows using Doppler radars are limited due to safety issues and uncertainties in forecasting. Numerical simulations of tornado flow are performed in micro- and macro-scales. While extremely useful, macro-scale simulations cannot resolve the flow-structure interactions due to their limited spatial-temporal resolution. On the other hand, micro-scale Computational Fluid Dynamics (CFD) methods are unable to implement realistic physics and boundary conditions of the event and are mainly limited to modeling the flow within simulators. Therefore, there is a clear need to conduct properly scaled laboratory simulations which, similar to boundary layer wind tunnel experiments for the case of synoptic winds, have the advantage of controllable conditions and repeatability.

The number of available full-scale measurements is gradually increasing owing to the developing of mobile Doppler radar technology and the improving knowledge of weather forecasting. Researchers have collected Doppler radar data from a significant number of tornadoes in various field projects such as VORTEX1 (1994-1995), ROTATE (1996–2001; 2003–2008; 2012-2013) and VORTEX2 (2009-2010). From the wind engineering point of view, the most restricting factor in full-scale measurements of tornadic flows is that the radar beams can be blocked by obstacles. Therefore, radar data are limited to elevations higher than few tens of meters above the ground while, the tornado structure

near to the ground is of high interest as most residential, industrial and public buildings have elevations of 50 m or less. Currently, a very limited number of full-scale data sets from elevations less than 50 m are made available (e.g. Spencer, SD 1998, Stratford, TX 2003, Happy, TX 2007 and Goshen County (LaGrange), WY 2009).

Numerical simulations of tornado-like flows are increasingly available due to recent advances in computational resources and reduced costs. Lewellen and Sheng [1] evaluated the interaction between the surface and the tornado using Large Eddy Simulations (LES) of turbulent transport for two swirl ratios and found that an increase in the surface roughness reduces swirl flow-like behavior. Natarajan and Hangan [2] extended the study of this interaction to a range of swirl ratios, surface roughness and translation. They showed that increasing roughness has a similar effect as a reduction in the swirl ratio and translation reduces the maximum mean tangential velocity for low swirl whereas it causes a slight increase in the maximum mean tangential velocity for higher swirl.

Wilson and Rotunno [3] studied the dynamics of a laminar columnar vortex using axisymmetric numerical simulations. They demonstrated that viscous effects are limited to a thin layer at the inflow along the surface and at the core along the axis. This outcome allowed for analytical solutions of tornado-like vortices (e.g. Xu and Hangan [4]) with reasonable agreement with experiments and numerical simulations. Lewellen *et al.* [5] performed unsteady, three-dimensional simulations of tornado interaction with surface and found the maximum inflow at lowest elevations. A similar conclusion was reached by Kuai *et al.* [6] who performed CFD simulations of the flow in a model domain representing a laboratory simulator.

Reynolds-averaged Navier-Stokes (RANS) simulations of tornado-like vortices were performed by Hangan and Kim [7] to investigate the flow dynamics as a function of the swirl ratio. An attempt was made to establish a relationship between the swirl ratio and the extensively used Fujita scale. This led to a potential relationship between an F4 tornado and a swirl ratio S=2 tornado-like vortex.

Tornado-like flows were first simulated experimentally in 1969 by Ying and Chang [8]. They designed and built a tornado-like vortex generator and then used the simulator to investigate the velocity field [9, 10]. Later, Ward [11] improved the simulator designed by Chang and introduced the Ward-type Tornado Vortex Chamber (TVC), which turned into a prototype for further experimental investigation of tornadoes. The simple structure of this cylindrical tornado chamber incorporated a rotating mesh screen at the periphery to provide and control the circulation and, a fan at the top to provide the updraft. This configuration resulted in an independent control over the flow rate and the circulation component. Ward added a fine mesh honeycomb right before the exhaust to decouple rotation from the axial flow and to prevent the effects of backflow from downstream. This provided a realistic boundary condition for the simulated vortex.

Church *et al.* [12] used the TVC design concept to develop a tornado simulator at Purdue University. The Purdue simulator had the advantage of independent control over the aspect ratio, in addition to the swirl ratio and the radial Reynolds number, by adjusting the inflow depth and the updraft radius separately. However, they reported that the main flow was influenced by the sharp edge of the updraft hole and an unwanted circulating cell was formed in the upper chamber. The TVC designed and built at Kyoto University [13], consisted of four fans in an annular ring surrounding the inflow region as the source of circulation. However, this configuration resulted in undesirable turbulent vortices. Later, they replaced the fans with a relatively large number of vanes to reduce the vibration due to a rotating device and increase the accuracy of the simulation.

Lund and Snow [14] investigated the velocity field of tornadoes simulated in the second Purdue University TVC using Laser Doppler Velocimetry (LDV). They showed that radial profiles of the measured tangential and radial velocities exhibit similar features to the modified Rankine vortex flow combined with the boundary layer flow. In the second generation of vortex chambers at Purdue University, the rotating wire mesh was replaced with vanes to allow varying inflow angles and an adjustable flow straightener was used in the convection zone.

In 2001, a ward-type simulator was assembled at Texas Tech University (TTU) with an updraft radius of 0.19 m and an inflow height varying between 0.064 m and 0.19 m [15]. This simulator was then modified by Mishra *et al.* [16] with an intention to perform experiments towards wind engineering, rather than the atmospheric science applications. In this simulator, updraft and circulation were provided by means of a blower at the top of the convective chamber and, 16 slotted jets at the inflow, respectively. Mishra *et al.* examined the three-dimensional flow field characteristics and the surface static pressure distribution. They compared the results with full-scale measurement data from Manchester, SD tornado of May 1998 [17] and Spencer, SD tornado of June 2003 [18]. Mishra *et al.* obtained a length scale of 1:3500 for the simulations and demonstrated that the measured surface pressures were in a good agreement with the full-scale data.

Although all the simulators discussed previously are, to some extent, capable of simulating tornadic winds in a laboratory, they all lack the translation feature of a real tornado. In addition, considering the reduced size of the simulators and therefore, their geometric scaling ratio, modeling buildings and structures and measuring the wind-induced loads is not practical.

A more recent tornado simulator was developed at Iowa State University (ISU) by Haan *et al.* [19] to meet two important requirements: first, to accommodate models of reasonable size for measuring loads on structures and buildings and second, to translate along the ground plane for a realistic simulation of a natural tornado. This simulator consisted of a circular duct (5.49 m in diameter) that is suspended from an overhead crane which allows translation along a 10.36 m long ground plane. The updraft is provided by means of a fan located in the center of the duct. The design concept was based on the rotating forced downdraft technique in which the flow from the updraft is directed downward while rotated by means of vanes in an annular duct surrounding the inner region.

An important feature of a tornado-like vortex, namely transition from a laminar core to a turbulent one, is not captured in this simulator. This can be due to the instability of the

vortex. Besides, the tangential component and the total flow rate cannot be controlled separately in this simulator [19].

Hashemi Tari *et al.* [20], for the first time, quantified the turbulent characteristics of a tornado-like vortex. They performed Particle Image Velocimetry (PIV) measurements in a modified version of the ISU simulator for various swirl ratios. Hashemi Tari *et al.* found that by increasing the swirl ratio, mean radial and tangential velocity components as well as normal and shear stresses increase. In addition, they illustrated that the maximum turbulent kinetic energy production corresponds to the vortex touch-down case.

Herein, the design concept of the state-of-the-art wind facility, the Wind Engineering, Energy and Environment (WindEEE) Dome, is described. WindEEE is a three-dimensional wind testing chamber capable of physically simulating 3D and time-dependent high intensity wind systems such as tornadoes and downbursts. In this work, we focus on tornado simulations in the 1/11 scaled model of the WindEEE Dome. The simulated tornado flow field is characterized qualitatively and quantitatively using flow visualization methods, surface pressure tests and PIV. Swirl ratio effects on the velocity field of tornado-like vortices as well as radial Reynolds number dependency of the flow are investigated.

4.2 Experimental Set-up

4.2.1 Wind Engineering, Energy and Environment (WindEEE) Dome concept

WindEEE is a unique large, three-dimensional and time dependent wind testing chamber, or a “Wind Dome”, of 25 m inner diameter and 40 m outer diameter (including the return circuit, see Figure 4-1). By using a system of 100 dynamic fans on the six peripheral walls coupled with 6 larger fans at the ceiling level, WindEEE can produce any type of wind systems including 4 m in diameter translating tornadoes (see Figure 4-2) and downbursts as well as a variety of time dependent shear flows.

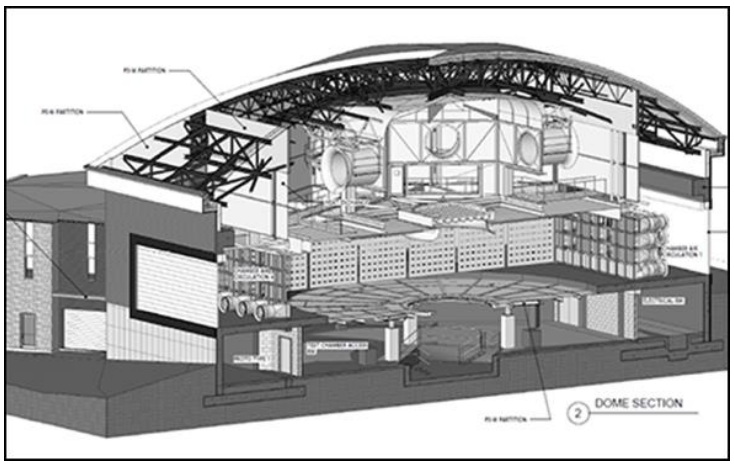

Figure 4-1: Cross-section of WindEEE Dome.

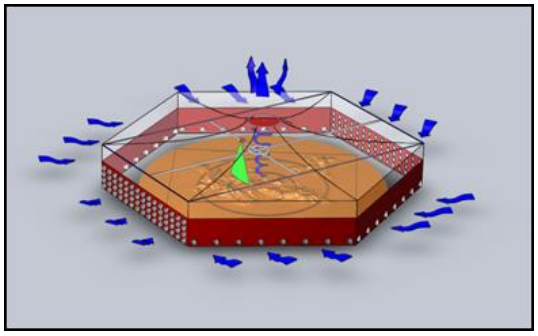

Figure 4-2: Preliminary design concept of tornado flow simulation in WindEEE Dome.

One of the 6 peripheral walls has a matrix of 4 rows x 15 columns fans which, if blowing inside the dome in conjunction with two porous curtains can form a versatile multi-fan wind tunnel. The flow can be varied to produce horizontal or vertical shear and the fans can be actuated at 1 Hz to produce a variety of turbulent flow fields. Also, the fans can be reversed blowing outside the dome on a platform used for full-scale testing of building components, solar panels or wind turbines.

In addition to the 60 fan wall, there are 8 fans at the base of each of the other 5 peripheral walls. Tornadoes are produced by positioning the vanes in front of each of the 6x8=40 lower level peripheral fans at various angles to produce various swirl ratios at the base. At the ceiling level, a bell-mouth connected to the 6 larger fans at the top, creates a

suction outlet. The coupling between the surface swirl and the ceiling suction can produce various types of tornadoes. Using a guillotine system, the bell-mouth and therefore the tornado can be translated at a maximum speed of 2 m/s over a distance of 5 m through the chamber.

The WindEEE dome, passed through conceptual and engineering design phases and construction, has just finished. A 1/11 scaled physical model of the dome, Model WindEEE Dome, reproducing most of the characteristics of the WindEEE Dome was operational since 2010 and has been instrumental to (i) validate the more than 75 CFD preliminary design simulations, (ii) implement the controls for the main operation scenarios and (ii) perform the present tornado simulations.

4.2.2 Model WindEEE Dome

The Model WindEEE Dome (MWD) was designed, constructed and commissioned in 2010 at Western University. It has the same number and distribution of the 100 fans on the peripheral walls as the WindEEE Dome. Instead of using 6 larger fans at the top chamber, the MWD uses an equivalent 6 x 3 = 18 number of fans of the same type as the ones used on the peripheral walls (see Figure 4-3). This facility only replicates the closed-loop modes of the WindEEE Dome while performing identically with the WindEEE Dome in terms of tornado or downburst generation, including their translation. Each fan can be controlled individually and the upper fans are reversible. Adjustable vanes that are installed in front of all lower fans can be used to produce the desired swirl.

While the inflow height is fixed at 0.07 m, the updraft radius is variable between 0.07 m and 0.2 m, resulting in aspect ratios ranging from 0.35 to 1. Experimental investigations of tornado-like vortices performed by Davies-Jones [21] and Church *et al.* [22] suggested that two main flow characteristics, namely the core radius and the swirl ratio of transition, are independent of the aspect ratio. Therefore, a fixed aspect ratio of 0.35 was selected for all experiments performed here.

In the MWD, the flow enters the main lower chamber through the openings at the periphery and exits the chamber at the top through the updraft hole and then recirculates

through the return circuit. To prevent the effect of the fans at the top on the upstream flow, a honeycomb is installed at the entrance of the updraft. This honeycomb also removes any radial and tangential velocity components form the updraft flow to resemble the appropriate downstream boundary condition.

There are two different configurations for generating tornado-like vortices in this simulator: a) using top fans to provide updraft and periphery vanes at the lower chamber to control the swirl; b) running periphery fans at the lower chamber to increase the inflow with vanes to produce the swirl and top fans to provide suction. The preliminary flow visualizations inside the simulator have shown that using any of these arrangements generates tornadoes of different structures; the former configuration generates single-celled and two-celled tornado-like vortices while the latter one results in multi-celled vortex structures. In the current study, tornado-like flows were generated using the first configuration.

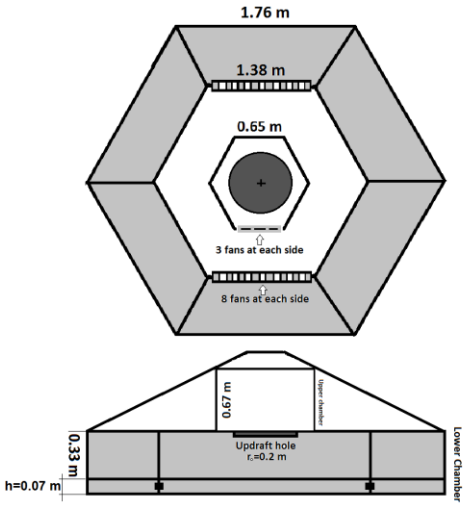

Figure 4-3: Schematic drawing of the MWD.

By starting the top fans, the flow is drawn into the chamber through the inlet at the periphery. The air passes the vanes which input both radial and tangential velocity components. At this moment, the flow contains only vertical vorticity which is carried towards the center. The vertical vorticity is then stretched vertically as approaching the

center of the simulator and initiates the rotating region. As the flow becomes steady-state, the lower surface radial boundary layer develops. At this point, the surface boundary layer provides the vorticity required to sustain the rotation in the core. The horizontal vorticity in the boundary layer is then tilted into the vertical direction by the radial gradient of the axial velocity close to the center and then stretched vertically by the axial gradient of the updraft in the core [12]. This develops the rotational core which extends to the updraft hole.

4.3 Flow parameters

The major dimensionless groups [11, 21-24] identified for TVC's are; the geometric aspect ratio (a), the kinematic swirl ratio (S) and the dynamic radial Reynolds number (Re_r). The aspect ratio is the ratio between the inflow height (h) and the updraft radius (r_0). The likely atmospheric range for the aspect ratio, as mentioned by Church *et al.* [22], is from 0.2 to 1. The radial Reynolds number is defined as $Re_r=Q/2\pi v$, where Q is the volumetric flow rate per unit axial length and v is the kinematic viscosity of the fluid. The radial Reynolds number of a real tornado is generally many orders of magnitude larger than that of simulated tornado-like vortices. However, it was previously shown that for a given geometry and for a smooth surface, above a certain critical value of Re_r, the core radius and the transition from a single vortex to multiple vortices are independent of Re_r and are strongly a function of swirl ratio [11, 21, 22, 25].

The swirl ratio represents the ratio between the rotational energy to the convective energy in the vortex. It is defined as $S= r_0\Gamma/2Qh$, where Γ is the circulation at the rotating screen in TVCs. This non-dimensional parameter is an important controlling factor which characterizes the vortex breakdown and the transition to a turbulent flow and to multiple vortices [21, 26]. Although the swirl ratio remains the most important parameter for the characterization of tornado-like vortices, its definition is based on the simulator configuration and can vary from one simulator to another. As a result, calculating the swirl ratio in a non-TVC tornado simulator using the given equations is not practical. Variation in the swirl ratio definition introduces new challenges in characterizing tornado-like vortices; the swirl ratio corresponding to the transition from a laminar to a

turbulent flow and from one-celled to two-celled vortices varies from one simulation to another. For instance, in calculating the swirl ratio for the ISU simulator the updraft radius was replaced with the radius of maximum tangential velocity and circulation was determined at the core radius [19]. Therefore, the swirl ratio needs to be defined for any simulation and the exact values reported for critical swirl ratios by previous works cannot be directly used for comparison purposes.

4.3.1 Swirl ratio

The swirl ratio in the MWD apparatus can be defined as the ratio between the tangential to radial velocity at the inflow region, $S = (1/2a)V_{tan,i}/V_{rad,i}$. Based on this definition, $V_{tan,i}/V_{rad,i}$ equals to $tan(\theta)$, where θ is the vane angle with respect to the radial direction. The vane angle varies between 0˚ (completely open) and 90˚ (completely closed). However, preliminary tests showed that beyond 40˚, the flow structure was altered and tornado-like vortex characteristics (i.e. Rankine vortex surface pressure distribution and tangential velocity profile) were not observed. Varying the vane angle between 0˚ and 40˚, while providing constant flow rate, results in swirl ratios ranging from 0.12 to 1.2. Alternatively, the swirl ratio can be defined using the overall maximum circulation ($\Gamma_\infty = 2\pi r_{c,max} V_{tan,max}$) at a given flow rate: $S = r_0\Gamma_\infty/2Qh$. where, $V_{tan,max}$ is the overall maximum tangential velocity and $r_{c,max}$ is the radius corresponding $V_{tan,max}$. This approach requires the availability of vector maps of the tangential velocity inside the chamber which were obtained through PIV measurements (see Section 4.5 for PIV results).

Figure 4-4 compares swirl ratio values computed based on the vane angles and the maximum circulation (using PIV results). It is observed that swirl ratios are fairly matched, particularly for vane angles less than 25˚. The swirl ratio equation suggests a linear relationship between the swirl ratio and the maximum circulation providing that the aspect ratio and the flow rate are constant. The swirl ratio variation with the maximum circulation is also displayed in Figure 4-4. The linear trend observed here is in agreement with the expected relation between swirl ratio and circulation for constant flow rate and demonstrates an independent control over the radial Reynolds number and the swirl ratio.

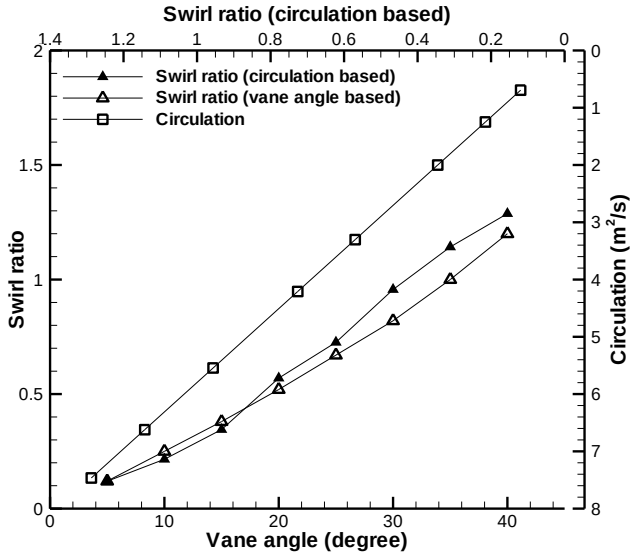

Figure 4-4: Swirl ratio variation with the vane angle as well as circulation as a function of the swirl ratio.

4.3.2 Radial Reynolds number

Since it is not possible to satisfy the radial Reynolds number dynamic similarity between the simulated and the real tornadoes, it is necessary to examine the dependence of the flow characteristics on the radial Reynolds number. Therefore, variations of tangential velocities with swirl ratio were studied for two different radial Reynolds numbers. The flow rate was calculated using the average axial velocity, V_{ax}, at the updraft. The axial velocity was determined by performing PIV measurements on a vertical plane at the updraft hole. The flow rate was also measured at the inlet of the simulator using a rotating vane anemometer. The results were in close agreement with the flow rate calculated based on PIV measurements. Note that this is a preliminary investigation of the Reynolds number effects on the flow characteristics. A more detailed study will be performed in the full-scale WindEEE Dome for a wide range of radial Reynolds number.

In order to examine the effect of the vane angle on the upper fan performance, the rotational speed of the fans was monitored for various vane angles. It was observed that,

even for high swirls, the fan performance was not affected by the vane angle and the flow rate was constant. As a result, the flow rate and the swirl component can be controlled independently in the MWD simulator similar to previous TVC experiments [12, 15]. This allows for validation and direct comparison of various tornado-like vortex characteristics between the present MWD and former TVC's.

Figure 4-5 displays time and azimuthally averaged tangential velocities (herein after called tangential velocities) 5 cm above the ground as a function of radius. Results are presented for various swirl ratios and for two different radial Reynolds numbers. The tangential velocity and the radius were normalized by the average axial velocity at the updraft and the updraft radius, respectively. It is observed that by increasing the flow rate in the simulator, the maximum tangential velocity increases slightly. However, the core radius is not affected by the change in the radial Reynolds number. This observation is supported by the experimental findings of Ward [11] and numerical simulations of Rotunno [26, 27]. Moreover, as suggested by Ward [11] and Davies-Jones [21] and observed in this study, the core radius size is mainly a function of the swirl ratio.

Normalized tangential velocities at S=0.35 and z=5 cm are compared in Figure 4-6 for the two radial Reynolds numbers. The maximum tangential velocity and the correspond radius were used to normalize tangential velocities and radial distance from the center, respectively. This figure shows again that the flow characteristics are insensitive to the radial Reynolds number as the tangential velocities match very well and show similar trend over the radial distance. Since the core size showed no dependence on the radial Reynolds number and normalized tangential velocities followed a closely similar trend for both radial Reynolds number, it can be concluded that for Re_r=6.7×10^4 and higher the flow has passed a certain critical turbulent state and therefore, the radial Reynolds number non-similarity would not significantly alter the experimental results. Similar results were observed for other heights and swirl ratios (not shown here).

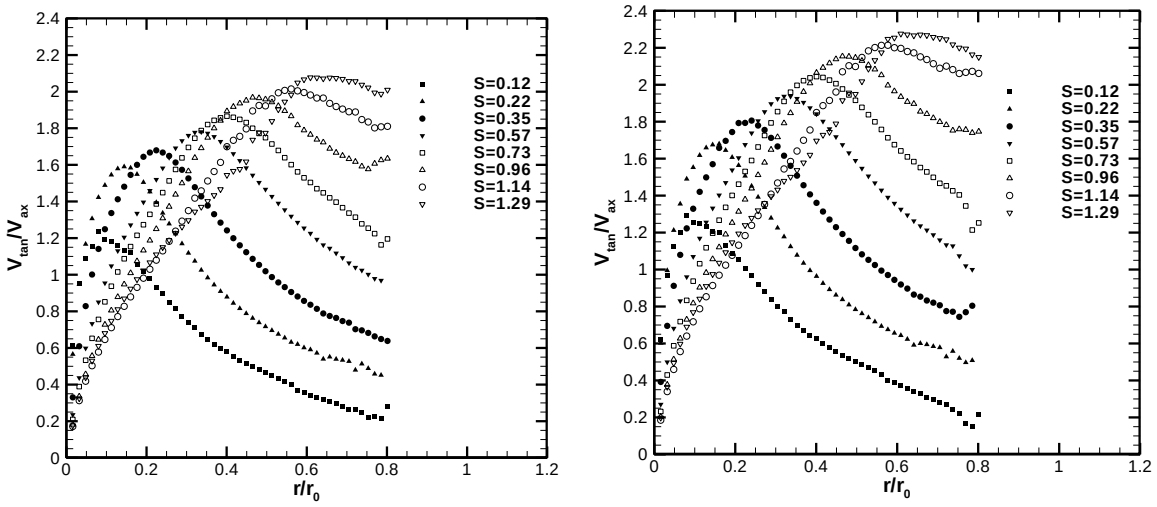

Figure 4-5: Radial profiles of the tangential velocity normalized with the axial velocity for various swirl ratios at *z*= 5 cm: a) $Re_r=6.7\times10^4$ and b) $Re_r=8.4\times10^4$.

4.3.3 Self-similarity

Tangential velocity profiles obtained from horizontal plane measurements 5 cm above the ground are plotted in Figure 4-7 for a wide range of swirl ratios and for two radial Reynolds numbers. For a given swirl ratio, results were normalized using the maximum tangential velocity and the corresponding radius (r_c). Except for S=0.12, the results tend to collapse on one graph. At S=0.12, the flow is laminar, unstable and its characteristics are mainly dominated by the wandering effects. This normalization leads towards the collapse of the rest of the radial profiles of the tangential velocity on one curve independent of swirl ratio and radial Reynolds number. This result indicates self-similarity and therefore, the scalability of the flow which is of crucial importance for simulating tornado vortices of various scales. It also suggests the potential of defining simple and robust models for tornado-like vortices.

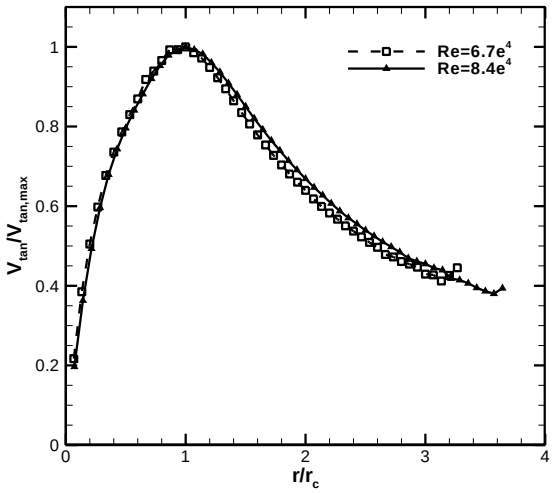

Figure 4-6: Comparison between normalized tangential velocities vs. radius for two radial Reynolds number. Data obtained for *S*=0.35 and at *z*= 5 cm.

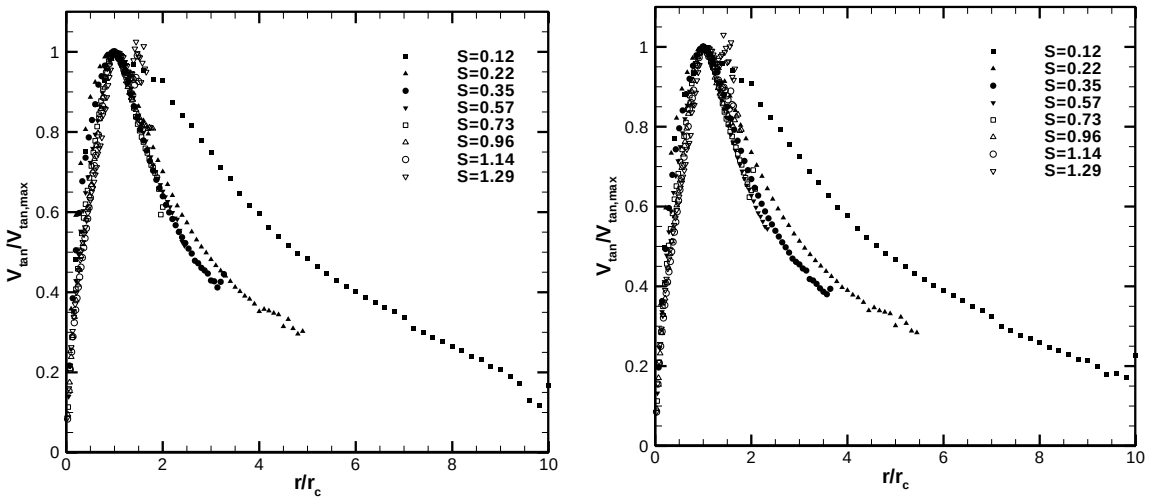

Figure 4-7: Normalized tangential velocities vs. radius for various swirl ratios at z= 5 cm: a) $Re_r=6.7\times10^4$ and b) $Re_r=8.4\times10^4$.

4.4 Measurement techniques

The tornado-like vortex flow field has been interrogated using flow visualization techniques, surface pressure measurements and Particle Image Velocimetry (PIV). Dry ice and helium bubbles were used for flow visualizations. The surface pressure

measurements employed several pressure taps at the surface and PIV measurements were performed at 8 horizontal planes above the surface and for two different flow rates. All experiments were carried out at 8 different vane angles ranging from 5˚ to 40˚, with 5˚ increments.

4.4.1 Flow visualizations

Flow visualizations were performed using dry ice and helium bubbles to obtain qualitative information on the structure of tornado-like vortices. These experiments were performed at a constant flow rate and variable vane angles to control the circulation. In order to fill the chamber with smoke, dry ice cubes were mixed with water and the resulting smoke was guided into the chamber through a hole on the ground plate at the center of the simulator. Alternatively, helium bubbles were used for visualization. The helium bubble generator produces neutrally buoyant, helium-filled bubbles of controlled size for visualizing complex airflow patterns. These bubbles are extremely durable and can be used to trace airflow patterns at speeds from 0 to 60 m/s. Two plastic tubes were used to transfer the helium bubbles from the generator to the simulator. The bubbles were fed into the chamber from one side far from the center of the simulator in order to minimize any disturbance in the flow structure.

Figure 4-8 displays images of the flow in MWD, visualized using dry ice (in column (i)) and helium bubbles (in column (ii)), at different swirl ratios and at $Re_r=6.7\times10^4$. The present visualizations are compared with previously simulated vortices in TVCs [11, 22] shown in column (iii). It is observed that the general flow pattern in MWD is in a very good agreement with the ones from TVCs.

For a low swirl ratio ($S=0.12$), the vortex core is laminar and extends upward from the ground panel to the updraft hole (Figure 4-8a). The core size variation with height is very small and the maximum updraft is observed at the central axis of the vortex. This is the so-called single-celled vortex. By increasing the swirl ratio, the flow structure changes (Figure 4-8b); the core abruptly broadens at higher elevations and becomes turbulent. This sudden increase in the rate of radial spread with height is known to be due to the

vortex breakdown which is the general characteristic of a quasi-cylindrical vortex core [28]. It is known that at this point [28], the vortex core develops an adverse axial pressure gradient which reduces the axial velocity at the centerline and shifts the location of the maximum axial velocity from the centerline to an annular ring surrounding the centerline.

Figure 4-8, illustrates the vortex breakdown as it occurs in MWD for swirl ratios ranging from 0.35 to 0.57. The breakdown bubble is further downstream in Figure 4-8b (ii). As the swirl ratio increases, the breakdown bubble moves toward the surface, as shown in Figure 4-8b (i), while radial spread of the core increases with height. The development of the free stagnation point towards the surface continues until it touches the ground at around $S \approx 0.57$ and the flow becomes fully turbulent. At this point, down-flow penetrates to the surface and two intertwined helical vortices and then a two-celled vortex ($S \geq 0.96$) forms (see Figure 4-8c and Figure 4-8d).

Figure 4-9 demonstrates the converging surface flow visualized using dry ice for a) a single-celled and b) a two-celled tornado-like vortex. The images were taken looking upwards through the chamber floor glass window. Smoke traces showed that these two vortices rotate around their own axis as well as the axis of the parent cell. Besides, the radial outward flow observed near the centerline is in good agreement with previous observations of Ward [11].

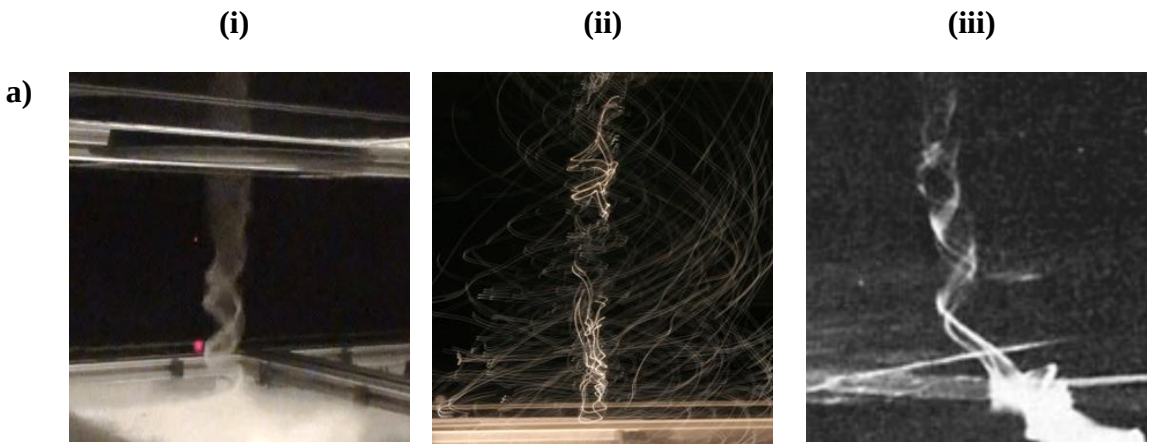

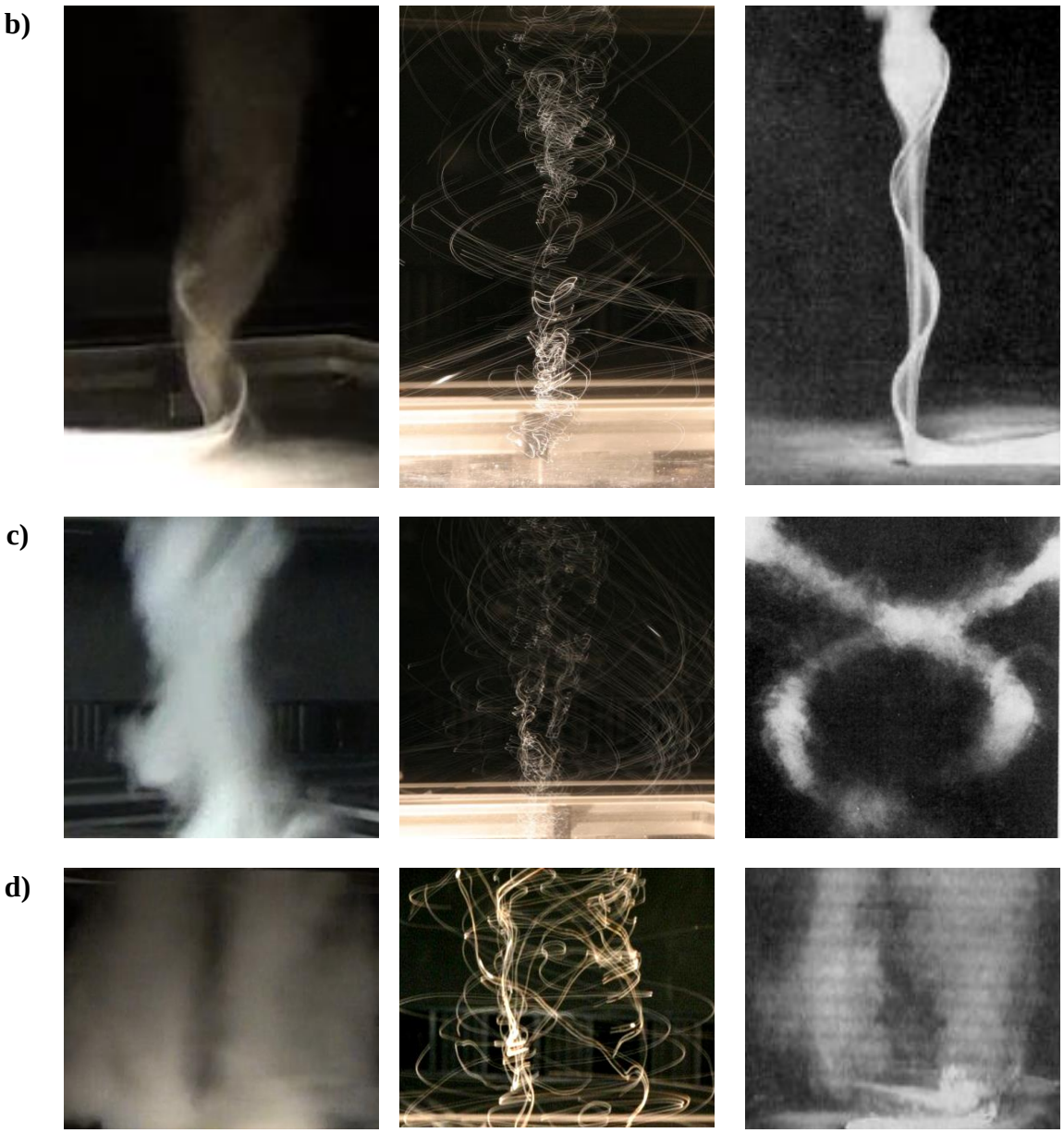

Figure 4-8: Tornado-like vortex produced in MWD and compared with previous works in TVCs: a) laminar core, *S*=0.12, b) vortex breakdown and touch-down, *S*=0.35-0.57, c) intertwined helical vortices, *S*=0.57-0.96 and d) two-celled vortex, *S*=0.96-1.29. (i) dry ice, MWD, (ii) helium bubbles, MWD and (iii) smoke, TVCs. Figures a(iii) [22] b(iii) [11] c(iii) [22] d(iii) [11] ©American Meteorological Society. Used with permission.

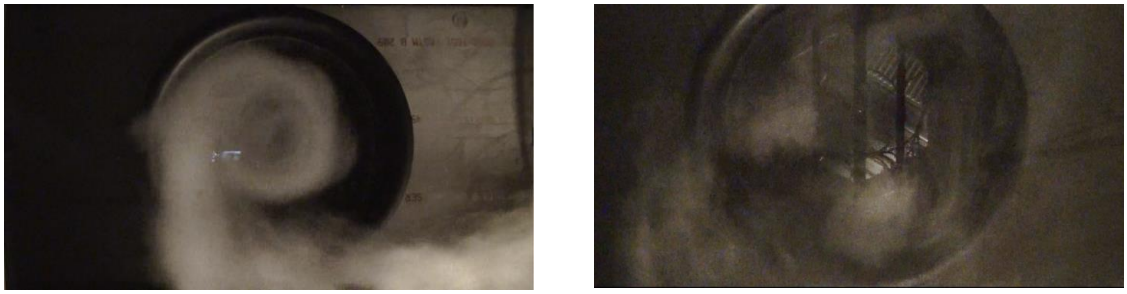

a) **b)**

Figure 4-9: Converging flow close to the surface visualized using dry ice; a) single-celled and b) two-celled tornado-like vortex.

4.4.2 Surface pressure

The pressure deficit is an important factor that distinguishes tornadoes from straight, boundary layer wind impacts on structures. The surface static pressure deficit of the simulated tornado-like vortex and its variation with the swirl ratio was investigated. Figure 4-10 presents radial profiles of the time and azimuthally averaged pressure deficits (ΔP) normalized with $1/2\rho V_{ax}^2$, for various swirl ratios at Re_r=6.7×10^4. Note that the radial Reynolds number of the pressure tests is less than the one chosen for PIV measurements. However, as discussed before, it is expected that for $Re_r \geq 6.7\times10^4$ the flow behaves independent of the radial Reynolds number.

For small swirls, the radius at which the minimum surface pressure occurs is not at the geometric center of the simulator. This offset is the result of the wandering characteristics of the vortex. By increasing the swirl ratio, the wandering effect decreases as a result of the transition from a laminar to a turbulent flow and the minimum pressure deficit location moves toward the center (r=0) at S=0.57.

The higher variation in the central pressure deficit at lower swirl ratios is attributed to the one-celled characteristics of the flow. A one-celled vortex is characterized by an axial upflow in the centerline region and increasing the swirl ratio, increases the axial velocity significantly. Therefore, central pressure deficit values increase.

Experimental results are compared with the surface pressure deficit suggested by the modified Rankine vortex model which is defined as $[P(r)-P(\infty)] = -\rho\Gamma_{\infty}^{2}/2\pi^{2}(r_c^{2}+r^{2})$. where ρ is the fluid density, r is the radial distance from the center of the vortex, r_c is the core radius of the vortex and $P(r)$ and $P(\infty)$ are static pressures at radius r and the atmospheric static pressure, respectively. The parameters in the modified Rankine equation were determined using PIV results. The overall maximum tangential velocity and the corresponding radius over all heights at a given swirl ratio were selected for this calculation. As shown in Figure 4-10, a better match is achieved at radial locations away from the center. Also, the analytical model estimation improves as the swirl ratio increases with the exception of S=0.96 which may be due to the transition of the flow from a single- to two-celled vortex at this swirl ratio.

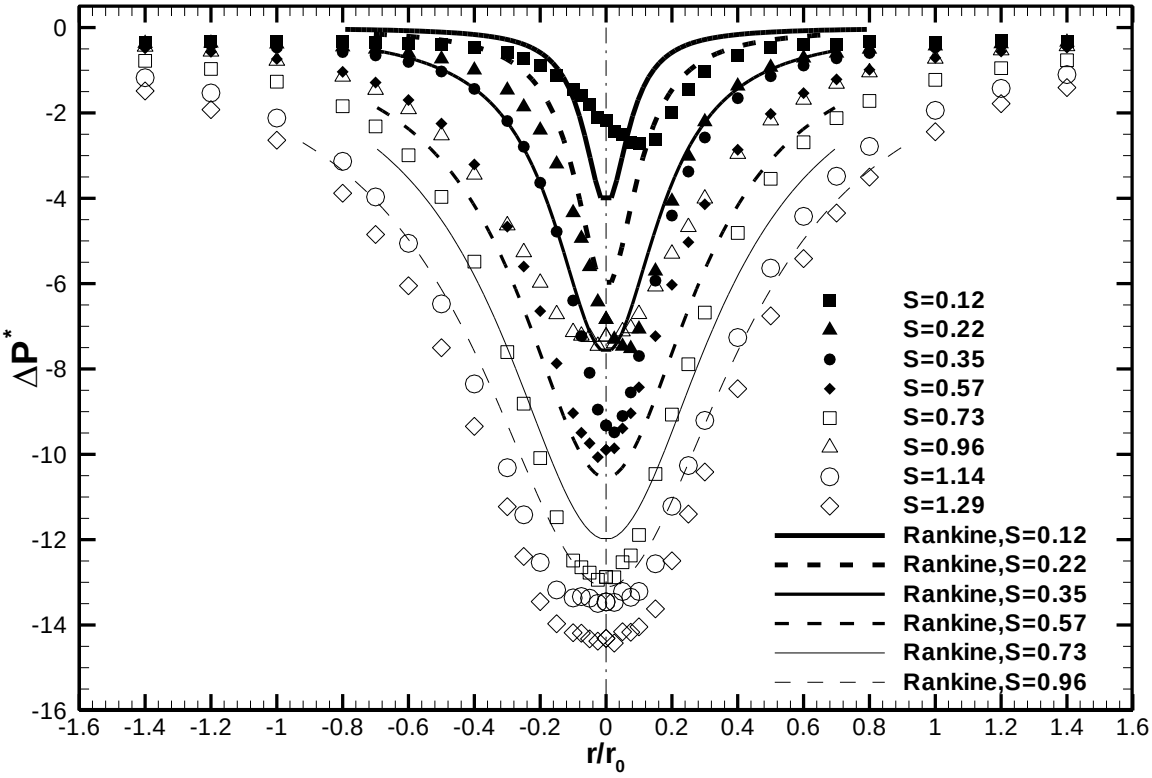

Figure 4-10: Surface static pressure deficits, averaged over time and azimuth for various swirl ratios at Re_r=6.7×10^4.

Figure 4-11 displays instantaneous maximum surface pressure deficits (square symbols) as well as time-averaged surface pressure deficits (circle symbols) at the radius corresponding the instantaneous maximum deficit. Results are normalized by $1/2\rho V_{ax}^2$ and are presented as a function of swirl ratio. There is a significant difference between the time-dependent and the time-averaged values. When compared to the pressure coefficients measured in the straight flows, the peak pressure deficits are larger by at least an order of magnitude. However, direct comparison should be avoided as it is known that increasing the surface roughness reduces the surface pressures substantially [29]. The trend observed in Figure 4-11 for the instantaneous pressure deficit variation with swirl ratio is very similar to the one reported by Pauley *et al.* [30] and recently by Natarajan and Hangan [2]. For $S<0.73$, constant increase in the pressure deficit is observed which is due to the intensification of the one-celled vortex as the swirl ratio increases. The largest pressure deficit is achieved at $S=0.73$ in the current experiments which, as explained by Snow *et al.* [31] and Pauley *et al.* [30], corresponds to the vortex breakdown penetration to the surface. For $0.73 \leq S \leq 0.96$, the turbulent vortex core expands rapidly and as a result, a reduction in the pressure deficit is observed. Flow visualizations suggested that at $S \approx 0.96$ or higher, the transition from a single turbulent vortex to a pair of vortices occurs. This transition is represented in Figure 4-11 as an increase in the surface pressure deficit which is consistent with the previous findings of Pauley *et al.* [30] and Natarajan and Hangan [2]. At this point, the minimum pressure is mainly associated with subvortices and is not located at the geometric center of the simulator (or, in other words, at the center of the parent vortex).

To further investigate the surface flow and confirm the existence of subvortices, instantaneous pressure deficits at various swirl ratios are plotted in Figure 4-12. The entire vortex evolution from a laminar single-celled structure with the maximum pressure deficit at the center to a two-celled set-up with localized peak pressure deficits at the centers of the subvortices is clearly observed in Figure 4-12. As the swirl ratio increases from 0.35 to 0.57, the vortex core broadens and the flow demonstrates axisymmetric characteristics. At this point, the minimum pressure is achieved at the central region of the flow. By further increasing the swirl ratio to 0.73, the flow develops asymmetric

characteristics and the minimum pressures move away from the center. Two local maximum pressure deficits confirm the presence of two sub-vortex in the flow. As the swirl increases to 1.29, the subvortices separate further and the core widens. Note that these subvortices are very unstable and constantly change size and relocate on the surface. Further investigations are required to identify any pattern in the structure and movement of the subvortices.

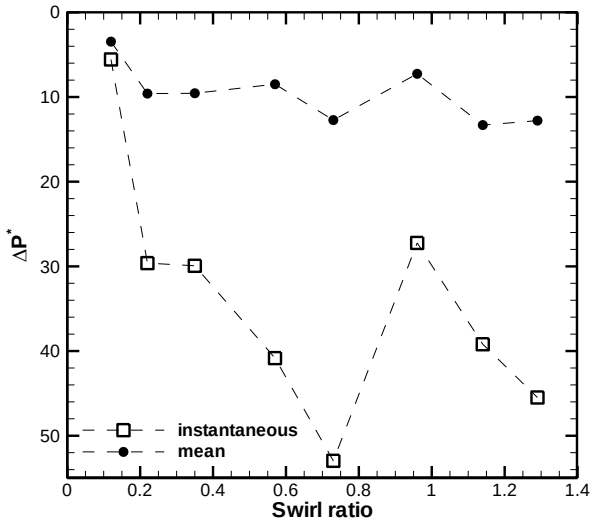

Figure 4-11: Time-dependent (square symbols) and time-averaged maximum surface pressure deficits as a function of swirl ratio for Re_r=6.7×10^4.

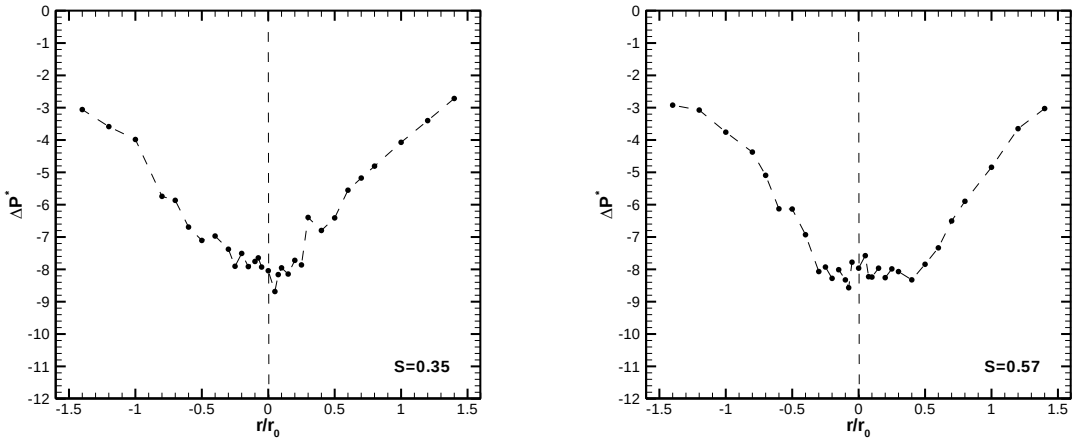

a) **b)**

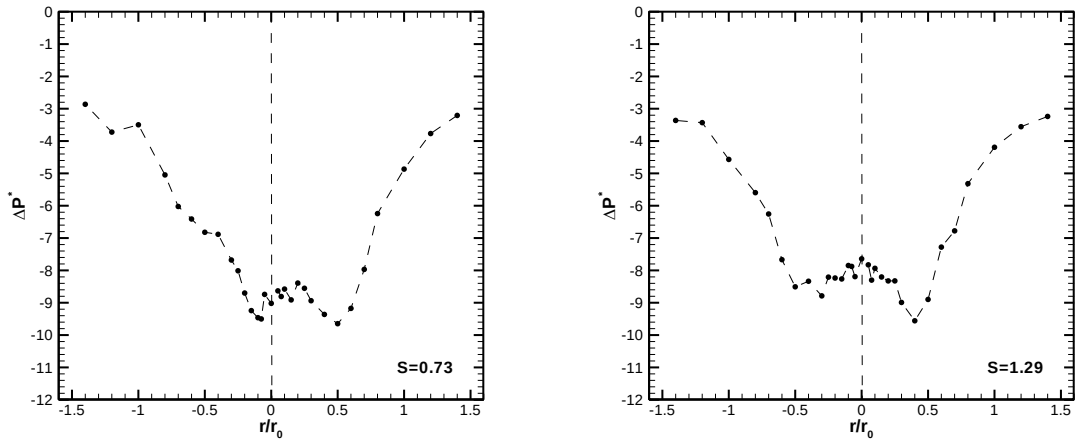

c) **d)**

Figure 4-12: Instantaneous pressure deficits over the surface as a function of radius for a) *S*=0.35, b) *S*=0.57, c) *S*=0.73 and d) *S*=1.29.

4.4.3 Particle Image Velocimetry (PIV)

A 120 mJ/pulse Nd:YAG laser along with a CCD camera with a spatial resolution of 2336 × 1752 pixels were used to perform PIV measurements. The camera was connected to a frame grabber that acquires 8-bit images. Using a calibration board, the field of view of the camera was set to 23.4 cm by 17.5 cm and pixel to meter conversion ratio was determined. A four-channel digital delay generator was used to control the timing of the laser light pulses. For each experimental run, 4000 images were acquired at a rate of 30 Hz resulting in 15 vector maps per second. A cylindrical lens was used to obtain a light sheet with a uniform thickness of 2 mm. The tornado chamber was seeded with Di-Ethyl-Hexyl-Sebacate (C26H50O4) particles, with an average diameter of 1 μm. These particles have a response time of 2.55×10^{-6} s which is 2 to 4 orders of magnitude smaller than Kolmogorov time scale of the simulated tornado (Kolmogorov time scale varies between 3.06×10^{-4} s and 1.2×10^{-2} s, depending on the swirl ratio). Therefore, these particles are sufficiently small to follow the fluid motion accurately and not alter the fluid properties or flow characteristics. The horizontal velocity field (radial and tangential

components) was measured at the center of the simulator and at 8 different swirl ratios and heights. The vertical velocity field (axial-radial) was only investigated at the updraft region to calculate the flow rate. The time interval between the two laser pulses was selected based on the mean velocity of the flow. These time intervals varied between 100 μs and 550 μs depending on the swirl ratio and the height at which measurements were performed. The adjustments were made to have a peak to noise ratio of 1.5 or higher in all experimental runs.

The captured images were processed using TSI software to extract vector maps. This software performs cross-correlations between interrogation windows in the first image and search windows in the second image. The interrogation windows were set to 64 by 64 pixels with 50% overlap, while the search regions were double in size. The same software was used for post-processing of the data. Spurious vectors were identified and removed using global and local filtering and then replaced by interpolated vectors. The total number of spurious vectors in each map did not exceed 1% of the total vectors. The velocity measurement errors were calculated for horizontal velocity fields and the maximum error was estimated to be 7.2%.

The spatial resolution of PIV measurements is determined by the interrogation window and is 3.2 mm. This resolution is 1 to 2 orders of magnitude larger than the Kolmogorov length scale which is ranging from 4.35×10^{-1} mm to 6.93×10^{-2} mm, depending on the swirl ratio. As a result, no attempt was presently made to resolve the smallest scales of the tornado-like flow.

4.5 Flow field

4.5.1 Tangential velocity profiles

Figure 4-13 displays radial profiles of tangential velocities for different swirl ratios at eight heights above the surface. Tangential velocities were averaged over azimuth and time. For a given swirl ratio, tangential velocities and radii were normalized by the maximum tangential velocity and the core radius corresponding to each height, respectively. As the swirl ratio increases, a smaller portion of the outer core region is

captured by the PIV measurements. This is due to the expanded core radius and the limited field of view of the camera.

Results are compared to the modified Rankine vortex model which is defined as $V_{tan}=r\Gamma_\infty/(r_c^2+r^2)\pi$. For a given swirl ratio, the overall maximum tangential velocity and the corresponding radius were used to calculate the tangential velocity estimated by the modified Rankine vortex. For S=0.12 and 0.22, before the vortex touch-down, most of the experimental results and the analytical model match fairly well with the exception of the data for S=0.22 and at z/r_0=0.4. This is probably due to an aloft vortex break-down around that level. For $S\geq$0.35 a clear dependency of the experimental values with height is observed initially in the outer, irrotational region and after touch-down in the core region as well. Also, most probably due to the increased surface friction at and after touch-down, the Rankine model shows agreement with only the upper level measurements. As explained by Snow [32], idealized profiles such as Rankine vortex model are most applicable above the surface layer, where radial velocities are relatively weak.

4.5.2 Radial velocity profiles

The azimuthally and time averaged radial velocities are shown in Figure 4-14 as a function of height for four swirl ratios and at four radial locations. The first radial location, r/r_0=0.048, resides inside the core region of the tornado-like vortex and the rest, r/r_0=0.125, r/r_0=0.6 and r/r_0=0.7, reside outside the core flow. Radial velocities are normalized by the average axial velocity, V_{ax}, at the updraft hole and a negative value of radial velocity represents a converging inflow.

The radial velocity values decrease as the flow approaches the centerline with the minimum velocity observed close to the center of the vortex. This trend is an immediate result of the radial velocity turning into the axial velocity in the core region and is in good agreement with previous observations by Hangan and Kim [7], Hashemi Tari *et al.* [20] and Zhang and Sarkar [33]. In addition, the radial velocity values close to the surface rise with increasing the swirl. This is attributed to the intensified tangential velocities

close to the ground. Except for S=0.12, the maximum radial velocity is observed at heights very close to the ground. For very low swirls, a laminar core develops at mid-heights above a ring-like separation zone around the center which prevents the radial converging flow reaching the centerline. Therefore, radial velocities are higher far from the surface. With an increase in the swirl ratio, the radial boundary layer thickness reduces and the height corresponding to the maximum radial velocity moves towards the surface. The variation of the radial velocity with height is more pronounced for flows with high swirl ratios which can be explained by the flow regime being fully turbulent for S≈0.57 or higher. Hashemi Tari *et al.* [20] reported discrepancies in the trend of radial velocity profiles obtained through the vertical and the horizontal planes. They concluded that the difference is due to the out of the horizontal plane motion close to the surface where axial velocities are dominant. The present trend of radial velocity profiles matches the ones resulting from the vertical plane measurements reported by Hashemi Tari *et al.*

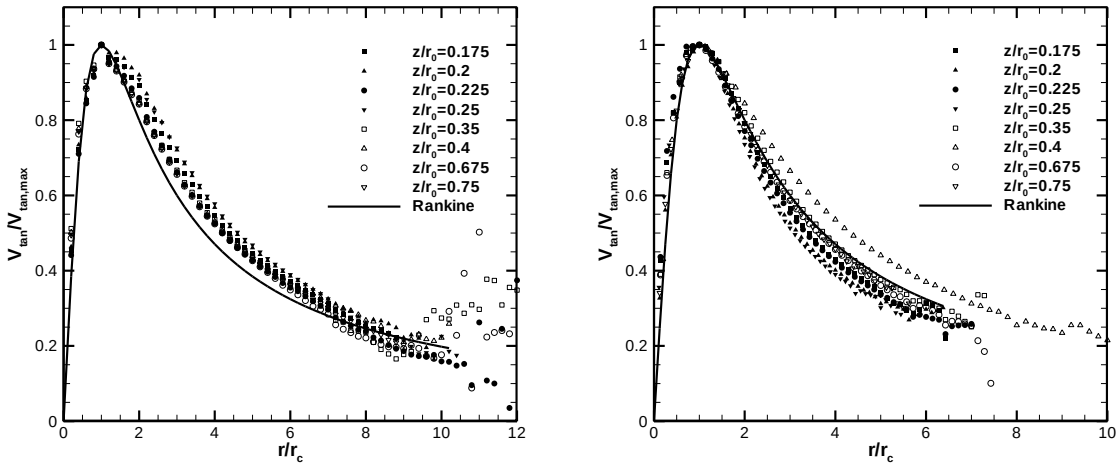

a) **b)**

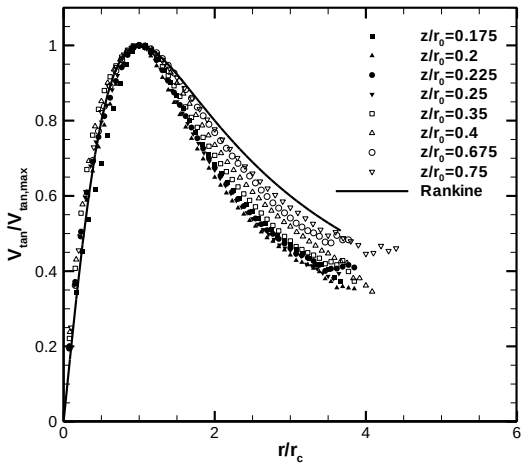
z/r0=0.175
z/r0=0.2
z/r0=0.225
z/r0=0.25
z/r0=0.35
z/r0=0.4
z/r0=0.675
z/r0=0.75
Rankine
Vtan/Vtan,max
r/rc

c)

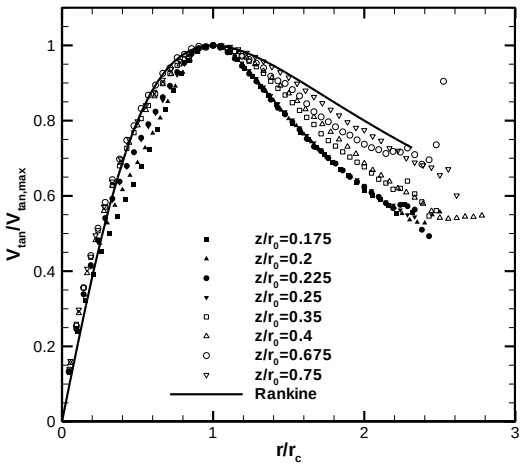
z/r0=0.175
z/r0=0.2
z/r0=0.225
z/r0=0.25
z/r0=0.35
z/r0=0.4
z/r0=0.675
z/r0=0.75
Rankine
Vtan/Vtan,max
r/rc

d)

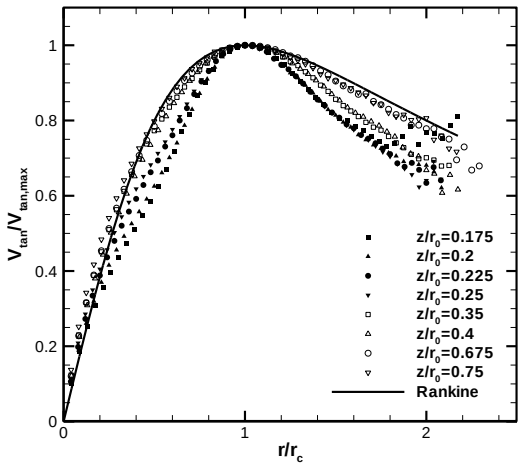
z/r0=0.175
z/r0=0.2
z/r0=0.225
z/r0=0.25
z/r0=0.35
z/r0=0.4
z/r0=0.675
z/r0=0.75
Rankine
Vtan/Vtan,max
r/rc

e)

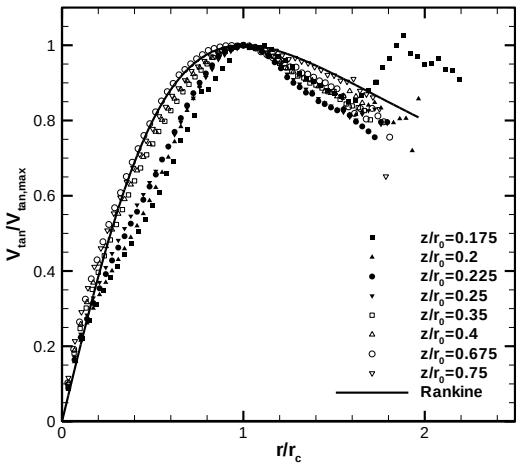
z/r0=0.175
z/r0=0.2
z/r0=0.225
z/r0=0.25
z/r0=0.35
z/r0=0.4
z/r0=0.675
z/r0=0.75
Rankine
Vtan/Vtan,max
r/rc

f)

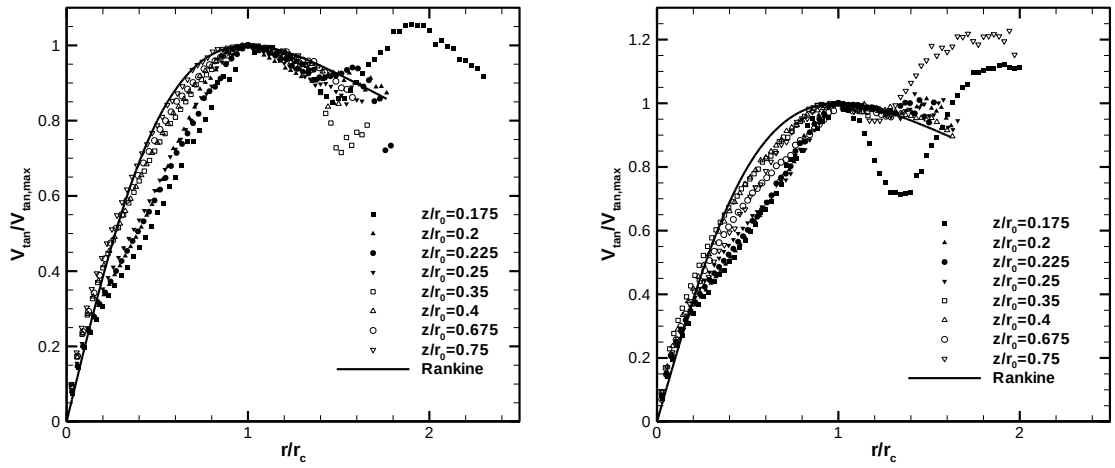

g) **h)**

Figure 4-13: Radial profiles of the normalized tangential velocity at various heights and for a) *S*=0.12, b) *S*=0.22, c) *S*=0.35, d) *S*=0.57, e) *S*=0.73, f) *S*=0.96, g) *S*=1.14 and h) *S*=1.29.

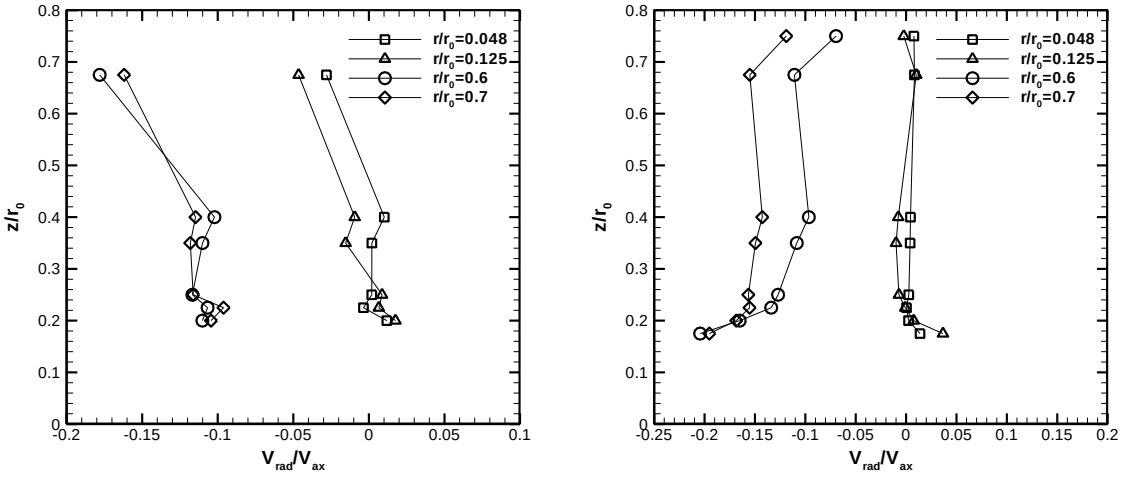

a) **b)**

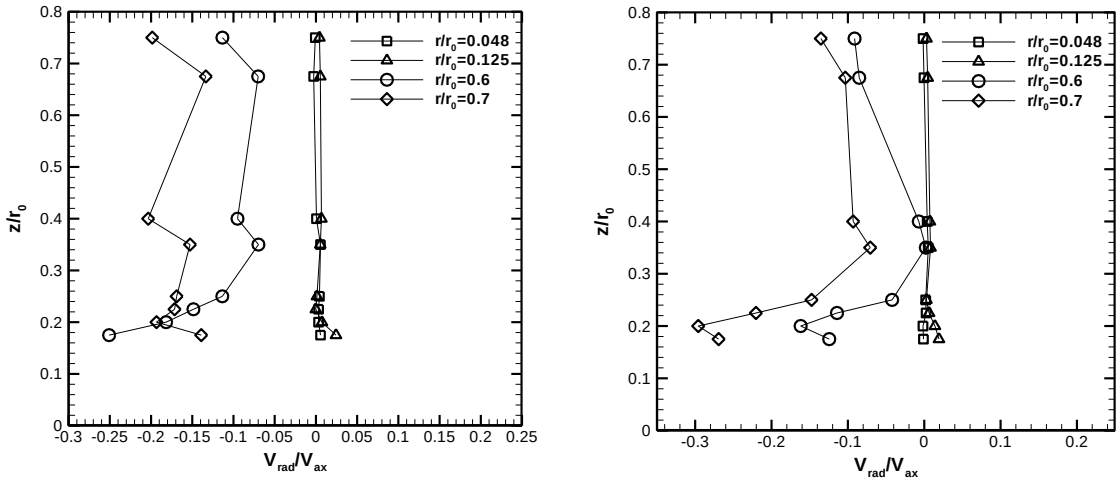

Figure 4-14: Vertical profile of the normalized radial velocity at four radial locations and for a) *S*=0.12, b) *S*=0.35, c) *S*=0.73 and d) *S*=1.14.

4.5.3 Vertical structure of the core region

The core radius was determined at each horizontal plane and its dependence on the swirl ratio is examined in Figure 4-15. As the swirl ratio increases, the core region of the tornado-like vortex grows. For a very small swirl ratio, the size of the core is only growing very slowly with height. By increasing the swirl ratio, the variation of the core radius with height is noticeable. For S=0.22, the core has a conical shape further aloft which corresponds to a vortex breakdown. In addition, a local maximum in the core size is detected at low elevations. After the vortex breaks down, it moves upstream and appears as a bulge in the flow as seen for $0.35 \leq S \leq 0.57$. The bulge develops at mid-heights and grows as the swirl ratio increases. This bulge reaches its maximum size at S=0.57 and the local maximum moves upstream until the touch-down occurs. For swirl ratios higher than 0.57, a broad core region is observed.

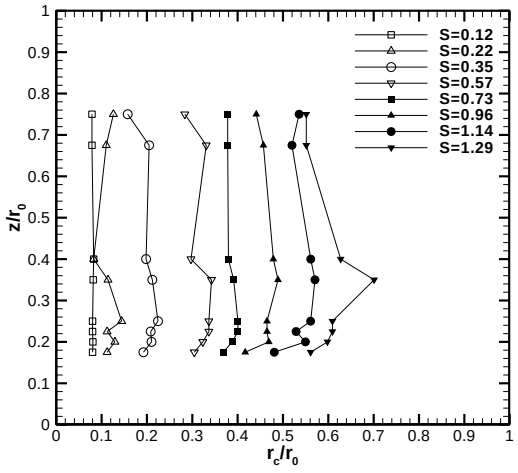

Figure 4-15: Vertical profile of the core radius for various swirl ratios.

Figure 4-16 presents maximum tangential velocities at each height for eight different swirl ratios. With the exception of low swirl (before the touch-down) the maximum tangential velocity is observed at heights very close to the ground. The position of the maximum tangential velocity close to the surface (ground) for tornadic flows is very different from a monotonic boundary layer profile and therefore it may be one of the differential factors between synoptic and non-synoptic wind systems with implications in structural damages. As the flow becomes fully turbulent and the transition from one- to two-celled vortex happens, there is less variation in the maximum tangential velocities with swirl ratio (see $S \geq 0.96$ in Figure 4-16).

The PIV measurements of horizontal velocities close to the ground were limited to z=3.5 cm due to accessibility issues. However, Ying and Chang [8], using laboratory simulations, demonstrated that the vertical profile of the tangential velocity very close to the surface is similar to the boundary layer profile of a uniform flow over a flat plate. Moreover, Baker and Church [34] have illustrated that maximum velocities drop rapidly for heights lower than the one corresponding to the maximum velocity.

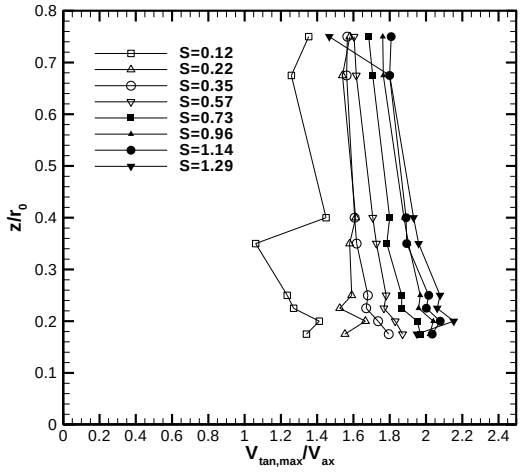

Figure 4-16: Maximum tangential velocitiy vs. height for $0.12 \leq S \leq 1.29$.

Overall, the vertical structure of the core is in agreement with previous experimental and numerical studies' findings [2, 34, 35]. For instance, the vertical profile of the maximum tangential velocity and the associated core radius at S=0.96 are well comparable with the ones reported by Baker and Church [34] for a turbulent vortex with Re_r=4.82×10^4 at S=0.97.

4.5.4 Vortex structure

A reconstruction of the three-dimensional structure of the tornado-like vortex was attempted using data obtained from horizontal PIV planes. Figure 4-17 presents streamlines superimposed on instantaneous vertical vorticity contour maps. Results are demonstrated for S=0.22, 0.57 and 0.96 and, at three different heights above surface: z=3.5, 7 and 15 cm.

Before touch-down, for S=0.22 (Figure 4-17a), the core size variation with height is almost negligible . The maximum vorticity is observed at the center of the vortex and the flow shows axisymmetric characteristics. Close to touch-down at S=0.57, a one-celled axisymmetric vortex with the core radius of 6 cm is observed at elevations very close to the surface (see Figure 4-17b). The maximum vertical vorticity is located in the core

region and the rest of the flow is nearly free of vorticity. By moving downstream (or upwards), the downflow intensifies and as a result the core region expands while developing asymmetric characteristics. This trend continues until the vortex structure breaks into a two-celled vortex for z>7 cm. The direction of the rotation is similar for the two cells as illustrated in Figure 4-17. At z=8 cm (not shown here), the two vortex cells are very close to each other. However, by moving downstream the cells separate further and their core region enlarges. The overall maximum vorticity is observed at z=15 cm with two local peaks associated with each cell. For S=0.96, the flow shows the most asymmetric characteristics when compared with S=0.22 and S=0.57 (see Figure 4-17c). The vortex breakdown has already propagated to the surface and as a result, a two-celled vortex is formed at the lowest elevations. The maximum vorticity magnitude is captured at the center of each individual vortex and the parent vortex core size has intensified.

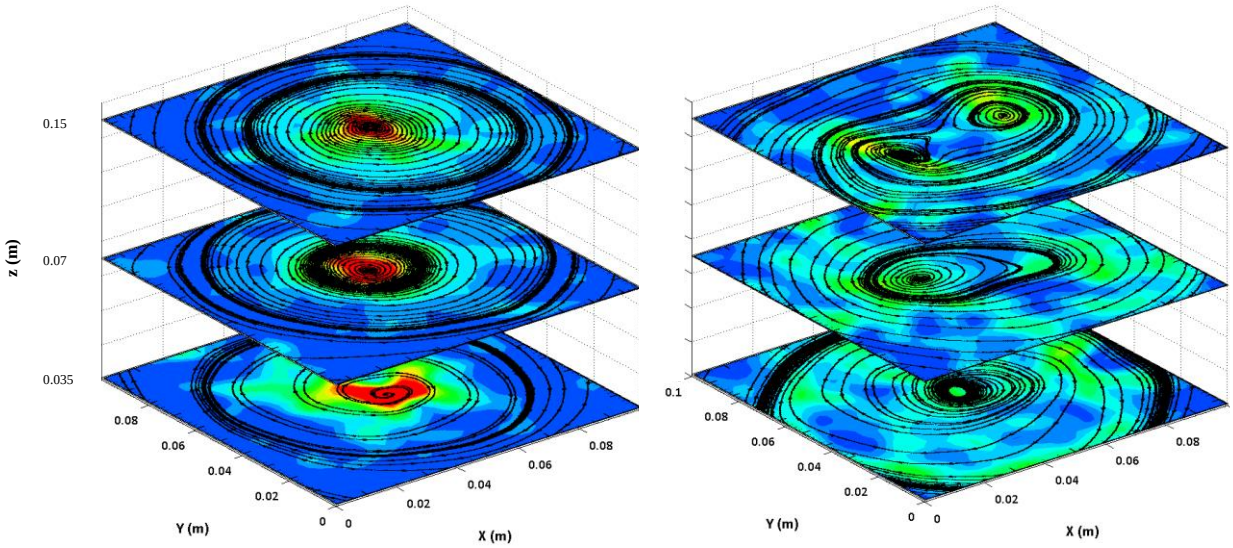

a) **b)**

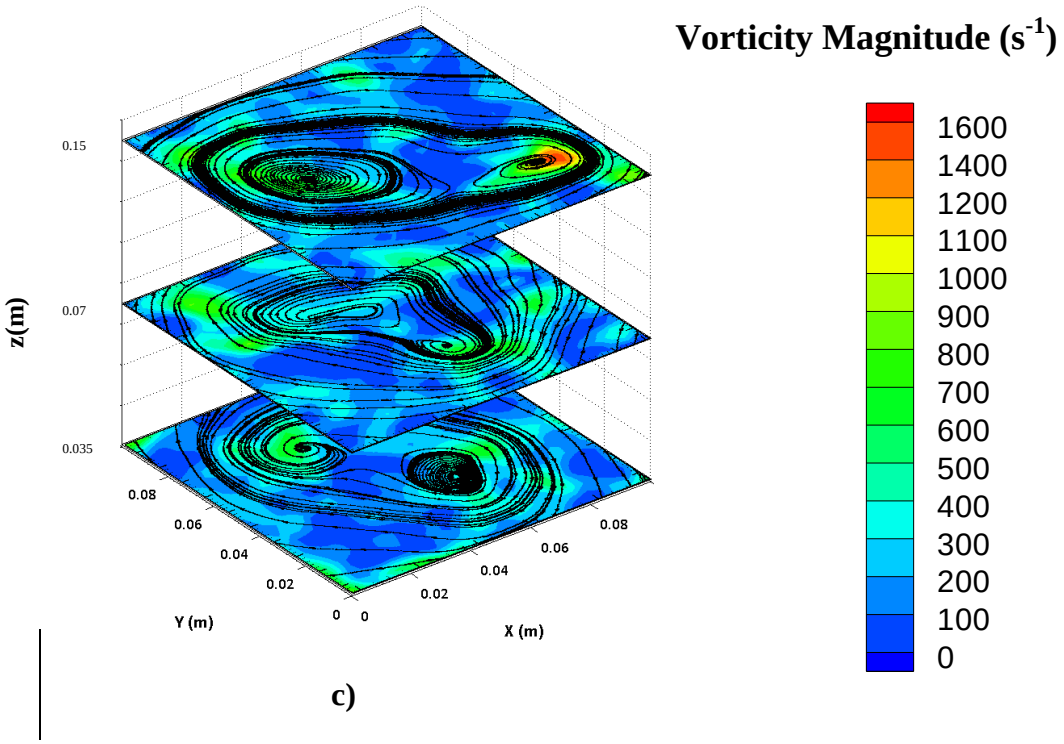

Figure 4-17: Streamlines superimposed on the instantaneous vertical vorticity contour maps at *z*=0.035, 0.07 and 0.15 m for a) *S*=0.22, b) *S*=0.57 and c) *S*=0.96.

4.6 Concluding remarks

Experimental investigations of tornado-like vortices were carried out in 1/11 scaled model of the WindEEE testing chamber at Western University. It has been shown that the aspect ratio, the flow rate and the rotational component can be varied independently in this simulator. The radial Reynolds number dependence of the flow was assessed. It was concluded that for $Re_r \geq 6.7\times10^4$, the core radius is nearly insensitive to the radial Reynolds number.

The evolution of the tornado-like vortex with variations in the swirl was documented using visualization techniques. This yielded a laminar single-celled vortex at S=0.12, a vortex breakdown bubble formation at $S\approx0.35$, a touch-down at $S\approx0.57$ and a fully turbulent two-celled vortex at S=0.96 or higher. Surface static pressure measurements showed a maximum pressure at the center of the vortex for single-celled cases and at the

center of each sub-vortex for two-celled set-ups. The instantaneous maximum pressure deficit variation with swirl ratio was investigated. Results showed good agreement with previous measurements and numerical simulations. A constant increase in the central pressure deficit with the swirl ratio was apparent for $S<0.73$. Significantly large surface static pressure deficits were recorded for simulated vortices with the overall maximum being at $S=0.73$.

The mean velocity field of the tornado-like vortex was measured using Particle Image Velocimetry. The radial profiles of the normalized tangential velocities were in close agreement with that of the modified Rankine vortex model in the main body of the flow not-influenced directly by boundaries. The near-surface flow showed intensified radial velocities and local maxima in the tangential velocities. These local maxima, along with the pressure deficit characteristics, differentiate tornadic winds from the atmospheric boundary layer flows and are believed to be responsible for the damage to structures and buildings in tornadic winds.

Although the results presented here are in good agreement with the modified Rankine vortex model and the previous experimental and numerical studies of tornado-like vortices, the relationship between the simulated tornadoes in MWD and natural tornadoes is yet to be determined. In an accompanying paper, scaling issues associated with tornado-like flow simulations are discussed in detail. A method is proposed which identifies the scaling ratio of the simulated tornadoes and the swirl ratio of the full-scale tornadoes.

References

[1] Lewellen, W. S., and Sheng, Y. P., 1979, "Influence of surface conditions on tornado wind distribution," Preprints, 11th Conf. on Sev. Loc. Stroms, AMS, Anonymous Boston, MA, pp. 375.

[2] Natarajan, D., and Hangan, H., 2012, "Large Eddy Simulations of Translation and Surface Roughness Effects on Tornado-Like Vortices," Journal of Wind Engineering and Industrial Aerodynamics.

[3] Wilson, T., and Rotunno, R. A., 1986, "Numerical Simulation of a Laminar End-Wall Vortex and Boundary Layer," Physiscs of Fluids, **29**pp. 3993-4005.

[4] Xu, Z., and Hangan, H., 2009, "An Inviscid Solution for Modeling of Tornado-Like Vortices," ASME Journal of Mechanics, **76**.

[5] Lewellen, D.,C., Lewellen, W.,S., and Xia, J., 2000, "The Influence of a Local Swirl Ratio on Tornado Intensification Near the Surface," Journal of the Atmospheric Sciences, **57**(4) pp. 527-544.

[6] Kuai, L., Haan, F. L., Gallus, W. A., 2008, "CFD Simulations of the Flow Field of a Laboratory-Simulated Tornado for Parameter Sensitivity Studies and Comparison with Field Measurements," Wind and Structures, **11**(2) pp. 1-22.

[7] Hangan, H., and Kim, J., 2008, "Swirl Ratio Effects on Tornado Vortices in Relation to the Fujita Scale," Wind and Structures, **11**(4) pp. 291.

[8] Ying, S. J., and Chang, C. C., 1970, "Exploratory Model Study of Tornado-Like Vortex Dynamics," Journal of the Atmospheric Sciences, **27**(1) pp. 3-14.

[9] Chang, C. C., 1971, "Tornado wind effects on buildings and structures with laboratory simulation," Anonymous Proceedings of the Third International Conference on Wind Effects on Buildings and Structures, pp. 231.

[10] Wan, C. A., and Chang, C. C., 1972, "Measurement of the Velocity Field in a Simulated Tornado-Like Vortex using a Three Dimensional Velocity Probe," pp. 116.

[11] Ward, N. B., 1972, "The Exploration of Certain Features of Tornado Dynamics using a Laboratory Model," Journal of Atmospheric Sciences, **29**pp. 1194.

[12] Church, C. R., Snow, J. T., and Agee, E. M., 1977, "Tornado Vortex Simulation at Purdue University," Bulletin of the American Meteorological Society, **58**pp. 900-908.

[13] Mitsuta, Y., and Monji, N., 1984, "Development of a Laboratory Simulator for Small Scale Atmospheric Vortices," Natural Disaster Science, **6**pp. 43-54.

[14] Lund, D. E., and Snow, J. T., 1993, "Laser Doppler Velocimetry Measurements in Tornado Like Vortices," Geophysical Monograp, **79**pp. 297.

[15] Wang, J., James, D. L., Letchford, C. W., 2001, "Development of a prototype tornado simulator for the assessment of fluid-structure interaction," Proceedings of the 1st Americas Conference on Wind Engineering, 4-6 June, Clemson Uni., SC.

[16] Mishra, A. R., Jamesa, D. L., and Letchford, C. W., 2008, "Physical Simulation of a Single-Celled Tornado-Like Vortex, Part A: Flow Field Characterization," J. Wind Eng. Ind. Aerodyn., **96**pp. 1243.

[17] Lee, J., and Samaras, T., 2004, "Pressure measurements at the ground in an F-4 tornado," Proceedings of the 22nd Conference on Severe Local Storms, Anonymous Hyannis, MA.

[18] Wurman, J., and Alexander, C. R., 2005, "The 30 may 1998 Spencer, South Dakota, Storm. Part II: Comparison of Observed Damage and Radar-Derived Winds in the Tornadoes," Monthly Weather Review, **133**(1) pp. 97-119.

[19] Haan Jr, F. L., Sarkar, P. P., and Gallus, W. A., 2008, "Design, Construction and Performance of a Large Tornado Simulator for Wind Engineering Applications," Engineering Structures, **30**pp. 1146.

[20] Hashemi Tari, P., Gurka, R., and Hangan, H., 2010, "Experimental Investigation of a Tornado-Like Vortex Dynamics with Swirl Ratio: The Mean and Turbulent Flow Fields," J. Wind Eng. Ind. Aerodyn., **98**pp. 936-944.

[21] Davies-Jones, R. P., 1973, "The Dependence of Core Radius on Swirl Ratio in a Tornado Simulator," Journal of Atmospheric Sciences, **30**pp. 1427.

[22] Church, C. R., Snow, J. T., Baker, G. L., 1979, "Characteristics of Tornado-Like Vortices as a Function of Swirl Ratio: A Laboratory Investigation," Journal of Atmospheric Sciences, **36**pp. 1175.

[23] Lewellen, W. S., 1962, "A Solution of Three Dimensional Vortex Flows with Strong Circulation," Journal of Fluid Mechanics, **14**pp. 420.

[24] Snow, J. T., 1982, "A Review of Recent Advances in Tornado Vortex Dynamics," Rev. Geophys., **20**pp. 953.

[25] Jischke, M. C., and Parang, M., 1974, "Properties of Simulated Tornado-Like Vortices," J. Atmos. Sci., **31**pp. 506.

[26] Rotunno, R. A., 1979, "A Study in Tornado-Like Vortex Dynamics," Journal of Atmospheric Sciences, **36**pp. 140.

[27] Rotunno, R. A., 1977, "Numerical Simulation of a Laboratory Vortex," Journal of Atmospheric Sciences, **34**pp. 1942-1956.

[28] Hall, M. G., 1966, "The Structure of Concentrated Vortex Cores," Prog. Aeronaut Sci., **7**pp. 53-110.

[29] Pauley, R. L., 1980, "Laboratory Measurements of Surface Pressure Minima in Simulated Tornado-Like Vortices," Purdu University, pp. 99.

[30] Pauley, R. L., Church, C. R., and Snow, J. T., 1982, "Measurements of Maximum Surface Pressure Deficits in Modled Atmospheric Vortices," Journal of Atmospheric Sciences, **39**pp. 368-377.

[31] Snow, J. T., Church, C. R., and Barnhart, B. J., 1980, "An Investigation of the Surface Pressure Fields Beneath Imulated Tornado Cyclones," J. Atmos. Sci, **37**pp. 1013-1026.

[32] Snow, J. T., 1984, "On the Formation of Particle Sheaths in Columnar Vortices," J. Atmos. Sci, **41**pp. 2477-2491.

[33] Zhang, W., and Sarkar, P. P., 2012, "Near-Ground Tornado-Like Vortex Structure Resolved by Particle Image Velocimetry (PIV)," Exp. Fluids, **52**pp. 479-493.

[34] Baker, G. L., and Church, C. R., 1979, "Measurements of Core Radii and Peak Velocities in Modeled Atmospheric Vortices," Journal of Atmospheric Sciences, **36**pp. 2413-2424.

[35] Church, C. R., and Snow, J. T., 1993, "Laboratory Models of Tornadoes," Geophysical Monograph, **79**.

Chapter 5

5 Three-dimensional axisymmetric wind field structure of five tornado events

5.1 Introduction

The high tornado count of 1,690 made 2011 the second most active year since the modern record began in 1950 [1]. The damage from tornado-related outbreaks in 2011 exceeded $10 billion, representing the highest property damage from severe weather in a single year since the property loss record keeping began in 1980. The annual total number of fatalities from tornadoes was 553, the most in the 62-year period of record. Damages from the May 22, 2011 EF5 Joplin, MO tornado alone exceeded $2.5 billion, the most on record for a single tornado in U.S. history. Fujita Scale (F-Scale) [2] or Enhanced Fujita Scale (EF-Scale) [3] is a forensic scale used to rate the intensity of a tornado by examining the damage caused by the tornado after it has passed over a structure. The strongest tornado of the 2013 season struck Moore, OK in May 20th, resulted in 25 dead and hundreds injured. Peak velocities of 330 km/hr were estimated by the National Weather Service (NWS) for this tornado after a damage survey was performed. This was the third time in the past 15 years that the city of Moore was hit by a strong tornado and it was perhaps the worst tornado disaster since the Joplin, MO tornado in May, 2011.

Designing structures and buildings for tornado-resistance requires a detailed knowledge of the nature of the wind threat including duration, speed, directional variability and debris loading. Characterizing the complex structure of tornadoes has challenged researchers for years, with the major barrier being the shortage of full-scale velocity field data from this phenomenon [4]. It is only recently that new techniques have emerged at the level of full-scale characterizations (portable Doppler radars), mathematical modeling (Ground-Based Velocity Track Display) as well as physical simulation (novel tornado-simulators). These advancements allow for an important break-through in investigating the effects of tornadoes on buildings and structures. Herein we show, for the first time, how these new techniques can be combined to characterize the flow structure of various tornado events. Single-Doppler radar data along with the Ground-Based Velocity Track

Display (GBVTD) method are used to extract the three-dimensional flow structure of five tornado events. These tornado structures are then related to previous physical experiments and to fluid mechanics parameters, such as swirl ratio, which can then be used to build a relationship between full-scale tornadoes and physically or numerically simulated tornado-like vortices. In addition, the data provided here will serve as the beginning of what will eventually be a database of full-scale tornado wind fields. This database is aimed for researchers focusing on experimental and numerical simulations of tornadic flows with the ultimate goal of studying wind loading effects on scaled models. Therefore, special attention is given to the dynamic structure of the natural tornado rather than the tornadogenesis.

5.2 Background

Physical [5-9] and numerical [10-13] simulations of tornado-like flows demonstrated the variation in the vortex intensity, structure and wind field which is mainly governed by the non-dimensional parameter known as the swirl ratio (S). The swirl ratio can be defined as the ratio between the tangential velocity (V_{tan}) at the edge of the updraft hole to the mean axial velocity (V_{ax}) through the updraft opening: $S=(1/2a)V_{tan}/V_{ax}$. where a, namely the aspect ratio, is the ratio between the inflow depth (h) and the updraft radius (r_0). As shown in Figure 5-1, variation of the swirl ratio results in various developments of the tornado-like vortices [14] among which are the vortex breakdown and the transition to turbulence. For very weak swirls, $S<0.2$, the flow in the boundary layer separates (Figure 5-1a). By increasing the angular momentum, a thin laminar swirling flow forms aloft while the separated flow is forced to reattach to the surface (Figure 5-1b). For moderate swirls, $0.2<S<0.4$, a turbulent vortex breakdown bubble forms aloft and moves towards the surface as the swirl ratio increases (Figure 5-1c). At this stage, the vortical flow consists of a thin laminar core close to the ground and a turbulent two-celled flow aloft. By further increasing the swirl ratio, a downdraft develops along the centerline and eventually the breakdown bubble touches the surface at $S\approx0.45$ (Figure 5-1d). For $0.8<S<1.4$, a two-celled vortex with a central downdraft impinging on the ground is observed (Figure 5-1e). The tornado vortex can split into 2 or more cells if the swirl

increases further (Figure 5-1f). Note that the swirl ratio values and ranges provided above correspond to measurements performed in a ward-type tornado simulator [15].

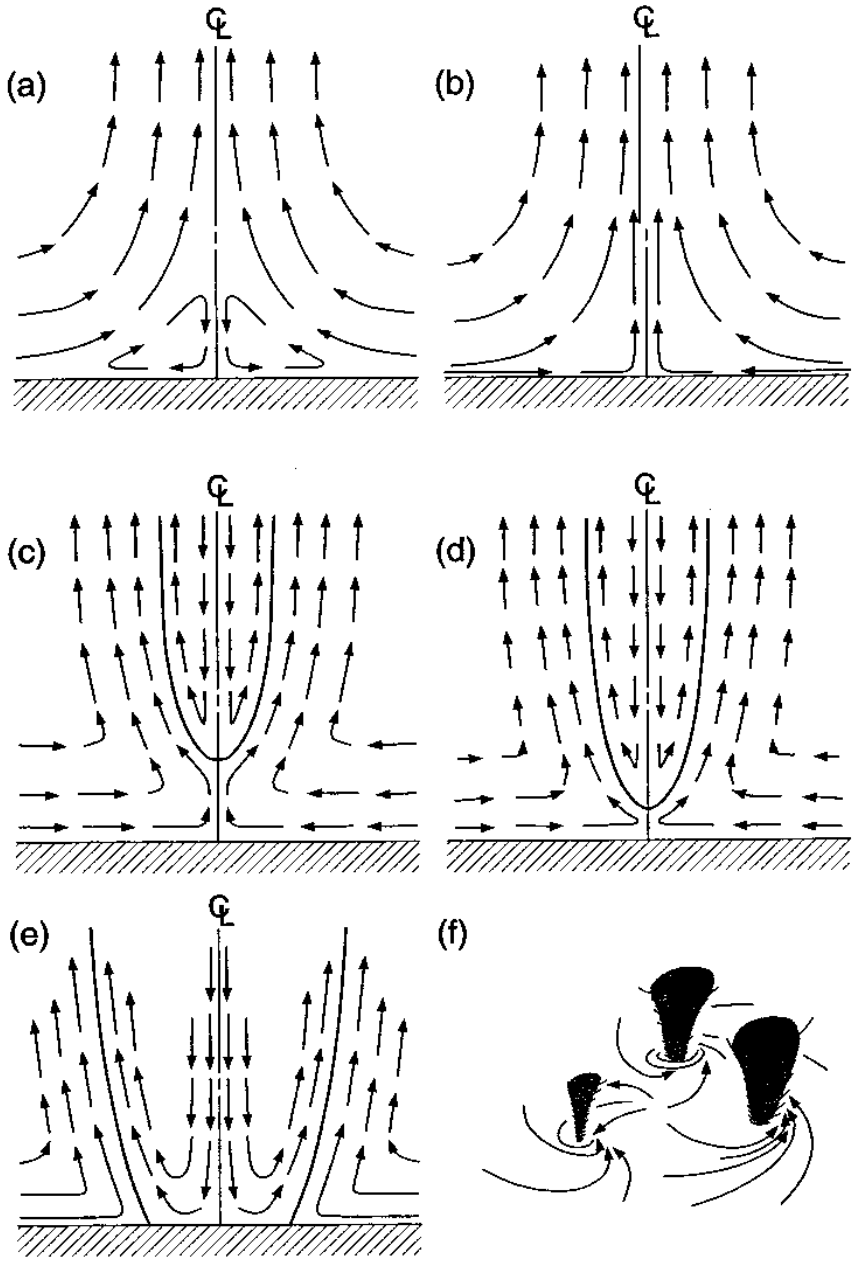

Figure 5-1: Swirl ratio effect on the structure of tornado vortices; a) very weak swirl, b) laminar core, c) breakdown bubble formation, d) drowned vortex jump, e) two-celled turbulent vortex and f) a family of three vortices - image from [14].

The Doppler on Wheels (DOWs) mobile radars were designed and constructed in 1995 [16, 17] to obtain data from small-scale, rapidly-evolving atmospheric events. Although a portable Doppler radar allows for investigators to measure tornado winds from close proximity (typically ~5-20 km), there are still measurement limitations/challenges. Since radar waves do not follow the earth's curvature and objects on the ground can block them, most data still are tens of meters above the ground level (AGL). In order to obtain data from regions very close to the ground (<10 m), Doppler radars need to be deployed very close (<5 km) to the tornado. Only on rare occasions [18, 19] researchers have been able to collect data from less than 10 m AGL.

To date, single- and dual-Doppler radar data from approximately 200 individual tornadoes have been collected during field projects such as VORTEX1 (1994-1995), ROTATE (1996–2001; 2003–08; 2012-13), VORTEX2 (2009-2010). The first three-dimensional maps of the tornado vortex inner and outer core flow with fine temporal and spatial resolution were obtained using the prototype DOW mobile radar in VORTEX1 [20]. These tornado wind maps allowed for recording the horizontal and vertical structure of the vortex and its evolution [21, 22]. ROTATE [23, 24] collected single- and dual-Doppler radar data from more than 140 different tornadic events which enabled scientist to study tornadogenesis [25-27], tornado structure [28-32] and the relationship between tornadic winds, debris, and damage [18, 33, 34].

The main objectives of the VORTEX2 [35] project were to collect wind, precipitation, and thermodynamic data, simultaneously in order to better understand the processes underlying tornado formation and to improve prediction of supercell thunderstorms and tornadoes. The data obtained during this project has been partially analyzed and published by various scientists [36-39] and are still being currently investigated. ROTATE (2012-13) is the most recent field study of tornadoes focused on the low-level winds and therefore of great interest for the wind engineering community. Using data collected during this field project, Kosiba and Wurman [19], for the first time, documented the fine-scale three-dimensional structure of the boundary layer in a tornado. They revealed that the inflow in this tornado is confined to 10-14 m AGL or less, which is much shallower than what is reported in previous works. Overall, the aforementioned

field projects increased the tornado warning lead-times, improved the quality of severe weather warnings, broadened our knowledge about tornadogenesis and extended the database of full-scale tornado wind fields.

Lee *et al.* [40] developed the GBVTD technique to retrieve the structure of a cyclone using single-Doppler radar data. Lee and Wurman [30] first applied the GBVTD technique to tornadoes to investigate the three-dimensional structure of the Mulhall, OK tornado (hereafter Ml tornado) on 3 May 1999. They focused on axisymmetric aspects of the flow and presented the tangential and radial winds at various radii and heights. Lee and Wurman reported peak axisymmetric tangential velocities of 84 m/s at 50 m altitude with the core region size ranging from 500 m to 1000 m for this multi-celled tornado.

Kosiba *et al.* [31] presented three-dimensional axisymmetric structure of the 12 May 2004 Harper, KS tornado retrieved from Doppler radar using an axisymmetric model. They concluded that an essential characteristic of the outer core region ($r>r_c$) is the significant spatial and temporal variability. GBVTD analyses were performed by Kosiba and Wurman [32] on data collected from the F4 rated Spencer, SD 1998 tornado using DOWs. The analysis revealed a two-celled vortex structure with significant downflow throughout the 8-minute observation period and significant inflow very close to the surface.

The June 9, 2009 long-lasting EF2-rated tornado of Goshen County (LaGrange), WY (hereafter GC tornado) was intercepted by DOWs during the VORTEX2 project [39, 41-43]. Single-Doppler radar data was obtained throughout the full lifetime of this tornado, with dual-Doppler measurement from before genesis through maturity. Photogrammetric and radar analysis of the GC tornado were conducted by Wakimoto *et al.* [36] and Atkins *et al.* [44]. They reported that damaging winds in the region few hundred meters above the ground extended radially beyond the funnel cloud. Later, Wakimoto *et al.* [37] published GBVTD analysis of the same tornado (GC tornado) combined with pictures of the funnel cloud. They focused mainly on identifying the relationship between velocity components, pressure gradients and the visual features of the tornado. Also, Wakimoto *et al.* examined the validity of GBVTD assumptions using dual-Doppler radar data. They

observed that the retrieved secondary circulation (axial and radial velocity components) near and within the core region is not accurate for small tornadoes with weak low-level inflow. Recently, Wurman *et al.* [45] combined in situ video and wind data obtained from the instrumented and armored Tornado Intercept Vehicle (TIV) with fine-scale DOW data for the GC tornado. In addition to characterizing the flow structure near the ground, this work revealed that horizontal velocity's variation from the lowest radar observed levels (~30 m AGL) to the in situ measurement level (3.5 m AGL) was negligible.

Lately, Nolan [46] performed a thorough review on the accuracy of the GBVTD method in retrieving velocity fields from single-Doppler radar data. He concluded that secondary circulations obtained through this mathematical method are biased, especially in weak tornadoes. This is due to the effect of centrifuging of debris and hydrometeors at low-levels which is shown to be more pronounced for tornadoes rated F2 or less. Nevertheless, retrieving the three-dimensional wind field of tornadoes is an ongoing research and improvements in the GBVTD method and in the correction for centrifuging effects are expected in the near future.

5.3 Data analysis

Single-Doppler radar data of five tornado events were analyzed in this study using the GBVTD method. The Spencer, SD 1998 (F4), Stockton, KS 2005 (F1), Clairemont, TX 2005 (F0), Happy, TX 2007 (EF0) and Goshen County, WY 2009 (EF2) tornadoes were selected for this purpose as these cover a wide range of vortex structures and intensities.

Data acquired through one complete radar scan of a tornado from regions very close to the ground to hundreds of meters aloft is termed as "volume". Nine volumes of radar data were investigated using the GBVTD method to retrieve axisymmetric three-dimensional structure of the parent vortex. Volumes were selected to cover wind speeds associated with EF0 to EF3 rated tornadoes. Note that the intensity ranking mentioned above for each tornado event is provided by the Storm Events Database [47] and is based on damage surveys. These ratings are influenced by accessibility, damage markers in the region and quality of structures and as a result, they are not a true representative of the tornado intensity. For instance, eye witnesses and DOW measured data suggest that the

Happy, TX 2007 tornado (hereafter Hp tornado) was stronger than EF0. Yet it travelled through open country terrain and as a result it is most likely under-rated.

The number of sweeps in a volume varied between 4 and 14 with the finest and coarsest elevation angles of 0.3˚ and 6˚, respectively. The minimum height scanned by the radar was affected by the terrain condition and the distance of the radar to the center of rotation. Volumes of radar data were first filtered subjectively using the SOLO II software [48], provided by National Center for Atmospheric Research (NCAR), to remove noise and any spurious data resulted from ground clutter and signal blockage near the surface. Then, the data were objectively analyzed using a bilinear interpolation scheme [49] to create a Cartesian grid (Δx, Δy, Δz). Next, the vortex center coordinates were identified. In theory, the vortex center can be defined using minimum pressure, circulation or reflectivity. Herein, the circulation center was considered as the vortex center. The Doppler velocity pattern of tropical cyclones was investigated by Wood and Brown [50]. They suggested that, given an axisymmetric flow field, center of the tropical cyclone is located on a circle that passes through the radar and Doppler velocity maxima. Therefore, the circulation centers were identified manually for every volume and at each elevation angle of the radar in accordance with Wood and Brown approach while taking into account the asymmetry inherited in the flow field of tornado vortices. The tornado circulation center at each elevation was then shifted to vertically align the centers in order to allow for a more accurate retrieval of the wind field.

The GBVTD analysis is applied to a ring with the circulation center of the vortex located at the center of this ring. The Doppler velocity (V_D) is expressed as a function of tangential (V_{tan}), radial (V_{rad}), translational (V_{trans}) and axial (V_{ax}) velocities of the atmospheric vortex as well as the terminal velocity of hydrometeors and debris (v_t):

$$V_D = V_{trans}\cos(\Upsilon-\theta_M)\cos\varphi - V_{tan}\sin\psi\cos\varphi + V_{rad}\cos\psi\cos\varphi + (V_{ax}-v_t)\sin\varphi$$

where, φ is the elevation angle of the radar beam, θ_M is the direction of the mean wind flow and, ψ and Υ are mathematical angles as shown in Figure 1 of the work by Lee *et al.* [40] (see Appendix E). Contributions from V_{ax} and v_t are first neglected to simplify the analysis. The horizontal velocities (tangential and radial components of the velocity)

consist of axisymmetric and asymmetric components. This results in a complex wave form for the Doppler velocity which can be decomposed into Fourier terms. In the GBVTD analysis, it is assumed that the flow field is dominated by strong axisymmetric tangential velocities. After simplifying equations and implementing the complex geometrical relationship between an atmospheric vortex and a ground-based Doppler radar, a system of equations relating Doppler velocities to the tangential and radial velocities are solved to retrieve the three-dimensional vortex structure. Azimuthally averaged tangential and radial velocities can be extracted using this mathematical method. The axial velocity at each grid point is then determined through upward integration of the continuity equation with a no slip boundary condition at the ground. Mathematical representation of this method and full assumptions are explained in detail by Lee *et al.* [40].

Figure 5-2 shows a contour map of Doppler velocities for the Hp tornado at 0203:20 UTC. The wind field of this tornado was reconstructed for a volume from 0203:20 UTC to 0204:17 UTC (hereafter v2). This volume consisted of 13 radar sweeps with elevation angle increments ranging from 0.3˚ to 3˚.

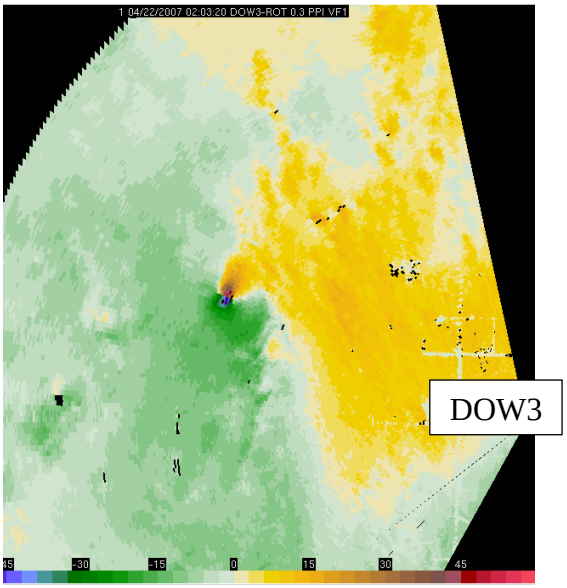

Figure 5-2: Doppler velocity (m/s) contour map of the Happy, TX 2007 tornado at 0203:20 UTC (Hp v2) and at 0.3˚ radar beam angle showing the tornado vortex location relative to the Doppler radar.

Figure 5-3a demonstrates vertical velocity (radial and axial components) vectors superimposed on the contour map of tangential velocities for Hp v2 tornado extracted using the GBVTD method. It is observed that the tangential velocity approaches its maximum of 37.9 m/s at regions very close to the ground with corresponding core radius (r_c) of 160 m. The central downdraft aloft is weakening as reaching the ground and the overall vertical flow pattern suggests that the vortex breakdown bubble formed aloft has just touched the ground and the flow has become fully turbulent.

As previously addressed [46, 51], radial and consequently axial velocities obtained from the GBVTD analysis can be significantly biased by the centrifuging of hydrometeors and debris. Using a linear analytical model for a translating tropical cyclone, Kepert [52] showed that in a rotating boundary layer there must exist a radial inflow at and around the radius of overall maximum tangential velocity. However, the net pressure force that accelerates the flow inward is weak compared to the centrifugal force that moves dense particles outward relative to the air and, as a result, the expected low-level inflow is not observed in retrieved data. To account for the centrifuging effect of hydrometeors and debris, the radial velocity components were modified ($V_{rad,mod}$) using an equation proposed by Nolan [46]:

$$V_{rad,mod}=V_{rad} - V_{rad,bias}=V_{rad} - C_{max}\,[\,(V_{tan}^2/r) / max\,\{V_{tan}^2/r\}\,].$$

where, $V_{rad,bias}$ is the positive bias in the radial velocity values due to the centrifuging of particles and C_{max} is the terminal fall speed of dominant particles in the flow (e.g. raindrops, hailstones, debris) as provided by Dowell *et al.* [51]. In order to modify the radial velocities (and consequently the axial velocities), information about the size and type of scatterers is needed. This information can be provided by the observers at the site of a tornado or can be estimated based on the topography of the site and whether the tornado has passed through structures or not. For the tornadoes that are analyzed here, such information is partially available for the Spencer, SD 1998 (hereafter Sp tornado) and GC tornadoes as they have been extensively investigated before ([29, 32, 34, 51] and [36-39], respectively). Since observational information is not available for the rest of

tornado events studied here, the radial wind field of these events is only corrected for small raindrops (0.5 mm in diameter).

Figure 5-3b displays the flow field of the Hp v2 corrected for centrifuging influence of small raindrops. When compared to Figure 5-3a, it is seen that the divergence at lower elevations has decreased while the updraft has slightly intensified. Note that the research on the debris centrifuging effect is at its early stages and is not yet mature. For instance, currently most algorithms, including the one employed in this work, assume that the centrifuging effect is evenly distributed over the whole flow field. However, an important consideration is that large debris will be confined to lower parts of the tornado. Therefore, when correcting for the centrifuging effects of large scatterers, it is important to have an estimate of the affected depth of the flow.

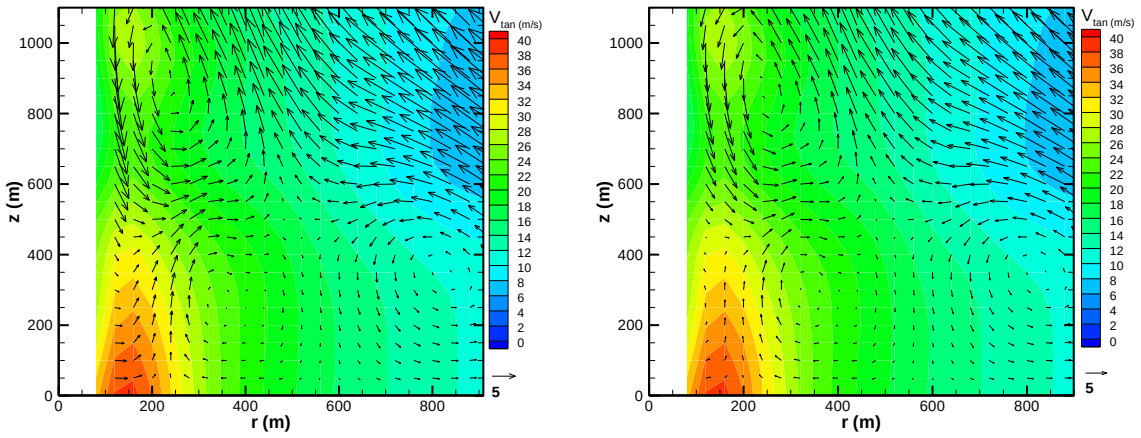

Figure 5-3: GBVTD retrieved structure of the Hp v2 at 0203:20 UTC, vertical velocity vector maps superimposed on tangential velocity contours, a) without and b) with correction for centrifuging.

A summary of the main information regarding each volume of data analyzed here as well as the parameters used in and extracted from the GBVTD analysis are provided in Table 5-1. In this table, volumes are grouped by the tornado events and the F- and EF-Scale for each tornado event was determined using the Storm Events Database [47]. The time

interval and the radar beam angle associated with each volume, the analysis grid size (Δx, Δy, Δz) and the minimum height (z_{min}) scanned by the radar are also presented in Table 6-1. The maximum values of grid spacing are dictated by the radar resolution near the center of the tornado. Δx and Δy should be smaller than about 1/3-1/2 of the largest radar resolution (Δr *and* $\Delta\theta$) at the tornado center. Choosing a larger value for the grid size, results in missing some of the information in the analysis while selecting a much smaller value adds noise to the calculation [53, 54]. The translational speed of the tornado was approximated based on the distance that the tornado had traveled over a certain period of time. The overall maximum tangential velocity ($V_{tan,max}$) obtained for each volume from the GBVTD analysis and the corresponding radius ($r_{c,max}$) and height (z_{max}) are also provided in Table 5-1

Sensitivity of the GBVTD analysis to the vortex center location as well as the grid spacing was examined. Errors smaller than 20% of the radius of the maximum tangential velocity (r_c) in the center location identification and changes in the grid size by ±8% of the largest radar resolution at the tornado center, resulted in negligible changes in the tangential velocity profiles and the flow structure.

Table 5-1. Summary of GBVTD analysis results for various volumes of radar data.

	Clairemont, volume1 (Clr v1)	Happy, volume1 (Hp v1)	Happy, volume2 (Hp v2)	Goshen Co, volume1 (GC v1)	Goshen Co, volume2 (GC v2)	Goshen Co, volume3 (GC v3)	Stockton, volume1 (Stc v1)	Spencer, Volume1 (Sp v1)	Spencer, Volume2 (Sp v2)
EF	F0	EF0	EF0	EF2	EF2	EF2	F1	F4	F4
Time interval (UTC)	2328:32-2328:44	0159:53-0200:57	0203:20-0204:09	2216:06-2216:45	2218:07-2218:42	2218:50-2219:39	2240:26-2240:38	0135:20-0135:52	0140:02-0140:41
Beam angles (degree)	0.3,1,1.7,2.4	0.3,0.6,1,1.5,2,2.5, 3,4,5,6,7.1,9,11,13.1		1,2,3,4,5,6	1,2,3,4,5,6	0.5,1,2,8, 10,12,14,16	0.3,1,1.7,2.4	2.5,3.4,5.4,7.6,10.2, 13.1,16.3,20.6	1,1.5,2.5,3.4,5.5, 7.4,10.5,13.3,16.5
$\Delta x=\Delta y$ *(m)*	18	40	50	25	25	25	20	16	16
Δz *(m)*	40	50	50	42	40	41	40	40	40
z_{min} *(m)*	25	71	38	97	75	30	43	51	85
V_{trans} *(m/s)*	1.2	19.4	19.4	9.49	9.49	9.49	10.95	15	15
$V_{tan,max}$ *(m/s)*	36.3	39	37.9	41.6	42	42.9	50.2	58.2	62
$r_{c,max}$ *(m)*	96	160	160	150	150	100	220	192	208
z_{max} *(m)*	200	250	50	42	160	41	40	40	40

5.4 Results and discussion

Figure 5-4 to Figure 5-12 display the GBVTD-extracted axisymmetric structure of each volume with and without corrections for the centrifuging effects. In these figures, the vertical velocity vector map is superimposed on the contour map of the tangential velocity. Results are corrected for relevant hydrometeor and debris size to examine the effect of correcting for centrifuging of particles on the flow structure. The vertical wind field of each volume is qualitatively compared with Figure 5-1 to determine the vortex structure which is important when simulating tornado vortices experimentally or numerically.

The very weak tornado of the Clairemont, TX (hereafter Clr tornado) was formed at 2305 UTC on June 12, 2005. This tornado was scanned by DOW3 using four elevation angles ranging from 0.3˚ to 2.4˚, resulting in measurement data at as low as 25 m AGL. The secondary flow vector map of this tornado at 2328:32 UTC (v1), shown in Figure 5-4a, suggests a downdraft that is weakening as it approaches the surface. Also, the maximum tangential velocity is observed at higher elevations. This configuration matches Figure 5-1c very well which corresponds to a stage of tornado vortex evolution just before the touch-down. The flow field corrected for centrifuging of small raindrops (see Figure 5-4b) shows a slight increase in the inflow and updraft.

A weak tornado was intercepted by DOW3 in the evening of April 21, 2007 near the town of Happy, TX (Hp tornado). This tornado was scanned from 0158:16 UTC to 0207:22 UTC and for various elevation angles ranging from 0.3˚ to 13.1˚. Figure 5-5a illustrates a single-celled structure with an updraft close to the center of the vortex at 0159:53 UTC (v1). A very weak outflow is detected at 400 m AGL and higher elevations. Applying the correction for centrifuging of small rain drops (C_{max}=2 m/s) increases the maximum inflow by 34% and intensifies the updraft at the centerline. Approximately 3.5 min later, at 0203:20 UTC (v2), a downdraft of 12 m/s is observed at very high elevations (~900 m AGL) while the updraft is shifted away from the centerline (Figure 5-6b). Also, the overall maximum tangential velocities are now moved towards

the surface. Whether this configuration represents right before or after the touch-down of the breakdown bubble is debatable as the core region is not fully resolved. Without considering the contributions from the centrifuging of raindrops, the flow in the core region and at the radius of the maximum tangential velocity is purely outward (see Figure 5-6a).

The GC tornado event has been thoroughly investigated over its life time through photogrammetric analysis combined with single- and dual-Doppler radar analysis. This long lasting tornado started at 2152 UTC and ended at 2231 UTC [47]. In the most recent work by Wakimoto *et al.* [37], the three-dimensional structure of this tornado was extracted using the GBVTD method for two different volumes; 2216:08-2216:45 UTC (v1) and 2218:07-2218:42 UTC (v2). Three volumes of the GC tornado, including the two that have been previously analyzed by Wakimoto *et al.* [37], were selected for analysis in the current study. This provides the opportunity to examine the accuracy of the retrieval analysis.

The flow field approximated for GC v1 is shown in Figure 5-7a. The lowest height scanned by the radar is relatively high (97 m AGL) and therefore, reduces the accuracy of the vertical wind retrieval process. The core region of the flow, which is about 300 m wide, and the surrounding area are dominated by a downdraft. A very week updraft is observed away from the core at r=350 m. The overall reconstructed flow field is in very good agreement with the one reported by Wakimoto *et al.* [37]. Since the flow field is dominated by a downdraft, it is difficult to characterize the vertical structure of the flow. However, axial downdrafts exceeding 17 m/s very close to the centerline together with weak updrafts that are located at the periphery of the funnel as shown by Wakimoto *et al.* [37], suggest a two-celled vortex pattern. After 2 min (see Figure 5-8a), the velocity field is still dominated by downdrafts and outflows while a local peak in the value of the overall maximum tangential velocity is apparent at 160 m AGL. The lowest radar data available for this volume is at 75 m AGL which means, the inflow layer is not resolved in this case. The retrieved flow field of the GC v2 is well matched with the one presented by Wakimoto *et al.* [37]. When compared to GC v1, the downdraft has weakened slightly

while there is no evidence of updraft at the periphery of the funnel. These observations combined with the fact that the overall maximum tangential velocity is captured at relatively high elevations suggest that the tornado vortex is at the transition stage. Figure 5-9a depicts the GBVTD-extracted velocity field of the third volume of the GC tornado (2218:50 UTC). The core area shrinks by 30% when compared with GC v1 and GC v2 and the overall maximum tangential velocity shifts back towards the ground. Relatively strong downdrafts confined to the core along with updrafts right outside of the vortex core are consistent with the vertical structure of a two-celled vortex shown in Figure 5-1. A persistent downdraft in all three volumes of the GC tornado confirms that the tornado is at the dissipation stage. Further investigations of the axial profile of the tangential velocity for GC v1-v3, presented later in this study, may provide more insights towards the vertical field of the vortex.

Using high-definition video footage as well as observations from personnel in the region, Wakimoto *et al.* [37] concluded that the centrifuging of hydrometeors, dirt and gravel has biased the estimate of the radial velocity field. However, to estimate the effect of centrifuging, they used a different approach proposed by Dowell *et al.* [51]. Following this method, they simulated the motion of particles and estimated the positive bias to the radial velocities. Afterwards, they subtracted the particles velocity field from the GBVTD-derived wind field and presented the modified vertical wind field. Based on the results provided by Wakimoto *et al.*, centrifuging of particles has introduced a maximum bias of 9 m/s to the radial velocities in regions very close to the ground. This positive bias decreases as moving upwards and reaches 2 m/s at ~750 m AGL. As mentioned before, the correction approach used in the current study is only suitable for small particles and hydrometeors. Therefore, the velocity fields of GC volumes are only corrected for the centrifuging effect of small raindrops with a mean diameter of 0.5 mm. Figure 5-7b, Figure 5-8b and Figure 5-9b depict that this correction slightly decreases the divergence in the flow.

DOW3 intercepted a tornado near Stockton, KS on June 9, 2005 (hereafter Stc tornado) at 2157 UTC. Although this tornado was rated F1, wind speeds as high as 50 m/s were

measured by DOW3 in this event. The Stc tornado was briefly (from 2239:11 UTC to 2240:38 UTC) scanned by DOW3 and the GBVTD-retrieved velocity field of one volume (v1) of data is presented in Figure 5-10. The vortex core is approximately 440 m wide with the lowest height scanned by the radar being 43 m AGL. The flow is dominated by inflows and consequently updrafts of approximately 21 m/s in the core region and the single-celled structure of the vortex remains unchanged after removing the bias in the radial velocity due to the centrifuging of small raindrops.

On May 31, 1998 an F4 rated tornado hit the city of Spencer, SD killed 6 people and left behind $17 million worth of property damage. DOW3 collected data from this tornado at 0100 UTC for approximately 45 min. Herein, two volumes of Sp tornado data, at 0135:20 UTC (v1) and 0140:02 UTC (v2) were investigated. The Sp tornado vortex core reached the city at 0138:08 UTC and exited at 0139:30 UTC. In a case study, Dowell *et al.* [51] investigated the effect of scatterer size and type on the Doppler radar observations of this tornado. They reported a horizontal inflow over the tornado core, at the lowest elevations, before it hit the city. Then after it entered the city, a significant change was observed in the Doppler velocity signature. Dowell *et al.* related this abrupt change to the change in the debris size as the tornado hit the city. Based on the mean horizontal divergence distribution (in the core and at the low-levels) over time, they concluded that the scatterer type has changed from small raindrops (C_{max}=2 m/s) at or before 0138 UTC to plywood sheets (C_{max}=20 m/s) at 0139:18 UTC. However, 1.5 min after the tornado exited the city Dowell *et al.* still noticed low-level divergence in the core. Whether this divergence is due to the existence of smaller debris in the flow or due to an error in resolving the surface layer (tornado was moving away from the radar at this point) is not clear. As a result, Sp v1 was corrected for small raindrops and since the discussion on the scatterer size and type for Sp v2 is not conclusive, C_{max}=2 m/s was used to correct the bias in the radial flow in this volume.

The vertical structure of the flow in Figure 5-11a for Sp v1 indicates two-celled vortex characteristics with a very strong downdraft of 62 m/s close to the center at 720 m AGL. As noted by Fiedler and Rotunno [55] such a strong downdraft is a characteristic of two-

celled tornadoes. The overall maximum tangential velocity of 58.2 m/s is obtained at 40 m AGL and at a radius of 192 m. Radar measurements are available for this volume at 51 m AGL or higher. Figure 5-11a illustrates a local peak in the tangential velocity values at higher elevations (~350 m AGL). As discussed by Kosiba and Wurman [32], this could be a retrieval analysis error due to the temporal resolution of the radar. In other words, the tornado intensification between successive scans is represented as a local peak in the tangential velocities aloft.

The axisymmetric structure of the Sp v2 is displayed in Figure 5-12. Similar to the Sp v1, a wide rotation is accompanied by a strong downdraft close to the centerline. The vertical wind map is in very good agreement with Figure 5-1e which suggests a two-celled vortex flow. Maximum tangential velocities are observed close to the surface and the updraft is shifted away from the centerline. The overall maximum tangential velocity of 62 m/s at a radius of 208 m is estimated for this volume. As expected, modifying the radial component of the velocity in such a strong tornado to account for the centrifuging effect of small raindrops has minimal influence on the flow structure.

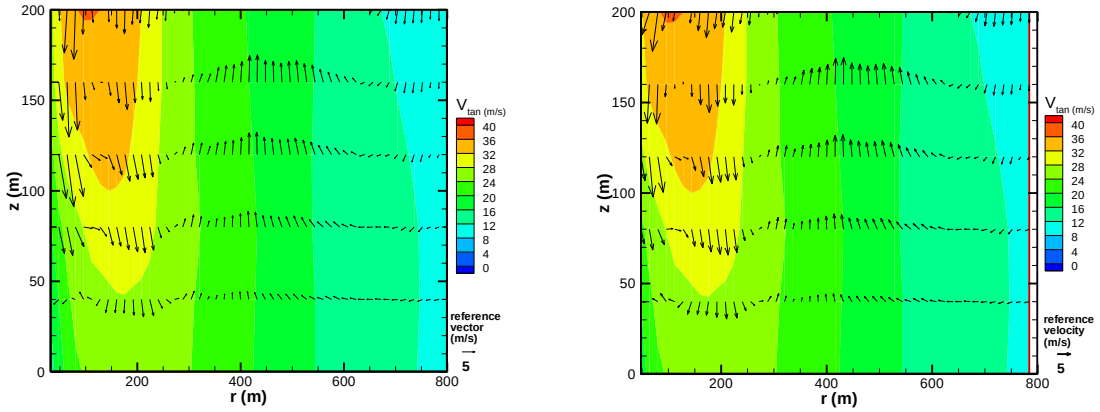

a) **b)**

Figure 5-4: Vertical velocity vectors superimposed on tangential velocity contours for Clr v1 at 2328:32 UTC with a) C_{max}=0 m/s and b) C_{max}=2 m/s.

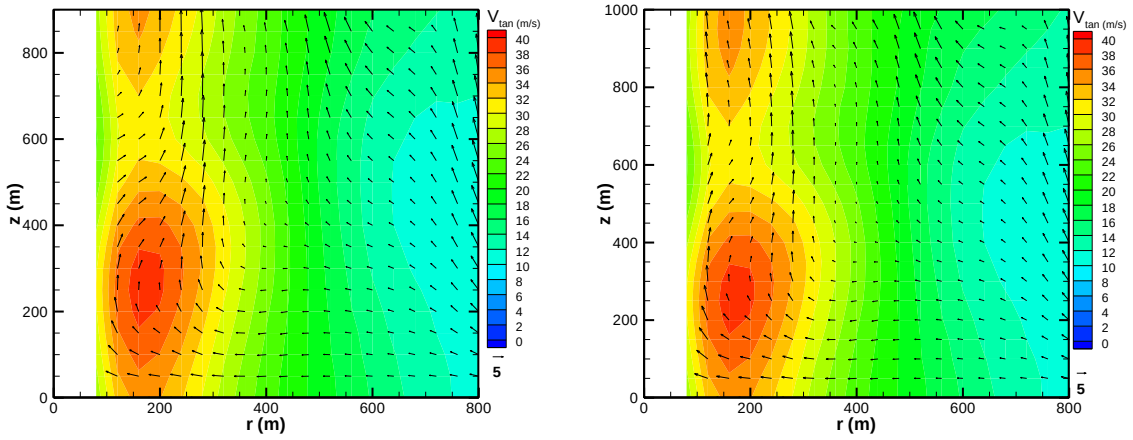

a) **b)**

Figure 5-5: Vertical structure of the vortex along with the tangential velocity contours for Hp v1 at 0159:53 UTC with a) C_{max}=0 m/s and b) C_{max}=2 m/s.

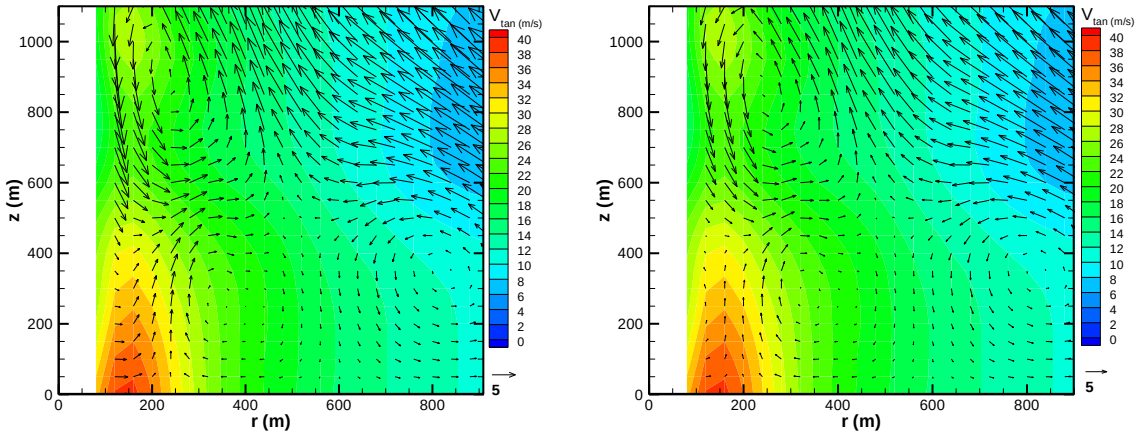

a) **b)**

Figure 5-6: Vertical structure of the vortex along with the tangential velocity contours for Hp v2 at 0203:20 UTC with a) C_{max}=0 m/s and b) C_{max}=2 m/s.

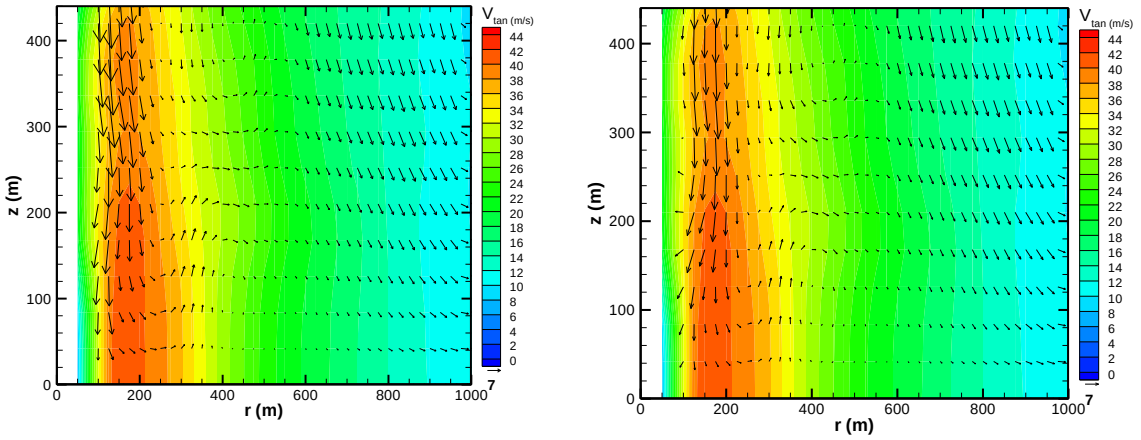

a) **b)**

Figure 5-7: Vertical velocity vector maps superimposed on tangential velocity contours for GC v1 at 2216:08 UTC with a) C_{max}=0 m/s and b) C_{max}=2 m/s.

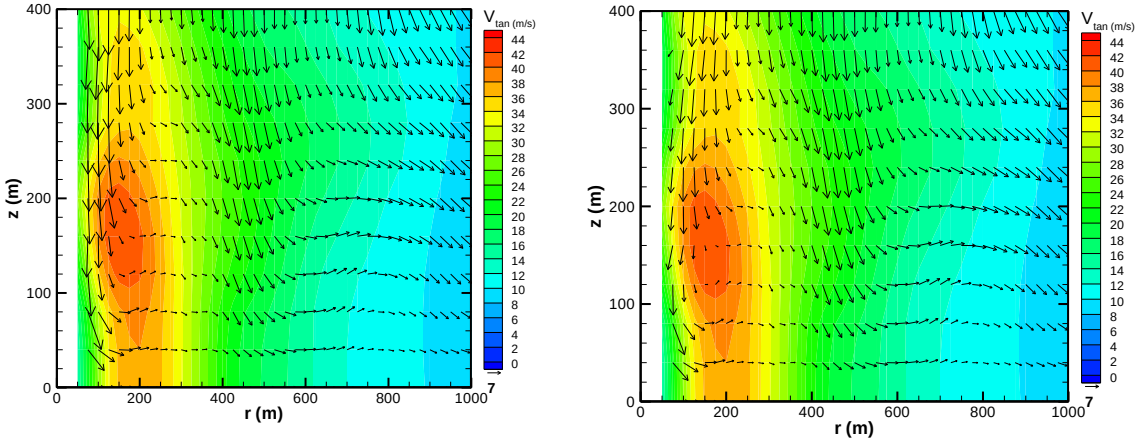

a) **b)**

Figure 5-8: Vertical velocity vector maps superimposed on tangential velocity contours for GC v2 at 2218:07 UTC with a) C_{max}=0 m/s and b) C_{max}=2 m/s.

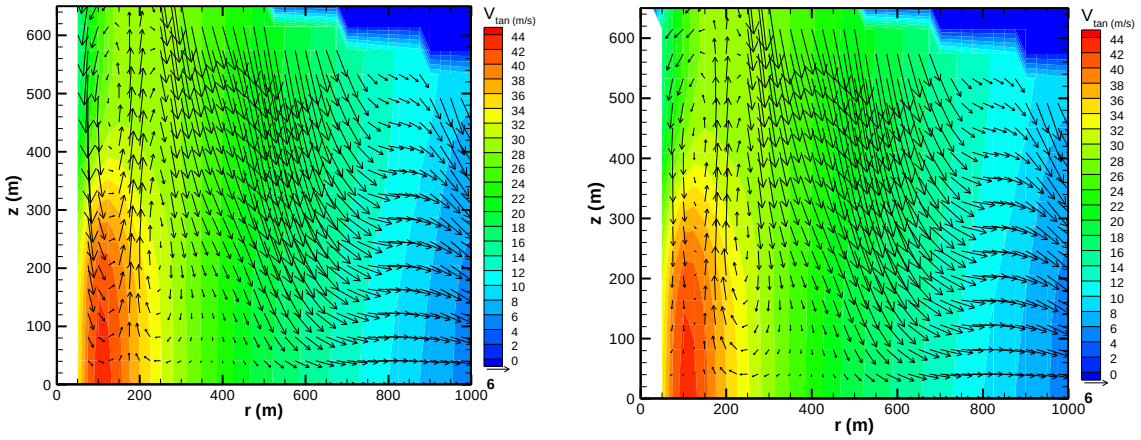

Figure 5-9: Vertical velocity vector maps superimposed on tangential velocity contours for GC v3 at 2218:50 UTC with a) C_{max}=0 m/s and b) C_{max}=2 m/s.

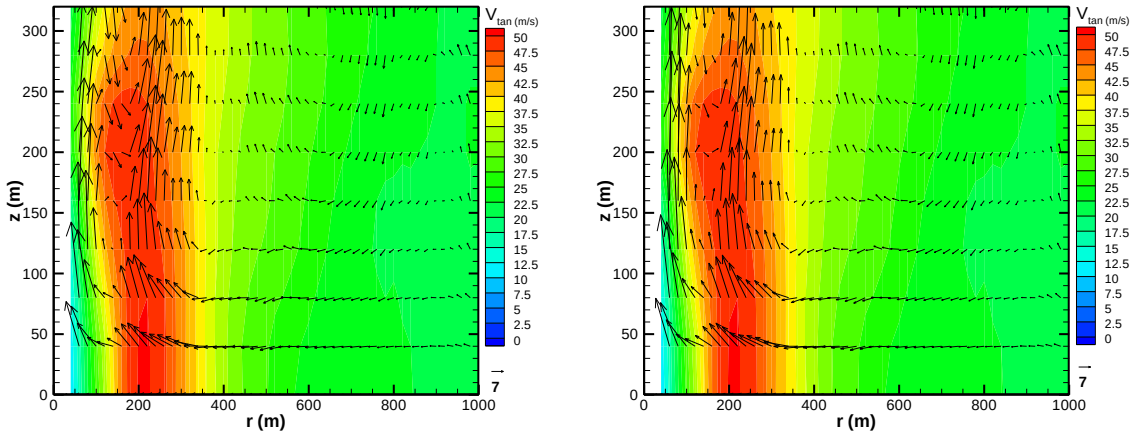

Figure 5-10: Vertical velocity vector maps superimposed on tangential velocity contours for Stc v1 at 2240:26 UTC with a) C_{max}=0 m/s and b) C_{max}=2 m/s.

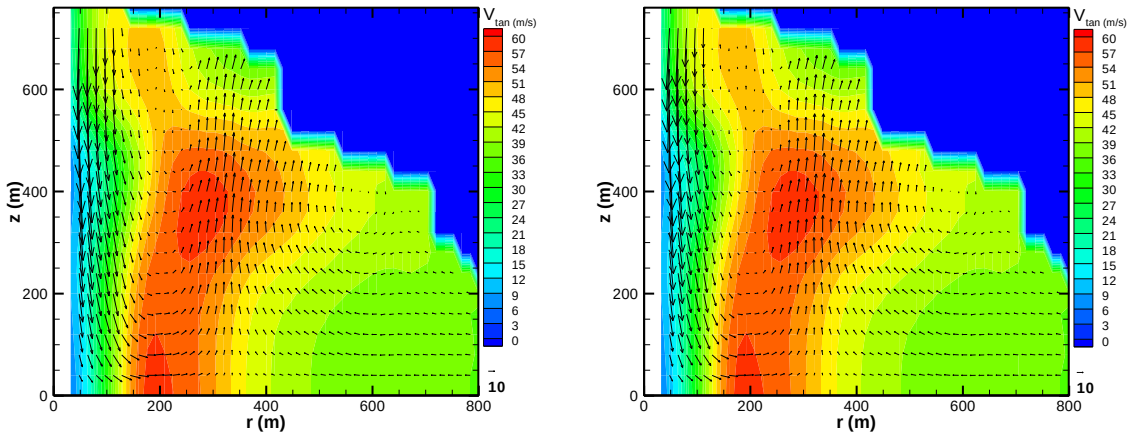

a) **b)**

Figure 5-11: Vertical velocity vectors superimposed on tangential velocity contours for the Sp v1 at 0135:20 UTC with a) C_{max}=0 m/s and b) C_{max}=2 m/s.

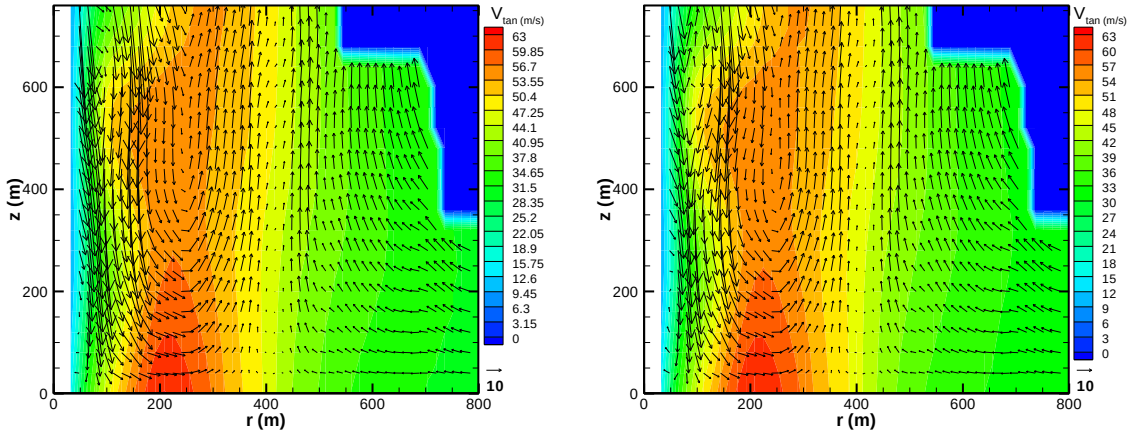

a) **b)**

Figure 5-12: Vertical velocity vectors superimposed on tangential velocity contours for Sp v2 at 0140:02 UTC with a) C_{max}=0 m/s and b) C_{max}=2 m/s.

The velocity profiles of the tornadoes investigated in here can be used as a benchmark for experimental and numerical simulations of tornado-like vortices. It was shown that the radial and, consequently, the axial velocities are very sensitive to the correction for centrifuging effects. In addition, detailed information about scatterers' size and type were not available for most of the tornado events studied here. As a result, only tangential velocity profiles are trusted and presented. The tangential velocity variation with radius is plotted in Figure 5-13 for all volumes of data and at various heights. Velocities and radii are normalized using the maximum tangential velocity and the core radius corresponding to each height, respectively. Results are compared with the modified Rankine vortex model in which the tangential velocity is estimated using $V_{tan}=r\Gamma_{\infty}/(r_c^2+r^2)\pi$. where, Γ_{∞} is the maximum circulation defined as $\Gamma_{\infty}=2\pi r_{c,max}V_{tan,max}$. The overall maximum tangential velocity ($V_{tan,max}$) of each volume and the corresponding radius ($r_{c,max}$) were used to calculate the tangential velocity of the Rankine model. Overall, the Rankine vortex is in good agreement with the field measurements. Discrepancies are spotted at lower heights and at the outer core region of the vortex. As explained by Snow [56], idealized profiles such as Rankine vortex are most applicable above the surface layer, where radial velocities are relatively weak. The Clr v1 and Hp v1 are exceptions as the best agreements are achieved at lower elevations. This can be explained by their laminar core at lower elevations, which means less surface interactions. In addition, the discrepancies between the tangential velocities of Sp v1 and Sp v2 and, the Rankine model estimation at radial distances far from the vortex core may be due to the presence of subvortices in the full-scale data.

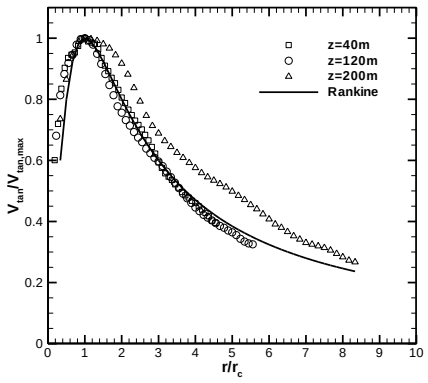
z=40m
z=120m
z=200m
Rankine
$V_{tan}/V_{tan,max}$
r/r_c

a)

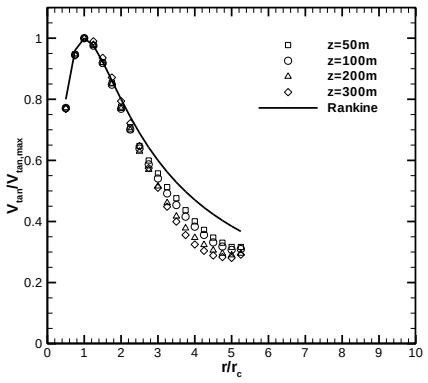
z=50m
z=100m
z=200m
z=300m
Rankine
$V_{tan}/V_{tan,max}$
r/r_c

b)

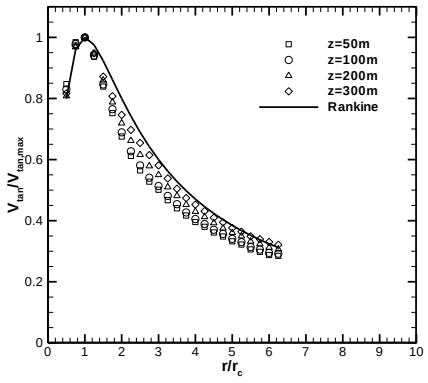
z=50m
z=100m
z=200m
z=300m
Rankine
$V_{tan}/V_{tan,max}$
r/r_c

c)

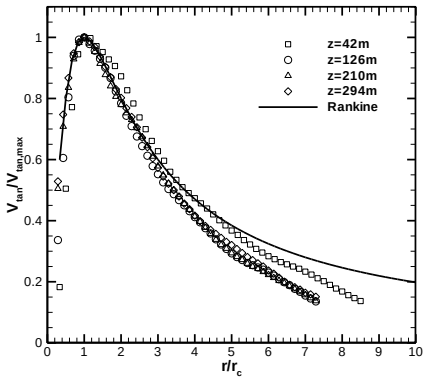
z=42m
z=126m
z=210m
z=294m
Rankine
$V_{tan}/V_{tan,max}$
r/r_c

d)

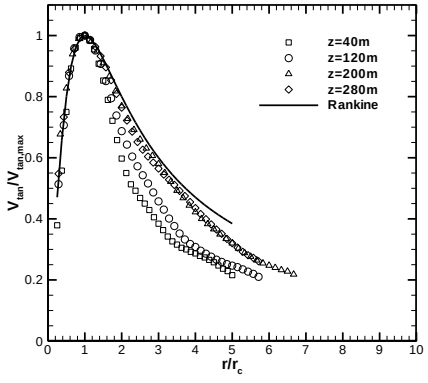
z=40m
z=120m
z=200m
z=280m
Rankine
$V_{tan}/V_{tan,max}$
r/r_c

e)

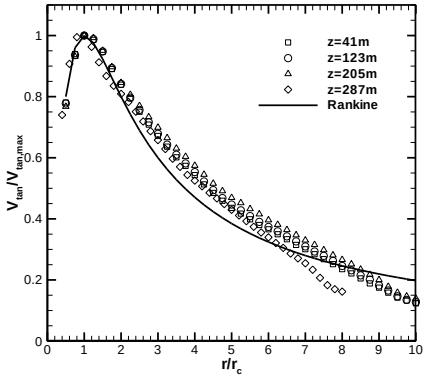
z=41m
z=123m
z=205m
z=287m
Rankine
$V_{tan}/V_{tan,max}$
r/r_c

f)

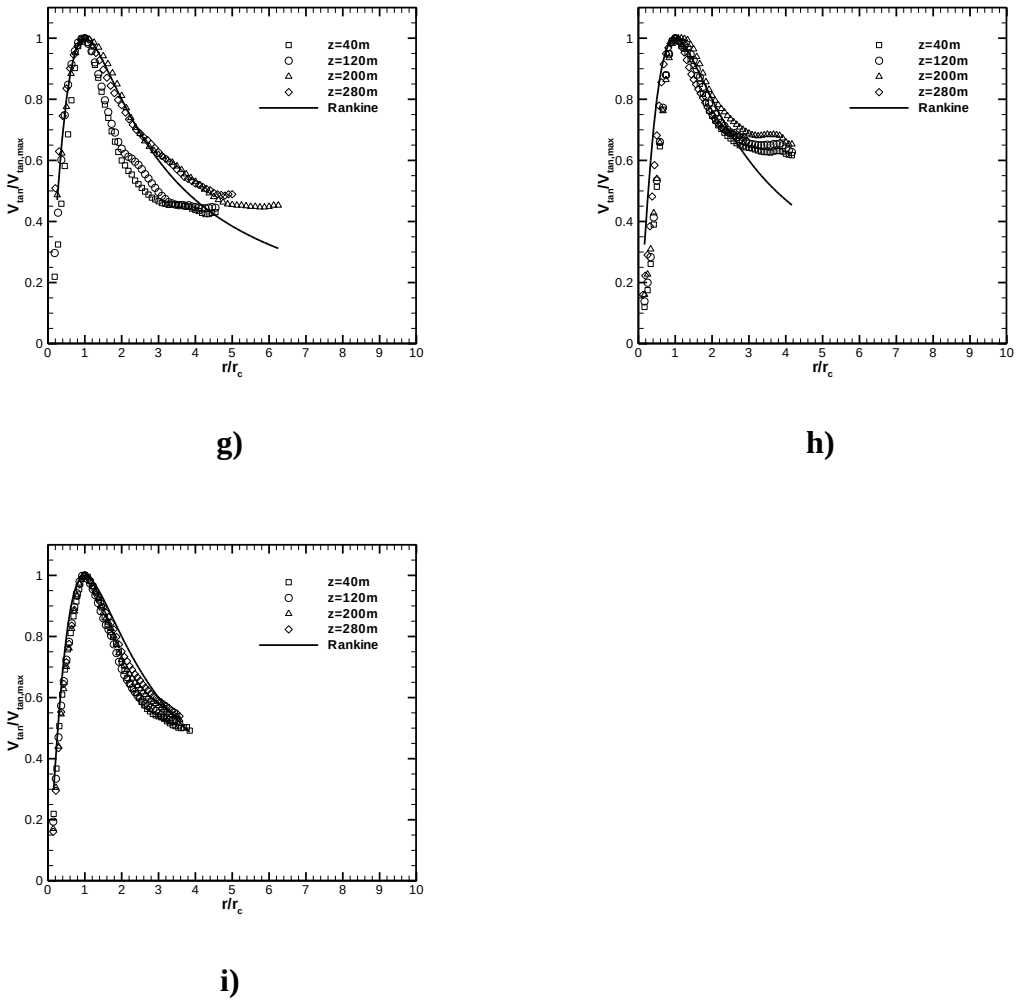

Figure 5-13: Radial profiles of the tangential velocity at different heights compared with Modified Rankine vortex model for a) Clr v1, b) Hp v1, c) Hp, v2, d) GC v1, e) GC v2, f) GC v3, g) Stc v1, h) Sp v1 and i) Sp v2.

Experimental [57] and numerical [58] simulations of tornado-like vortices have shown that the axial profile of the tangential velocity is characterized by a local peak very close to the surface ("nose" structure). This local maximum distinguishes tornadic flows from straight boundary layer flows and is thought to be responsible for the severe damage to structures. As a result, the axial profiles of the maximum tangential velocity are extracted and presented in Figure 5-14 for all volumes of data. Except for the Clr v1, Hp v1 and

GC v2, the maximum tangential velocity increases as moving towards the ground. However, there is no evidence of a local maximum of tangential velocities close to the surface. In a recent study performed by Kosiba and Wurman [19], the near surface flow of the EF2 rated Russell, KS tornado of May 2012 was retrieved and the maximum tangential velocities were located at the lowest heights (z<10 m AGL). Therefore, it can be inferred that the nose (maximum) in the current data is at elevations that are not resolved by the radar measurements, particularly for weaker tornadoes. On the other hand, Figure 5-14 demonstrates minimal variations in the tangential velocities at the lowest data points. Similar trend was reported by Kosiba and Wurman [19]. They observed a gradual decrease of about 10% in the Doppler velocities from 10 m to 40 m AGL. Therefore, one can conclude that the axial profiles of the tangential velocity reported here correspond to the regions right above the inflow or the boundary layer of the tornado vortex.

Although measurement data is not available for regions below the height corresponding to the maximum tangential velocities, previous experimental and numerical investigations of tornado-like vortices [59, 60] have shown that the axial profile of the tangential velocity very close to the surface is similar to a boundary layer profile, i.e. peak velocities drop rapidly towards the ground.

Clr v1, Hp v1 and GC v2 are an exception to all previous discussions as the peak tangential velocity is captured at high elevations (z>160 m AGL) for these volumes. This is attributed to the vortex structure and dynamics. For a single-celled vortex with a breakdown bubble aloft, the vortex core is laminar close to the surface. As the vortex breaks down aloft, the flow develops an adverse pressure gradient at the centerline which is a well-known characteristic of quasi-cylindrical vortices [61, 62]. along this point, the flow becomes turbulent and maximum velocities shift away from the centerline while surrounding the breakdown bubble [58, 63]. Capturing the overall maximum tangential velocity for Clr v1, Hp v1 and GC v2 cases implies that the vortex is at transition, from laminar to turbulent, which is consistent with the retrieved vertical structure of Clr v1 and Hp v1.

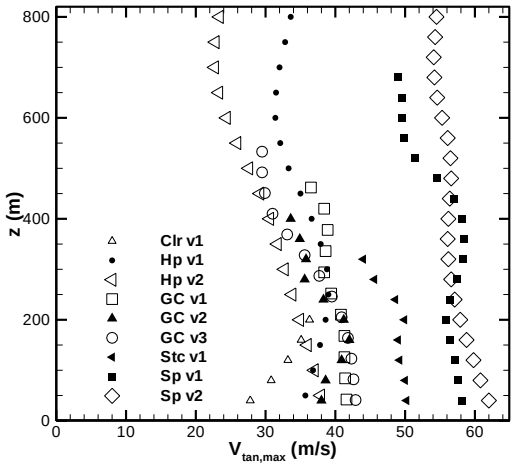

Figure 5-14: Variation of the maximum tangential velocity with height for various volumes of radar data.

As discussed before, experimentally and numerically simulated tornado vortices are governed by the swirl ratio. However, determining the swirl ratio of a field tornado is very challenging as this parameter is dependent on location and in physical simulations it was defined based on the boundaries of simulators. Calculating the swirl ratio has been attempted by Lee and Wurman [30] and Kosiba and Wurman [32] for the Ml and the Sp tornadoes, respectively. They estimated swirl ratios of 2 to 6 and 1 to 7 for the Ml and the Sp tornadoes, respectively. In both studies, it is stated that this range of swirl ratios is consistent with the multiple vortex radar signatures observed in these events. However, Kosiba and Wurman acknowledged that due to the underrepresentation of the radial inflow in radar measurements, the swirl ratio values might have been overestimated. The swirl ratio in both aforementioned studies is calculated using the V_{tan} and V_{ax} at the updraft radius. Alternatively, the swirl ratio can be expressed using the maximum circulation and the volumetric flow rate (Q') through the updraft: $S=r_0\Gamma_\infty/2Q'$. In this equation, Γ_∞ is calculated using the overall maximum tangential velocity and the corresponding radius. Computing the swirl ratio of the field data using the circulation may result in more accurate values as it reduces the error associated with subjectively choosing the representative values. Herein, the swirl ratio associated with each volume

was determined by calculating the average flow rate through the updraft and the maximum circulation. The estimated swirl ratios and the values chosen for calculating *S* are reported in Table 5-2. Since the flow was dominated by downdraft for the GC volumes, it was not possible to estimate the updraft region and therefore, swirl ratio is not reported for these volumes. It is seen that swirl ratio values vary between 1 and 5 for the volumes studied here. It was expected to obtain the maximum swirl ratios for Sp v1 and Sp v2 as they showed a two-celled vortex structure with large tangential velocities. Yet, the maximum swirl ratios were computed for Clr v1 and Stc v1. Further assessments showed that the last radar scan in aforementioned volumes was limited to 200 m and 320 m AGL, respectively. This results in an underestimation of the flow rate aloft and therefore, high values of the swirl ratio.

Table 5-2: Estimated swirl ratio and its the subjectively chosen parameters for each volume.

volume	$r_{c,max}$ (m)	$V_{tan,max}$ (m/s)	r_0 (m)	Q' (m^3/s)	S
Clr v1	96	36.3	608	1472813	4.5
Hp v1	160	39	600	11267893	1.04
Hp v2	160	37.9	720	13501478	1.01
Stc v1	220	50.2	600	4091612	5.08
Sp v1	192	58.2	512	8261078	2.17
Sp v2	208	62	608	8238670	2.98

To further study the relation between full-scale and simulated tornadoes, the calculated swirl ratio values are presented in Figure 5-15 as a function of EF-Scale. Note that the overall maximum tangential velocity of each volume ($V_{tan,max}$) is used to identify the EF-

Scale as a damage-based ranking is limited to the availability if damage indicators and as can be very subjective. Taking Clr v1 and Stc v1 out of the discussion, one can infer that the swirl ratio increases as the tornado vortex intensifies which is consistent with laboratory observations. More full scale data and further investigations are needed in order to confirm this trend. Overall, discrepancies between the swirl ratios calculated using the full-scale data and the laboratory measurements are highly expected due to the uncertainties in identifying the updraft region and in the retrieved axial velocities.

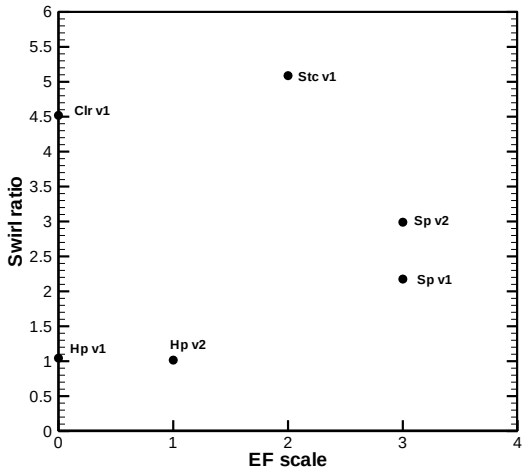

Figure 5-15: Variation of the estimated swirl ratio with the EF-Scale for each volume.

5.5 Conclusions

As a first attempt to create a database of full-scale tornado wind fields, nine volumes of single-Doppler radar data were analyzed. These volumes were selected to cover a wide range of wind speeds and vortex structures. The well-established mathematical analysis, Ground-Based Velocity Track Display (GBVTD) was implemented to reconstruct the axisymmetric three-dimensional velocity field of these tornado volumes. Identification of the vortex structures in tornadoes, i.e. single-celled vortex, vortex breakdown bubble aloft, touch-down and two-celled vortex, is of particular interest in laboratory and

numerical simulations of tornado-like vortices. Therefore, tangential velocity contour maps combined with the vertical velocity vectors, all retrieved by the GBVTD, were used to determine the vortex structure. The radial velocities were modified to remove the centrifuging effect of hydrometeors and debris. The corrections need to be performed with special caution as they can alter the flow pattern. Among the nine volumes of data studied herein, Hp v1 and Stc v1 showed single-celled characteristics, vortex breakdown bubble was evident in Clr v1 and, GC v1, GC v3, Sp v1 and Sp v2 showed two-celled vortex characteristics. Maximum velocities deduced from the full-scale data ranged between 36.3 m/s and 62 m/s. The radial profiles of the tangential velocity were compared with the modified Rankine vortex model and a good agreement was found between the full-scale measurements and the analytical model, particularly at higher altitudes. In addition, it was observed that the maximum tangential velocities increase as approaching the surface which is very different than the atmospheric boundary layer characteristics. For the first time, the swirl ratio of full-scale data was computed using the flow rate through the updraft and the maximum circulation in the flow and was related to the forensic EF-Scale. This resulted in a good agreement between the calculated swirl ratios and the vortex intensity and size. This dataset along with the calculated swirl ratios provide an insight into the flow field of tornadoes for a limited but good variety of vortex structures and intensities. Following the approach developed herein, the dataset can be extended and can be used to properly scale and simulate tornado-like vortices both physically and numerically.

References

[1] Carbin, G., 2013, "United States Tornadoes of 2012," NOAA/NWS/Storm Prediction Center.

[2] Abbott, P.L., 2002, "Natural Disasters," McGraw-Hill, pp. 422.

[3] Wind Science and Engineering Centre, 2004, "A Recommendation for an Enhanced Fujita scale (EF-Scale)," Texas Tech University, 79409-1023.

[4] Zhang, W., and Sarkar, P. P., 2012, "Near-Ground Tornado-Like Vortex Structure Resolved by Particle Image Velocimetry (PIV)," Exp. Fluids, **52**pp. 479-493.

[5] Ward, N. B., 1972, "The Exploration of Certain Features of Tornado Dynamics using a Laboratory Model," Journal of Atmospheric Sciences, **29**pp. 1194.

[6] Davies-Jones, R. P., 1973, "The Dependence of Core Radius on Swirl Ratio in a Tornado Simulator," Journal of Atmospheric Sciences, **30**pp. 1427.

[7] Davies-Jones, R. P., 1976, "Laboratory simulations of tornadoes," Anonymous **Texas Tech. University,** pp. 151-174.

[8] Church, C. R., Snow, J. T., Baker, G. L., 1979, "Characteristics of Tornado-Like Vortices as a Function of Swirl Ratio: A Laboratory Investigation," Journal of Atmospheric Sciences, **36**pp. 1175.

[9] Snow, J. T., 1982, "A Review of Recent Advances in Tornado Vortex Dynamics," Rev. Geophys., **20**pp. 953.

[10] Rotunno, R. A., 1979, "A Study in Tornado-Like Vortex Dynamics," Journal of Atmospheric Sciences, **36**pp. 140.

[11] Lewellen, W. S., and Sheng, Y. P., 1979, "Influence of surface conditions on tornado wind distribution," Preprints, 11th Conf. on Sev. Loc. Stroms, AMS, Anonymous Boston, MA, pp. 375.

[12] Lewellen, D.,C., Lewellen, W.,S., and Xia, J., 2000, "The Influence of a Local Swirl Ratio on Tornado Intensification Near the Surface," Journal of the Atmospheric Sciences, **57**(4) pp. 527-544.

[13] Kuai, L., Haan, F. L., Gallus, W. A., 2008, "CFD Simulations of the Flow Field of a Laboratory-Simulated Tornado for Parameter Sensitivity Studies and Comparison with Field Measurements," Wind and Structures, **11**(2) pp. 1-22.

[14] Davies-Jones, R.P., 1986, "Tornado dynamics. Thunderstorms morphology and dynamics," 2d ed. E. Kessler, Ed., University of Oklahoma Press, pp. 197-236.

[15] Pauley, R. L., Church, C. R., and Snow, J. T., 1982, "Measurements of Maximum Surface Pressure Deficits in Modled Atmospheric Vortices," Journal of Atmospheric Sciences, **39**pp. 368-377.

[16] Wurman, J., Randall, M., and Zahrai, A., 1997, "Design and Deployment of a Portable, Pencil-Beam, Pulsed, 3-Cm Doppler Radar," J. Atmos. Oceanic Technol, **14**pp. 1531-1539.

[17] Wurman, J., 2001, "The DOW mobile multiple-Doppler network," Preprints, 30th Conf. on Radar Meteorology, Anonymous Amer. Meteor. Soc., Munich, Germany, pp. 95-97.

[18] Wurman, J., Alexander, C., and Robinson, P., 2007, "Low Level Winds in Tornadoes and Potential Catastrophic Tornado Impacts in Urban Areas," Bull. Amer. Meteor. Soc, **88**pp. 31-46.

[19] Kosiba, K., and Wurman, J., 2013, "The Three-Dimensional Structure and Evolution of a Tornado Boundary Layer," Weather Forecasting.

[20] Rasmussen, E. N., Straka, J. M., Davies-Jones, R., 1994, "Verification of the Origins of Rotation in Tornadoes Experiment: VORTEX," Bull. Amer. Meteor. Soc., **75**pp. 995-1006.

[21] Wurman, J., Straka, J., and Rasmussen, E., 1996, "Fine Scale Doppler Radar Observation of Tornadoes," Science, **272**pp. 1774-1777.

[22] Wurman, J., and Gill, S., 2000, "Fine-Scale Radar Observations of the Dimmitt, Texas (2 June 1995) Tornado," Monthly Weather Review, February.

[23] Wurman, J., 1998, "Preliminary results from the ROTATE-98 tornado experiment," Proc. 19th Conf. on Severe Local Storms, Minneapolis, MN, Anonymous Amer. Meteor. Soc., pp. 120-123.

[24] Wurman, J., 2003, "Multiple-Doppler observations of tornadoes and tornadogenesis during the ROTATE-2003 project," Preprints, 31st Conf. on Radar Meteorology, Seattle, WA, Anonymous Amer. Meteor. Soc., pp. P4A.1.

[25] Dowell, D. C., and Bluestein, H. B., 2002, "The 8 June 1995 McLean, Texas, Storm. Part I: Observations of Cyclic Tornadogenesis," Monthly Weather Review, **130**(11) pp. 2626-2648.

[26] Bluestein, H. B., Weiss, C. C., and Pazmany, A. L., 2003, "Mobile Doppler Radar Observations of a Tornado in a Supercell Near Bassett, Nebraska, on 5 June 1999. Part I: Tornadogenesis," Monthly Weather Review, **131**(12) pp. 2954-2967.

[27] Wurman, J., Richardson, Y., Alexander, C., 2007, "Dual-Doppler Analysis of Winds and Vorticity Budget Terms Near a Tornado," Monthly Weather Review, **135**(6) pp. 2392-2405.

[28] Wurman, J., 2002, "The Multiple-Vortex Structure of a Tornado," American Meteorological Society, June pp. 473-505.

[29] Alexander, C. R., and Wurman, J., 2005, "The 30 may 1998 Spencer, South Dakota, Storm. Part I: The Structural Evolution and Environment of the Tornadoes," Monthly Weather Review, **133**(1) pp. 72-97.

[30] Lee, W. C., and Wurman, J., 2005, "Diagnosed Three-Dimensional Axisymmetric Structure of the Mulhall Tornado on 3 may 1999," American Meteorological Society, **62**pp. 2373-2393.

[31] Kosiba, K., Trapp, J., and Wurman, J., 2008, "An Analysis of the Axisymmetric Three-Dimensional Low Level Wind Field in a Tornado using Mobile Radar Observations," Geophys. Res. Lett., **35**.

[32] Kosiba, K., and Wurman, J., 2010, "The Three-Dimensional Axisymmetric Wind Field Structure of the Spencer, South Dakota, 1998 Tornado," Journal of Atmospheric Sciences, **67**pp. 3074-3083.

[33] Burgess, D. W., Magsig, M. A., Wurman, J., 2002, "Radar Observations of the 3 may 1999 Oklahoma City Tornado," Weather and Forecasting, **17**(3) pp. 456-471.

[34] Wurman, J., and Alexander, C. R., 2005, "The 30 may 1998 Spencer, South Dakota, Storm. Part II: Comparison of Observed Damage and Radar-Derived Winds in the Tornadoes," Monthly Weather Review, **133**(1) pp. 97-119.

[35] Wurman, J., Dowell, D., Richardson, Y., 2012, "The Second Verification of the Origins of Rotation in Tornadoes Experiment: VORTEX2," Bulletin of the American Meteorological Society, **93**(8) pp. 1147-1170.

[36] Wakimoto, R. M., Atkins, N. T., and Wurman, J., 2011, "The LaGrange Tornado during VORTEX2. Part I: Photogrammetric Analysis of the Tornado Combined with Single-Doppler Radar Data," Monthly Weather Review, **139**(7) pp. 2233-2258.

[37] Wakimoto, R. M., Stauffer, P., Lee, W. C., 2012, "Finescale Structure of the LaGrange, Wyoming Tornado during VORTEX2: GBVTD and Photogrammetric Analyses," Monthly Weather Review, **140**pp. 3397-3418.

[38] Atkins, N. T., McGee, A., Ducharme, R., 2012, "The LaGrange Tornado during VORTEX2. Part II: Photogrammetric Analysis of the Tornado Combined with Dual-Doppler Radar Data," Monthly Weather Review, **140**(9) pp. 2939-2958.

[39] Kosiba, K., Wurman, J., Richardson, Y., 2013, "Genesis of the Goshen County, Wyoming, Tornado on 5 June 2009 during VORTEX2," Monthly Weather Review, **141**(4) pp. 1157-1181.

[40] Lee, W. C., Jou, J. D., Chang, P. L., 1999, "Tropical Cyclone Kinematic Structure Retrieved from Single-Doppler Radar Observations. Part I: Interpretation of Doppler Velocity Patterns and the GBVTD Technique," Monthly Weather Review, **127**pp. 2419-2439.

[41] Markowski, P., Richardson, Y., Marquis, J., 2012, "The Pretornadic Phase of the Goshen County, Wyoming, Supercell of 5 June 2009 Intercepted by VORTEX2. Part I: Evolution of Kinematic and Surface Thermodynamic Fields," Monthly Weather Review, **140**(9) pp. 2887-2915.

[42] Markowski, P., Richardson, Y., Marquis, J., 2012, "The Pretornadic Phase of the Goshen County, Wyoming, Supercell of 5 June 2009 Intercepted by VORTEX2. Part II: Intensification of Low-Level Rotation," Monthly Weather Review, **140**(9) pp. 2916-2938.

[43] Marquis, J., Richardson, Y., Markowski, P., 2014, "An Investigation of the Goshen County, Wyoming, Tornadic Supercell of 5 June 2009 using EnKF Assimilation of Mobile Mesonet and Radar Observations Collected during VORTEX2. Part I: Experiment Design and Verification of the EnKF Analyses," Monthly Weather Review, **142**(2) pp. 530-554.

[44] Atkins, N. T., McGee, A., Ducharme, R., 2012, "The LaGrange Tornado during VORTEX2. Part II: Photogrammetric Analysis of the Tornado Combined with Dual-Doppler Radar Data," Monthly Weather Review, **140**(9) pp. 2939-2958.

[45] Wurman, J., Kosiba, K., and Robinson, P., 2013, "In Situ, Doppler Radar, and Video Observations of the Interior Structure of a Tornado and the Wind Damage Relationship," Bulletin of the American Meteorological Society, **94**(6) pp. 835-846.

[46] Nolan, D. S., 2012, "On the use of Doppler-Radar-Derived Wind Fields to Diagnose the Secondary Circulation of Tornadoes," Journal of Atmospheric Sciences, Preliminary Accepted Version.

[47] Storm Events Database , Www.Ncdc.Noaa.Gov/stormevents/, Aug 2013.

[48] Oye, R., Mueller, C., and Smith, C., 1995, "Software for radar translation, visualization, editing, and interpolation," Preprints, 27th Conference on Radar Meteorology, Vail, CO, Anonymous Amer. Meteor. Soc., pp. 259-361.

[49] Mohr, C. G., Jay Miller, L., Vaughan, R. L., 1986, "The Merger of Mesoscale Datasets into a Common Cartesian Format for Efficient and Systematic Analyses," Journal of Atmospheric and Oceanic Technology, **3**(1) pp. 143-161.

[50] Wood, V. T., and Brown, R. A., 1992, "Effects of Radar Proximity on Single-Doppler Velocity Signatures of Axisymmetric Rotation and Divergence," Monthly Weather Review, **120**(12) pp. 2798-2807.

[51] Dowell, D. C., Alexander, C. R., Wurman, J. M., 2005, "Centrifuging of Hydrometeors and Debris in Tornadoes: Radar-Reflectivity Patterns and Wind-Measurement Errors," Monthly Weather Review, **133**(6) pp. 1501-1524.

[52] Kepert, J., 2001, "The Dynamics of Boundary Layer Jets within the Tropical Cyclone Core. Part I: Linear Theory," Journal of the Atmospheric Sciences, **58**(17) pp. 2469-2484.

[53] Trapp, R. J., and Doswell, C. A., 2000, "Radar Data Objective Analysis," Journal of Atmospheric and Oceanic Technology, **17**(2) pp. 105-120.

[54] Majcen, M., Markowski, P., Richardson, Y., 2008, "Multipass Objective Analyses of Doppler Radar Data," Journal of Atmospheric and Oceanic Technology, **25**(10) pp. 1845-1858.

[55] Fiedler, B. H., and Rotunno, R., 1986, "A Theory for the Maximum Windspeeds in Tornado-Like Vortices," Journal of the Atmospheric Sciences, **43**(21) pp. 2328-2340.

[56] Snow, J. T., 1984, "On the Formation of Particle Sheaths in Columnar Vortices," J. Atmos. Sci, **41**pp. 2477-2491.

[57] Refan, M., and Hangan, H., 2014, "Qualitative and Quantitative Characterization of the Tornado-Like Flow Field in a New Model Scale Wind Dome," Unpublished Results, .

[58] Natarajan, D., 2011, "Numerical Simulation of Tornado-Like Vortices," PhD Thesis, the University of Western Ontario.

[59] Ying, S. J., and Chang, C. C., 1970, "Exploratory Model Study of Tornado-Like Vortex Dynamics," Journal of the Atmospheric Sciences, **27**(1) pp. 3-14.

[60] Baker, G. L., and Church, C. R., 1979, "Measurements of Core Radii and Peak Velocities in Modeled Atmospheric Vortices," Journal of Atmospheric Sciences, **36**pp. 2413-2424.

[61] Hall, M. G., 1966, "The Structure of Concentrated Vortex Cores," Prog. Aeronaut Sci., **7**pp. 53-110.

[62] Hall, M. G., 1972, "Vortex Breakdown," Annual Review of Fluid Mechanics, **4**(1) pp. 195-218.

[63] Church, C. R., and Snow, J. T., 1985, "Measuremenets of Axial Pressures in Tornado-Like Vortices," J. Atmos. Sci, **42**pp. 576-582.

Chapter 6

6 Reproducing tornadoes in laboratory using proper scaling

6.1 Introduction

The National Oceanic and Atmospheric Administration (NOAA) reported that in 2011 tornadoes killed 553 people in the United States with approximately $10 billion in damage. These recent catastrophes have led researchers to investigate the characteristics of this phenomenon in more depth.

Limited full-scale and significant numerical and experimental research has been carried out on tornado-like vortices. While extremely useful, full-scale measurements of tornado flows using Doppler radar are limited due to the dangerous environment and unpredictable path of tornadoes. Macro-scale simulations have the advantage of taking into consideration the correct physics and boundary conditions of weather events but their spatial-temporal resolution is limited mostly for the case of local storm systems such as tornadoes. On the other hand, micro-scale Computational Fluid Dynamics (CFD) methods are not capable of simulating a large domain to accommodate a tornado vortex with proper boundary conditions while resolving in detail the flow-structure interactions problems. As for the case of non-synoptic winds, properly scaled and well conducted laboratory simulations have the advantage of controllable conditions and repeatability.

The first step in simulating tornadoes is to satisfy the proper geometric, kinematic and dynamic similarities between the real flow and the simulated one. Velocity, length and time scales determined through similarity analysis will then be used to properly recreate tornado-like vortices through physical laboratory simulations and apply their flow field to models of buildings and structures to study tornado-related loading and damage. The main non-dimensional parameters [1-3] encountered in Tornado Vortex Chambers (TVC's) are the geometric ratio between the inflow height and the updraft radius ($a = h/r_0$), the velocity ratio between the far-field tangential and radial velocities termed as swirl ratio, $S = (1/2a)\, V_{tan}/V_{rad}$, and the ratio between momentum and friction forces in the

flow characterized as the radial Reynolds number (Re_r). As in many laboratory simulations of wind flows, it is generally accepted that above a certain critical value the influence of the Reynolds number on the flow is reduced.

The flow characteristics of various tornadoes vary not only in terms of maximum wind speed but also in terms of the overall flow structure. In laboratory the flow structure of tornado-like vortices is governed by the swirl ratio which remains the main non-dimensional parameter of tornado-like vortices. Real tornadoes are characterized by Fujita Scale (F-Scale) or Enhanced Fujita Scale (EF-Scale), which are forensic parameters related to damage and associated to wind speed ranges, while simulated ones are mainly characterized by the swirl ratio. It is difficult to calculate the swirl ratio for real tornadoes as this non-dimensional parameter is location dependent and in full-scale there is no clear definition of the location of the inlet/outlet boundary conditions as in a TVC. As a result, to simulate tornado-like vortices either numerically or experimentally and study the damage associated with them, it is important to search and establish a relationship between the laboratory swirl ratio and the full-scale Fujita- or Enhanced Fujita-Scale. This way, scaling parameters may be identified for each simulation and can be used for modeling different types of tornadic winds.

Baker and Church [4] measured the average maximum core velocity (V_m) and the mean updraft velocity (V_{ax}) for various swirl ratios in Purdue University vortex simulator which was 1.5 m in diameter and 0.6 m in height at the convergence zone. Since the ratio between these two velocities remained constant through a wide range of swirl ratios, they suggested that V_m/V_{ax} can be used as a scaling parameter. Recent full-scale investigations by Nolan [5] showed that radial/axial velocities deducted from single-Doppler radar data using the Ground-Based Velocity Track Display (GBVTD) method are not accurate for tornadoes rated F2 or less. As a result, using V_m/V_{ax} as a scaling parameter is not a practical approach for the most occurring tornadoes.

Mishra *et al.* [6] determined the length scale of their simulation using the core radius of the vortex near the ground. They calculated the core radius of a single-celled tornado-like vortex simulated in Texas Tech University simulator using surface pressure data and

compared the results with that of the May 1998 Manchester, SD tornado obtained through cyclostrophic momentum balance. Mishra *et al.* showed that using this length scale, the surface pressure profiles of the simulated and Manchester tornadoes are well matched and therefore, this particular simulation can be used for studying wind loading on scaled models. However, it is important that the radial profile of tangential velocity at various heights also be compared and matched in order to conclude that the simulated tornado is a valid representation of a single-celled tornado in nature. It should also be noted that obtaining pressure data from a real tornado is rare and more challenging than capturing velocity fields using radar.

Haan *et al.* [7] validated the Iowa State University (ISU) simulator through quantitative and qualitative comparisons between full-scale and simulator flow fields. They qualitatively compared the non-dimensional contour plots of simulated tornado corner flow structures at two different swirl ratios with that of Spencer [8] and Mulhall [9] tornadoes and inferred that the overall structure matches well. Also, they compared the azimuthally averaged tangential velocity profiles (hereinafter referred to as tangential velocity profile) of their simulated tornado at different swirl ratios with that of Spencer and Mulhall tornadoes at various heights and showed that the graphs match very well and collapse on each other. However, it should be noted that there are at least two geometric parameters of importance in a tornado-like vortex: the core radius at which the maximum tangential velocity happens and the height above the surface corresponding this maximum. By using non-dimensionalized graphs based on only the maximum tangential velocity and core radius, the radial profiles of tangential velocity are forced to collapse on one single graph but the height information is missing. Also, it seems that the geometric scaling of the ISU simulator is primarily determined based on the scale of the building model being used [7] and not on the scaling of the flow fields between real and simulated tornadoes.

Kuai *et al.* [10] numerically simulated the flow field of the ISU tornado simulator using Doppler radar data and laboratory velocity field measurements as boundary conditions. They evaluated the performance of a CFD model in capturing near ground flow field

characteristics of a full-scale and experimentally simulated tornado and compared the results of specific cases of numerical simulations with the tangential velocity field of the F4 rated tornado from Spencer, SD in 1998. In this comparison, the geometric and velocity length scales of the simulation were selected based on the inflow radius and maximum tangential velocity, respectively. However, there is no discussion about the similarity of the flow structure between the simulated tornado and the radar data.

Zhang and Sarkar [11] resolved the near ground structure of a simulated tornado vortex using Particle Image Velocimetry (PIV) and compared the tangential velocity profile of the simulated tornado with that of an actual tornado. In this work, Zhang and Sarkar acknowledged inherent uncertainties in the comparison approach and suggested that an extensive field database of tornadoes of various intensities and structures can overcome the existing problem in tornado simulations.

An attempt to determine a flow field relationship between simulated and full-scale tornado was made in 2008 by Hangan and Kim [12]. They proposed that by determining the overall maximum tangential velocity for a given swirl ratio and matching it with full-scale Doppler radar data, a velocity scaling could be approximated and a relationship between swirl ratio and Fujita-Scale may be obtained. Hangan and Kim compared radial profiles of the tangential velocity for numerically simulated vortices with various swirl ratios to that of the Doppler radar full-scale data from the F4 tornado, in Spencer, SD on May 30, 1998 [8]. They have considered the scaling of both the core radius and the height at which the maximum tangential velocity occurs. Hangan and Kim observed that the best fit between their tangential velocities at various heights and the full-scale data was found for a swirl ratio of approx. S=2. For the same swirl ratio (S=2), the length scales one based on the core radius and the other one based on the height corresponding the maximum tangential velocity overlapped. This matching could therefore be used to infer the existence of a relationship between a fluid mechanics parameter (swirl ratio) and a forensic tornado parameter (Fujita Scale) suggesting the possibility to scale laboratory simulations with real tornadoes. Nevertheless, this matching was only performed for one full-scale tornado.

Detailed literature review performed on tornado-like vortex simulations reveals the lack of a comprehensive and conclusive study of scaling which is mainly due to the shortage of full-scale data. In this study, a dataset of three-dimensional axisymmetric velocity fields of tornadoes obtained through a preliminary GBVTD analysis is presented. Afterwards, results of the very recent experimental simulations of tornado-like flows performed by Refan and Hangan [13] are matched with the full-scale data. Based on the matching process, the scaling ratios of simulated tornadoes and a first relationship between modeled and full-scale tornadoes are inferred.

6.2 Full-scale data

In recent years, advances with portable Doppler radars and development of mathematical models, such as the Ground-Based Velocity Track Display (GBVTD) technique [14], have enabled scientists to investigate three-dimensional velocity fields of tornadoes in nature. Although a portable Doppler radar allows for investigators to monitor unpredictable tornadoes from a safe distance, it introduces new limits for measurement. Radar waves do not follow the earth's curvature and objects on the ground can block them. Therefore, Doppler radar cannot measure regions immediately above the ground but are best suited for elevations of tens of meters above the ground.

Field projects such as VORTEX1 (1994-1995), ROTATE (1996–2001, 2003–2008 and 2012-2013), VORTEX2 (2009-2010) and ROTATE2012 (2012), allowed researchers to capture single- and dual-Doppler radar data from quite a significant number of tornadoes of various patterns and intensities. Scientists, for the first time, investigated the entire evolution of a tornado in VORTEX1. ROTATE collected single- and dual-Doppler radar data from more than 140 different tornadic events. To date, VORTEX2 remains the most ambitious filed study of tornadoes with more than 100 scientists involved. ROTATE2012 is the most recent field study of tornadoes focused on the low-level winds and therefore of great interest for the wind engineering community. The most important outcomes of these field projects are improved severe weather warnings and the collection of considerable full-scale data from tornadoes of various flow types and intensities.

The GBVTD technique was developed by Lee *et al.* [14] to retrieve the structure of a tropical cyclone using single-Doppler radar data and later, this method was used to examine the three-dimensional structure of the Mulhall tornado [9].

The GBVTD analysis is performed on a ring with the circulation center located at the center of the ring. In this method, the Doppler velocity (V_D) is expressed as a function of tangential (V_{tan}), radial (V_{rad}), translational (V_{trans}), axial (V_{ax}) and terminal (v_t) velocities of the atmospheric vortex.: $V_D = V_{trans}\, cos(\Upsilon - \theta_{trans})\, cos\varphi - V_T\, sin\psi\, cos\varphi + V_R\, cos\psi\, cos\varphi + (V_{ax} - v_t)\, sin\varphi$. where, φ is the elevation angle of the radar beam, θ_M is the direction of the mean wind flow and ψ and Υ are mathematical angles as shown in Figure 1 of the work by Lee *et al.* [14]. To simplify the problem, contributions from the terminal velocity and the axial velocity are neglected. The tangential and radial velocities consist of axisymmetric and asymmetric components and as a result, the Doppler velocity has a complex waveform that can be decomposed into Fourier terms. The GBVTD method is based on the assumption that strong axisymmetric tangential velocities dominate the flow field. After simplifying equations and implementing the complex geometrical relationship between an atmospheric vortex and a ground-based Doppler radar, a system of equations relating observed Doppler velocities to the tangential and radial velocities will be solved to construct the three-dimensional structure of a tropical cyclone. Azimuthally averaged tangential and radial velocities can be extracted using this mathematical method after identifying the center location of the vortex. Mathematical representation of this method and full assumptions are explained by Lee *et al.* [14].

Kosiba and Wurman [15] performed GBVTD analysis on data collected from Spencer, South Dakota, 1998 tornado using Doppler on Wheels (DOWs) mobile radar. Their analysis revealed a two-cell vortex structure with significant downward flow throughout the 8-min observation period and significant inflow very close to the surface.

In 2009, DOWs intercepted a long-lasting EF2 rated tornado in LaGrange, WY and obtained single-Doppler radar data throughout the whole lifetime of this tornado. Wakimoto *et al.* [16] presented photogrammetric and radar analysis of this tornado and showed that the damaging wind in the region few hundred meters above the ground

extended beyond the funnel cloud. Afterwards, Wakimoto *et al.* [17] published GBVTD analysis of June 5th, 2009 LaGrange, WY tornado combined with pictures of the funnel cloud in order to identify the relationship between the three velocity components, pressure gradients and the visual features of the tornado. They also evaluated the validity of GBVTD assumptions using dual-Doppler radar data. Wakimoto *et al.* concluded that for tornadoes with weak low-level inflow and small core radius, the retrieved radial/vertical velocity profiles near and within the core region are not accurate. Recently, Nolan [5] performed a detailed literature review on the use of GBVTD. This study confirmed that radial and vertical velocities obtained through this method are biased (especially in weak tornadoes) due to the effect of centrifuging of debris at low-levels. Nevertheless, Doppler radar and GBVTD are the most promising means to retrieve the 3D velocity field in tornadoes to date and improvements are expected.

So far, the primary goal of full-scale measurements using Doppler radar in VORTEX1 and VORTEX2 projects has been to increase the understanding of the tornado formation for future forecast applications. However, this same valuable Doppler radar data can also be used to fill the current gap in the experimental/numerical investigations of tornado flow field for wind engineering: the relationship between the simulated and field tornadoes.

Now that full-scale Doppler radar data are increasingly available, there is a good opportunity to create a database of real tornadoes velocity fields retrieved by GBVTD, and employ data to determine velocity and length scale ratios of experimental and numerical simulations.

6.3 GBVTD analysis and results

Herein, single-Doppler radar data of the Spencer, SD 1998 (F4), Stockton, KS 2005 (F1), Clairemont, TX 2005 (F0), Happy, TX 2007 (EF0) and Goshen County (LaGrange), WY 2009 (EF2) tornadoes were investigated using the GBVTD method in order to create a dataset of full-scale tornado velocity fields. These preliminary analyses are accompanied by a detailed study [18] which focuses on the GBVTD analysis of these five tornado

events with necessary corrections and examines the flow pattern for each case in more depth.

Each tornado was studied at various instants of its life cycle. In total, nine volumes of data were analyzed with the GBVTD method [14] to extract axisymmetric three-dimensional structure of the parent vortex, mainly tangential velocity profiles at various heights. The term "volume" refers to one complete radar scan of the tornado from regions very close to the ground (~20m) to hundreds of meters aloft. The number of sweeps (quasi-horizontal planes) in a volume varied between 4 and 14 with the finest elevation angle of 0.3˚. Doppler data were first interpolated to a Cartesian grid and then the vortex center coordinates were identified. The vortex center can be defined using minimum pressure, circulation or reflectivity. Herein, the circulation center was considered as the vortex center. Wood and Brown [19] studied the Doppler velocity pattern of tropical cyclones and suggested that for an axisymmetric flow field, the center of the tropical cyclone is located on a circle which passes through Doppler velocity maxima and the radar. Following this approach, the circulation centers were identified manually for every volume and at each elevation angle of the radar. The tornado circulation center at each elevation was then shifted to align centers vertically to simplify the analysis (see Figure 6-1).

Figure 6-2 shows the contour map of Doppler velocities for Happy, TX 2007 (EF0) tornado at 0203:20 UTC with the approximate location of the vortex center marked with "X". The wind field of this tornado was reconstructed by the GBVTD technique for a volume from 0203:20 UTC to 0204:17 UTC (volume 2). This volume consisted of 13 radar sweeps with elevation angle increments ranging from 0.3˚ to 2˚. Figure 6-3 demonstrates vertical velocity vectors superimposed on the contour map of tangential velocities for volume 2 in Happy, TX 2007 tornado extracted by the GBVTD method. It is observed that the tangential velocity approaches its maximum of 37.9 m/s at regions very close to the ground with corresponding core radius of 160 m. The strong central downdraft aloft is weakening as reaching the ground and the overall vertical flow pattern

suggests that the vortex break-down bubble formed aloft has just touched the ground and the flow has become fully turbulent.

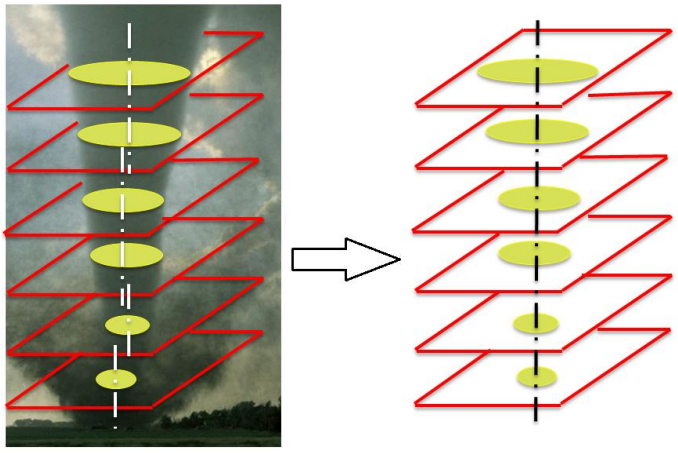

Figure 6-1. The process of identifying the tornado circulation center at each elevation and then shifting the centers to align them vertically.

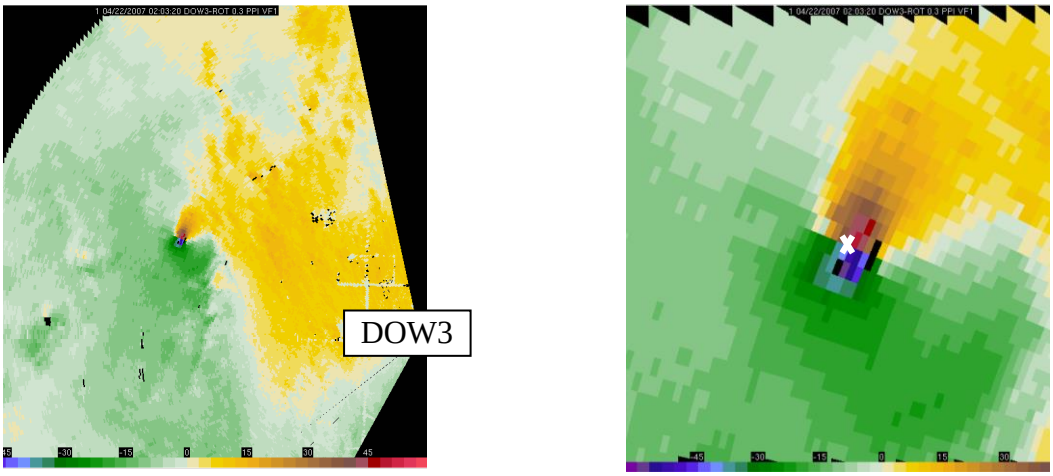

a) **b)**

Figure 6-2: Doppler velocity contours for volume 2 in Happy, TX 2007 tornado with a) radar location indicated and b) circulation center marked.

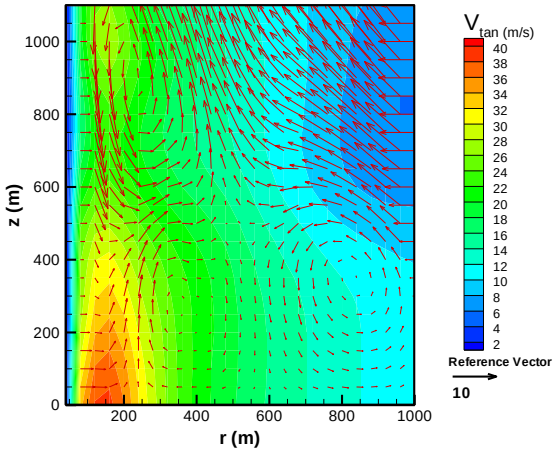

Figure 6-3: Vertical velocity vectors superimposed on tangential velocity contours for volume 2 in Happy, TX 2007 tornado.

The full-scale database created herein, consists of GBVTD-retrieved velocity profiles at various heights above the ground for 9 volumes of Doppler-radar data. Table 6-1 summarizes the GBVTD analysis results for each volume and provides damage- and velocity-based F/EF-Scales for each event. In this table, the radar data volumes are sorted in an increasing overall maximum tangential velocity value order. The Storm Events Database [20] was used to determine the F/EF ratings for each tornado based on the damage. However, assessing the intensity level of a tornado based on damage surveys is subjective, with various parameters, such as damage markers in the region and quality of structures, contributing to the complexity of the process. As a result, in this work only the velocity range associated with each category of the Enhanced Fujita Scale was used to categorize each volume of data. For instance, Goshen County (LaGrange), WY 2009 tornado was rated EF2 based on the damage survey while, volume 1 in this event was rated EF1 based on the maximum tangential velocity retrieved for that volume. Herein the rating of the tornado event was done based on maximum tangential velocity and has been kept consistent through the analysis. Radar volumes categorized as EF0-EF3, based on the maximum tangential velocity extracted by GBVTD, are presented in an increasing EF order in Table 6-1. The translational speed of each tornado as well as the flow

structure of each volume is also presented in this table. Translational speed was determined by estimating the distance that tornado center had traveled over a certain period of time. Hereafter, the abbreviations provided in Table 6-1 are used to refer to each volume of data. In order to identify the structure of the tornado, vertical velocity profiles for each volume extracted by GBVTD were compared with experimental observations of the flow field reported by Davies-Jones *et al.* [21].

Table 6-1: Summary of GBVTD analysis results for various volumes of radar data.

Event	Intensity (damage)	Abbreviation	$V_{tan,max}$ (m/s)	V_{trans} (m/s)	Intensity (velocity)	Structure
Clairemont, volume 1	F0	Clr v1	36.3	1.2	EF0	Vortex Break-down bubble aloft
Happy, volume 2	EF0	Hp v2	37.9	19.4	EF0	Touch-down
Happy, volume 1	EF0	Hp v1	39	19.4	EF1	Single-celled
Goshen County, volume 1	EF2	GC v1	41.6	9.49	EF1	Two-celled
Goshen County, volume 2	EF2	GC v2	42	9.49	EF1	Vortex Break-down bubble aloft
Goshen County, volume 3	EF2	GC v3	42.9	9.49	EF1	Two-celled
Stockton, volume 1	F1	Stc v1	50.2	10.95	EF2	Single-celled
Spencer, volume 1	F4	Sp v1	58.2	15	EF3	Two-celled
Spencer, volume 2	F4	Sp v2	62	15	EF3	Two-celled

6.4 Experimental simulations data

Comprehensive experimental data provided by Refan and Hangan [13] were employed for the scaling practice. They performed experimental investigations of tornado-like vortices using the Model WindEEE Dome (MWD) apparatus at Western University. MWD, the 1/11 scaled model of the WindEEE Dome, was designed, constructed and commissioned in 2010. It is a closed-loop three-dimensional "wind dome" made out of one hexagonal testing chamber (TC on Figure 6-4) with 100 fans distributed on the periphery, surrounded by a hexagonal return circuit (RC). Above the TC, a 3rd hexagonal ceiling chamber (CC) has another set of fans on the periphery (3x6 = 18). Each fan can be controlled individually and the upper fans are reversible. Adjustable vanes that are installed in front of all lower fans can be used to produce the desired swirl. The tornado-like vortices are generated in this simulator using top fans to provide updraft and periphery vanes at the lower chamber to control the swirl. The flow visualizations inside the simulator have shown that this configuration results in single-celled and two-celled tornado-like vortices.

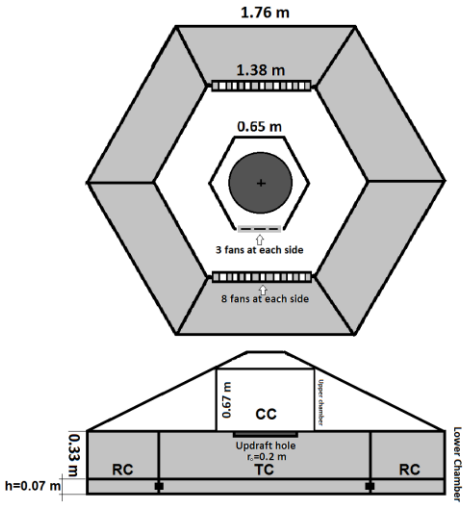

Figure 6-4: Schematic drawing of the MWD demonstrating TC, RC and CC zones.

In order to characterize the flow field in MWD, Refan and Hangan [13] carried out PIV measurements at eight horizontal planes over the height of the vortex. All experiments were performed at a constant flow rate and inflow depth. The updraft radius was set to 20 cm, which corresponds to a=0.35. Refan and Hangan measured swirl ratio, mean velocities and the tornado vortex core radius. They showed that tornado-like vortices with swirl ratios ranging from 0.12 to 1.29 can be generated in MWD. In addition, they captured a laminar single-celled vortex at S=0.12, a vortex breakdown bubble formation at S=0.35, a touch-down at S=0.57 and a fully turbulent two-celled vortex at S=0.96 or higher. Details on the MWD design and PIV experiments performed in this simulator are presented in [13].

6.5 Similarity analysis

6.5.1 Length and velocity scale ratios

In order to properly reproduce a tornado and then model a structure in a tornado simulator, a measureable geometric length scale (λ_l) should be determined. There are various geometric lengths in a tornado simulator such as updraft radius, inflow depth, core radius, inner chamber height as well as the core radius and the height corresponding the maximum tangential wind speed (r_c and Z_{max}, respectively). Among these lengths, only two are measureable in a real tornado; the core radius and the height corresponding the maximum tangential velocity. Therefore two length scale ratios are defined as the ratios between full-scale Doppler radar (index D) and Simulation (index S) data: $r_{c,D}/r_{c,S}$ and $Z_{max,D}/Z_{max,S}$.

As the radial Reynolds number of a real tornado is many orders of magnitude larger compared to those of generated ones, it can be concluded that dynamic scaling requirements are not satisfied. However, Ward [1], Davies-Jones [22], Jischke and Parang [2] and Church *et al.* [3] showed that for a given geometry and for a smooth surface, if the radial Reynolds number is large enough to ensure turbulent flow, the core radius and the transition from a single vortex to multiple vortices are independent of the radial Reynolds number and are strongly a function of swirl ratio. Since the dynamic

similarity is not satisfied in tornado simulations, the velocity scale (λ_v) needs to be determined independent of the radial Reynolds number condition. Tangential, axial and radial velocity components of an actual tornado can be deducted using the GBVTD technique. However, as previously addressed, radial and axial components calculated by this method are questionable, especially for weaker tornadoes. As a result, the ratio between the overall maximum tangential velocity of a real tornado and that of a simulated one ($V_{tan,max,D}/V_{tan,max,S}$) are used here to determine the velocity length scales for each simulated tornado.

6.5.2 Matching process

The single-Doppler radar data were analyzed using the GBVTD method and the resulting velocity fields were then matched with that of the physical simulations at Western to establish a relationship between simulated and real tornadoes. The matching process was performed on experimental simulations data from MWD for swirl ratios ranging from 0.12 to 1.29.

The overall maximum tangential velocity of the simulated tornado over various heights for a given swirl ratio, $V_{tan,max} = V_{tan}(r_{c,max}, z_{max})$, was determined and then compared with that of the full-scale measurements. This way, the velocity scaling could be approximated. Afterwards, the core radius and the height corresponding the overall maximum tangential velocity for the simulated vortex ($r_{c,max,S}$ and $z_{max,S}$, respectively) at each swirl ratios were compared to their counterparts in the natural tornado ($r_{c,max,D}$ and $z_{max,D}$, respectively) which resulted in two length scale ratios. Since in fluid mechanics simulations the length scale must be a single value, it is expected that the two length scale ratios converge towards one value at a certain swirl ratio. This is a key condition that, if satisfied, may then be used to relate swirl to Fujita Scale and therefore modeled tornado-like vortices (experimental or numerical) to full-scale tornadoes.

Figure 6-5 shows the length scale ratios as a function of the swirl ratio for nine tornadic events. As the swirl ratio increases, the two length scales show a clear converging behaviour for Hp v2, GC v1, GC v3 and higher EF ranking events. However, a different

trend is observed for Clr v1, Hp v1 and GC v2 events: the two length scales intersect at a certain swirl ratio. The swirl ratio at which the convergence or intersection occurs is considered to represent the swirl ratio of the real tornado. The following matching procedure is applied: (i) if there is a range of swirl ratios (rather than a single value) over which convergence/intersection occurs, the chosen swirl ratio is based on the vital structure of the tornado (i.e. single-celled, two-celled tornado, etc.), (ii) if there is a range of convergence that is consistent with the structure of the real vortex, the experimental results are scaled up using length scales corresponding to that range of swirl ratios and the radial profiles of the tangential velocities at various heights are compared to the ones extracted from the full-scale data. The length scale resulted in the most accurate estimation of the maximum tangential velocity and the corresponding core radius is then selected to represent the geometric scaling of the simulation. This point by point procedure has been applied to all the tornado volumes, and (iii) if the difference between the two length scale ratios at the convergence is significant, the priority is given to the length scale determined using $r_{c,max,D}/r_{c,max,S}$. This is due to the negligible variation of the maximum tangential velocity with height within several tens of meters close to the ground in real tornadoes. Also, the core radius is responsible for the wind shear experienced by a structure that is passed by the inner region of a tornado.

6.6 Results and discussion

6.6.1 Length scale

Figure 6-5a displays that the length scales intersect for $0.12<S<0.22$ for Clr v1. The full-scale data of Clr v1 showed a single-celled vortex with break-down bubble aloft. This structure corresponds to a simulated vortex in MWD with $0.22\leq S<0.57$. Therefore, it can be inferred that $S=0.22$ is a better match for Clr v1. Also, the difference between the two length scale ratios is significant at $S=0.22$. Based on the matching criteria, the priority was given to the length scale determined using $r_{c,max,D}/r_{c,max,S}$ and the length scale ratio of 3711 was selected for the Clr v1 event.

Figure 6-5c suggests that the swirl ratio of Hp v1 is 0.22 which is consistent with the one-celled structure of the full-scale vortex. The two length scales converge on swirl ratios ranging from 0.57 to 1.29 for Hp v2 and GC v1 events (see Figure 6-5b and Figure 6-5d). Based on the GBVTD-retrieved velocity fields, the Hp v2 is at the touch-down stage while the GC v1 is a two-celled vortex with a clear downdraft at the centerline. As a result, the length scales associated with S=0.57 and S=0.73 were chosen for Hp v2 and GC v1 events, respectively. However, further investigations are required to support the swirl ratio value selected for the GC v1 as two-celled vortices have been captured in MWD for swirl ratios higher than 0.57. Figure 6-5e demonstrates that the two scaling ratios match well at S=0.35 for GC v2. This swirl ratio is consistent with the vertical flow pattern of GC v2 which is estimated to be right before the penetration of the turbulent breakdown bubble. Based on the GBVTD analysis, the GC v3 has two-celled vortex characteristics with slightly higher velocities when compared to GC v1. The convergence swirl ratio of 0.96 for GC v3, as seen in Figure 6-5f, is supported by the structure of the flow.

A convergence trend in the length scale values of the Stc v1 is detected for S>0.57. The Stc v1 is a single-celled vortex with strong and broad rotation and with the overall maximum tangential velocity close to the surface. This pattern is consistent with a vortex after the transition from laminar to turbulent in which the vortex core broadens and velocities intensify. For Sp v1 and Sp v2 volumes, the two length scales almost converge at S=1.14-1.29. These volumes have shown two-celled structures which is consistent with the range of convergence. Therefore, the length scales for Stc v1, Sp v1 and Sp v2 will be selected (as stipulated in the matching criteria) based on the best match achieved between the simulation and the full-scale tangential velocity profiles.

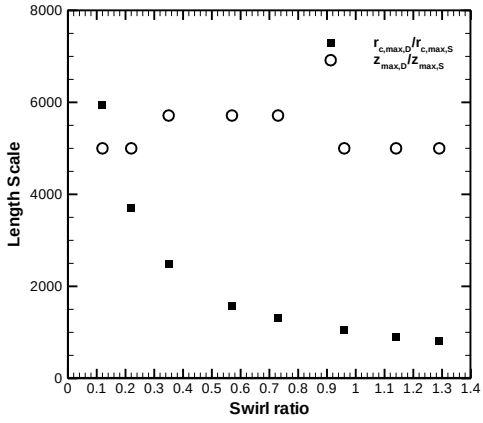
Length Scale
Swirl ratio
$r_{c,max,D}/r_{c,max,S}$
$z_{max,D}/z_{max,S}$

a)

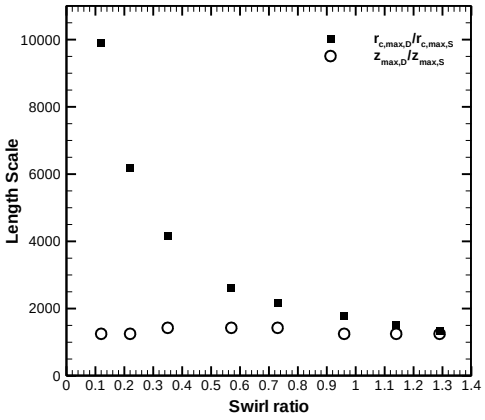
Length Scale
Swirl ratio
$r_{c,max,D}/r_{c,max,S}$
$z_{max,D}/z_{max,S}$

b)

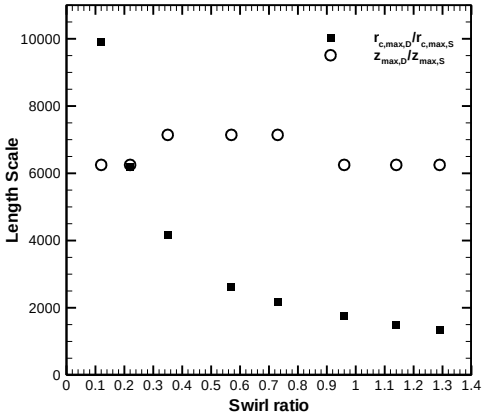
Length Scale
Swirl ratio
$r_{c,max,D}/r_{c,max,S}$
$z_{max,D}/z_{max,S}$

c)

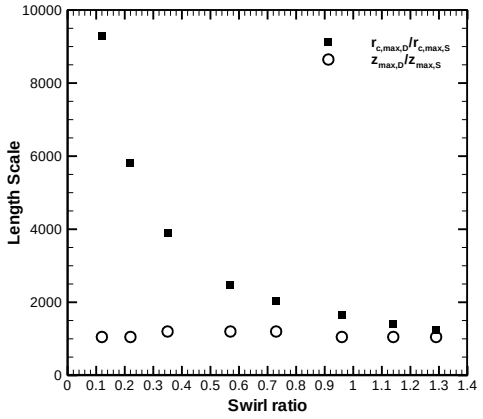
Length Scale
Swirl ratio
$r_{c,max,D}/r_{c,max,S}$
$z_{max,D}/z_{max,S}$

d)

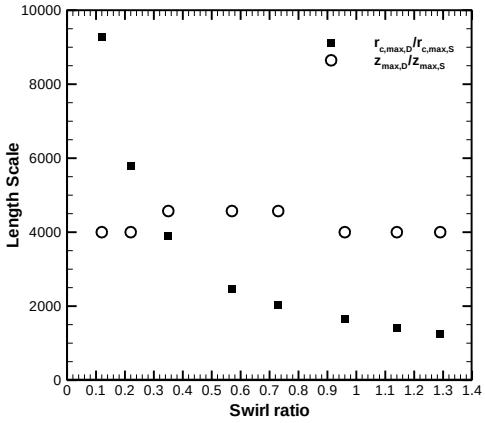
Length Scale
Swirl ratio
$r_{c,max,D}/r_{c,max,S}$
$z_{max,D}/z_{max,S}$

e)

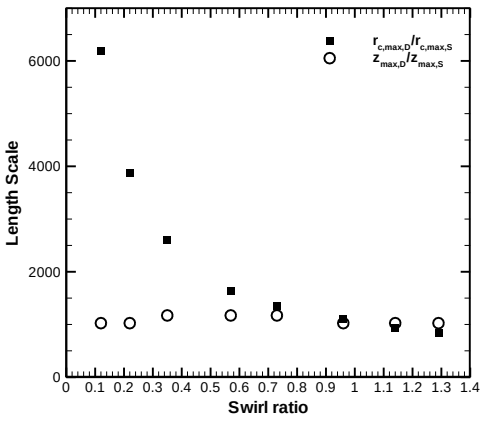
Length Scale
Swirl ratio
$r_{c,max,D}/r_{c,max,S}$
$z_{max,D}/z_{max,S}$

f)

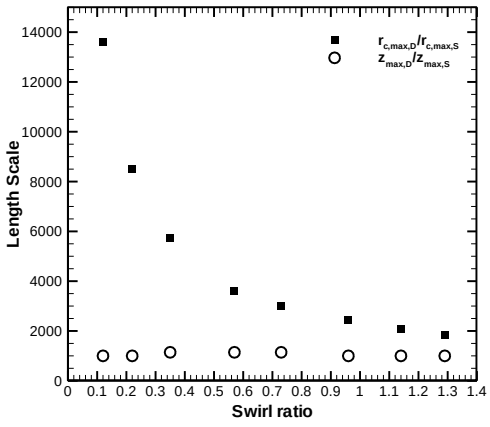

g)

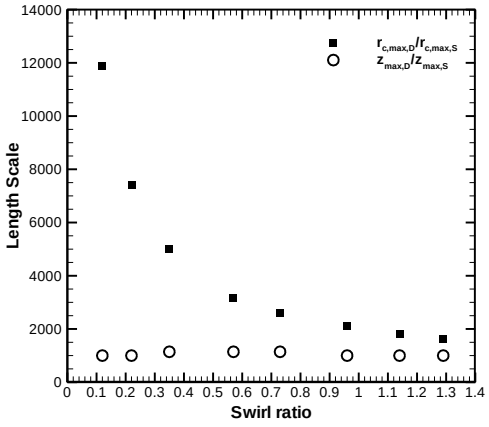

h)

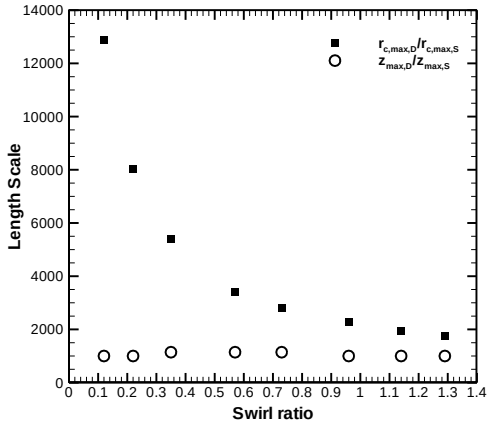

i)

Figure 6-5: Geometric scaling ratio as a function of swirl ratio for various volumes of full-scale data; a) Clr v1, b) Hp v2, c) Hp v1, d) GC v1, e) GC v2, f) GC v3, g) Stc v1, h) Sp v1 and i) Sp v2.

Figure 6-6 shows variations of the length scale with the swirl ratio for 9 volumes of radar scan. It is observed that as the swirl ratio increases, the length scale decreases. Also for the Clr v1, Hp v1 and GC v2 events that have swirl ratios less than 0.57, the length scale varies significantly from one event to another. However for volumes with swirl ratios higher than 0.57, the length scale does not greatly change. This trend can be explained by variations of the vortex structure with the swirl ratio in MWD and in real tornadoes. This

starts with a thin laminar core for very small swirls followed by a turbulent vortex break-down aloft for small swirls. By further increasing the swirl ratio, the vortex break-down bubble touches the ground, the flow becomes turbulent and maximum velocities move towards the ground. In MWD the vortex touch-down occurs at $S \approx 0.57$. Before the touch-down, the flow is highly unstable as it consists of three distinct dynamic regions: turbulent sub-critical region aloft followed by the break-down bubble in the middle and the narrow super-critical core close to the ground. As a result of the instabilities associated with the vortex break-down bubble and the transition from laminar to turbulent flow, one can expect considerable variations in the vortex characteristics and structure for swirl ratios less than 0.57.

Evaluation of the GBVTD-retrieved velocity fields along with the determined swirl ratios reveals that in Clr v1, Hp v1 and GC v2 events, the tornado vortex break-down bubble has not yet touched the ground. These events demonstrate single-celled structure with the vortex break-down bubble aloft. The maximum tangential velocity of Clr v1, Hp v1 and GC v2 events that is observed at higher elevations, when compared with other events, also confirms the existence of a laminar core with break-down bubble aloft. As a result, the length scale varies significantly, between 2600 and 6200, from one event to another. On the other hand, the tornado vortex in the GC v1, GC v3, Stc v1, Sp v1 and Sp v2 volumes is fully turbulent with a two-celled vortex pattern in some cases and therefore, the length scale variation is limited to 1100-2900 range.

Considering instabilities and transitions happening in the flow for swirl ratios less than 0.57 as well as the trend observed in Figure 6-6, one can divide the flow, for simulation purposes, into two categories; before and after the touch-down. While before touch-down there is a clear variability in the length scale, after touch-down the length scale may be considered quasi constant. Therefore, the average length scale of 1550 can be used for simulating mid-range EF1 to low-end EF3 rated tornadoes in MWD with fully turbulent flow characteristics.

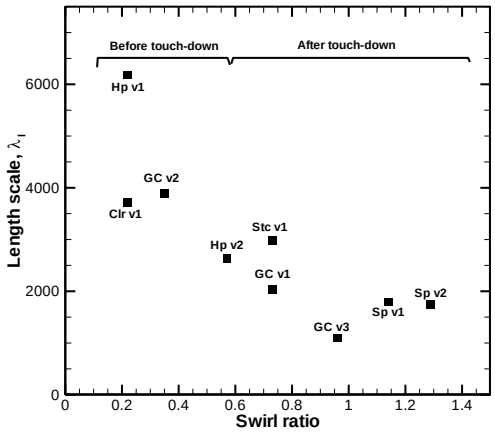

Figure 6-6: Length scales of the simulation as a function of swirl ratio.

6.6.2 Velocity scale

The experimentally measured tangential velocities reported by Refan and Hangan [13] are averaged over azimuth and time. The averaging time of the PIV measurements equals to the number of vector maps (2000) times the duration of acquiring one vector map (2/30Hz) which equals to approximately 132 sec. The length scale of simulating mid-range EF1 to low-end EF3 rated tornadoes in MWD was estimated to be λ_l=1/1550. Providing that the typical velocity scale of tornado simulations, based on F2 tornado wind speeds, is equal to λ_v=1/7.7 [7], the time scale of simulation is equal to λ_t=0.005. Therefore, an averaging time of 132 sec of PIV velocity measurements scales up to an averaging time of 26,400 s (7.2 hrs) of full-scale velocity data. This scaled up averaging time is far from reality as tornadoes usually last less than 30 min. Moreover, full-scale velocity data are instantaneous measurements even though it takes approximately 3 sec for a Doppler radar to scan the flow at a given beam angle. Therefore, direct comparison of current PIV measurements with full-scale velocity data is not possible. Two factors contribute to this issue: first, the low sampling rate of the PIV system and second, the small length scale of simulations.

In order to compare the PIV results with the full-scale data, it is necessary to account for the effect of averaging time on velocity values. The Durst curve [23] serves this purpose. This curve relates wind velocities averaged over *t* second to wind velocities, from the same storm, averaged over 3600 s (one hour). The velocity ratio between one second to 3600 s averaging time determined from the Durst curve (V_1/V_{3600}=1.57) can be used to adjust instantaneous wind velocities of full–scale data to equivalent wind velocities averaged over one hour. Note that Durst curve was developed for atmospheric boundary layer flows and there is a need to develop a similar curve for non-synoptic winds. In the meantime, the Durst curve provides an opportunity to compare velocity data from a 30 Hz PIV system to Doppler radar measured wind velocities as the velocity adjustment ratio is 1 for an averaging time of one hour or higher. Future work in the WindEEE Dome facility will benefit from larger simulation scale as well as time resolved PIV measurements. This will alleviate the velocity scaling issues raised herein.

Following the matching criteria, the length and velocity scale ratios corresponding to the convergence swirl ratios were determined and further implemented to scale up the experimental simulations of tornadoes. Figure 6-7 illustrates radial profiles of the tangential velocity as a function of height for simulated tornadoes (lines) compared with that of the full-scale (symbols). Overall, the laboratory simulated vortex well matches the full-scale one. This agreement is observed for the core radius and the corresponding tangential velocity at different heights.

The poorer match for the outer vortex core region, which is observed in some cases, is attributed to the effect of the boundary conditions. Experimental simulations use generic conditions and are limited in domain while the full-scale events have complex boundary conditions and are not limited in size. In addition, there are fluctuations in the tangential velocity values in the outer core region of the vortices with S=0.73-1.29. This is the result of the relatively large vortex core and the limited field of view in the experimental measurements.

The swirl ratio associated with each event is also noted in Figure 6-7. The accuracy of the length scale of the simulation and the corresponding swirl ratio for cases with a range of

convergence was further evaluated. Results are reported here for the Hp v2 event as the convergence was observed over a relatively wide range of swirl ratios ($0.57<S<1.29$) for this volume. The radial profiles of the tangential velocity obtained from the experiments were scaled up using the length scales associated with S=0.57-1.29. These experimental velocity profiles are compared with the full-scale data at z=100 m and are depicted in Figure 6-8. It is evident that the overall match between the physical simulations and the full-scale data is deteriorating as the swirl ratio increases. Therefore, the Hp v2 event can be reproduced in MWD with a tornado-like vortex with S=0.57. Following this approach, the swirl ratio associated with Stc v1, Sp v1 and Sp v2 were determined as 0.73, 1.14 and 1.29, respectively.

The velocity scale variation with swirl ratio is illustrated in Figure 6-9 for different volumes of full-scale data. It is seen that, with the exception of the two-celled vortices, i.e. Sp v1 and Sp v2, variation of the velocity scale with the swirl ratio can be considerd quasi-constant which has positive implications for the practical aspects of tornado simulations.

In order to identify a relationship between the simulated and full-scale tornadoes, the variation of the velocity-based EF-Scale with swirl ratio is presented in Figure 6-10 for nine volumes. This figure shows that the full-scale tornado vortex intensifies as the swirl ratio increases. Similar to the length scale trend, there is an apparent variability in the intensity of the vortices before touch-down. As expected, after the touch-down there is a linear relationship between the swirl ratio and the EF-Scale which validates the overall matching process.

The relationship between the swirl ratio and the EF-Scale observed in Figure 6-10 along with the length scale variation with the swirl ratio showed in Figure 6-6 enables reproducing tornado-like vortices in MWD using proper scaling. It is concluded that, the tornado-like vortices simulated in MWD with $0.12<S\leq0.57$ are representatives of EF0 to low-end EF1 rated tornadoes in nature and the ones simulated in MWD with $0.57<S<1.29$ correspond to full-scale tornadoes with mid-range EF1 to low-end EF3 intensity rating.

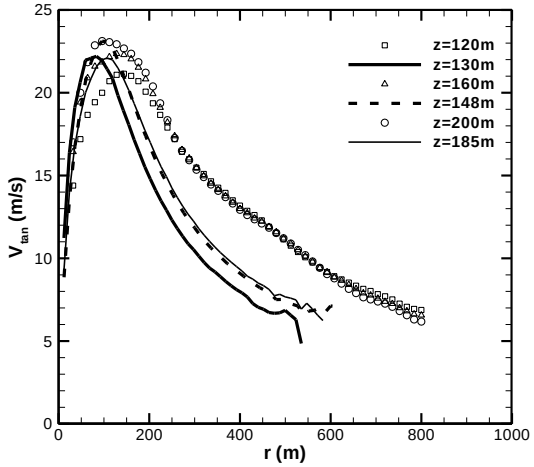
z=120m
z=130m
z=160m
z=148m
z=200m
z=185m
V_tan (m/s)
r (m)

a)

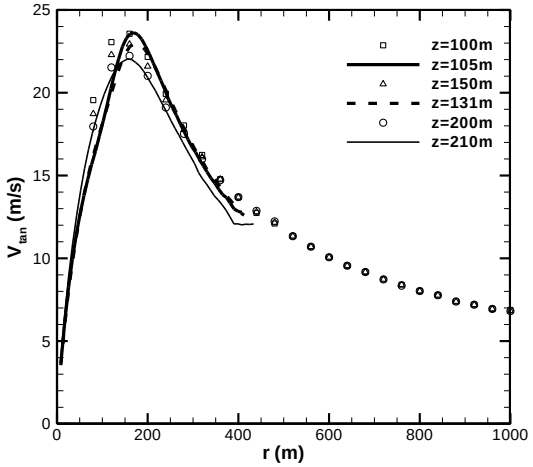
z=100m
z=105m
z=150m
z=131m
z=200m
z=210m
V_tan (m/s)
r (m)

b)

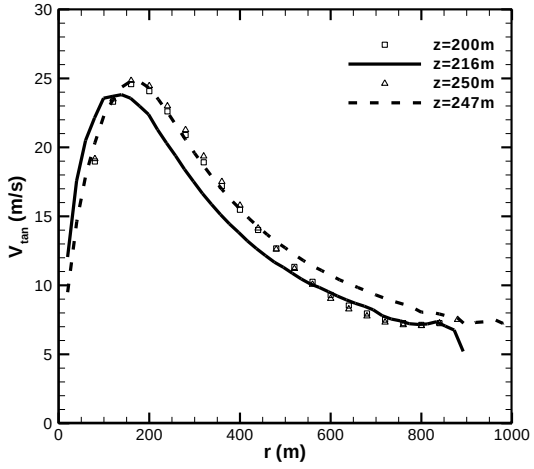
z=200m
z=216m
z=250m
z=247m
V_tan (m/s)
r (m)

c)

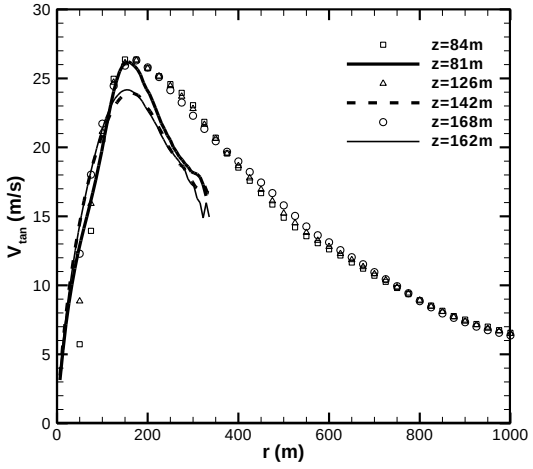
z=84m
z=81m
z=126m
z=142m
z=168m
z=162m
V_tan (m/s)
r (m)

d)

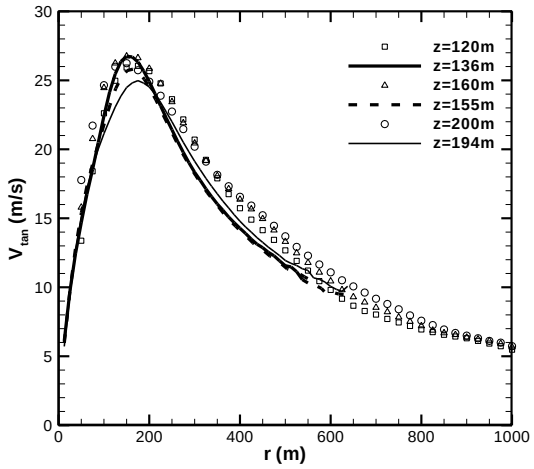
z=120m
z=136m
z=160m
z=155m
z=200m
z=194m
V tan (m/s)
r (m)

e)

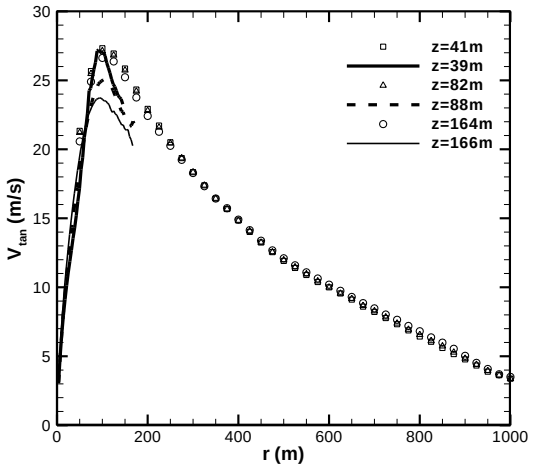
z=41m
z=39m
z=82m
z=88m
z=164m
z=166m
V tan (m/s)
r (m)

f)

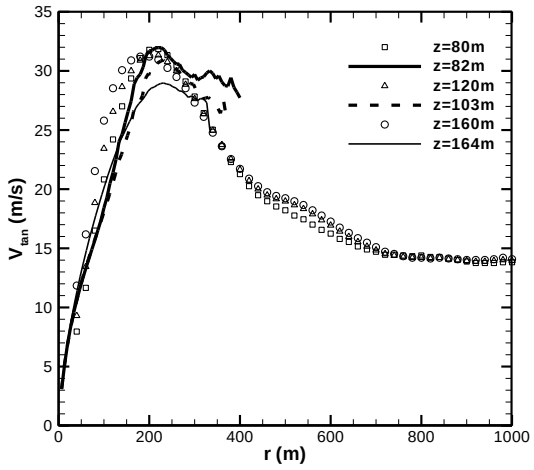
z=80m
z=82m
z=120m
z=103m
z=160m
z=164m
V tan (m/s)
r (m)

g)

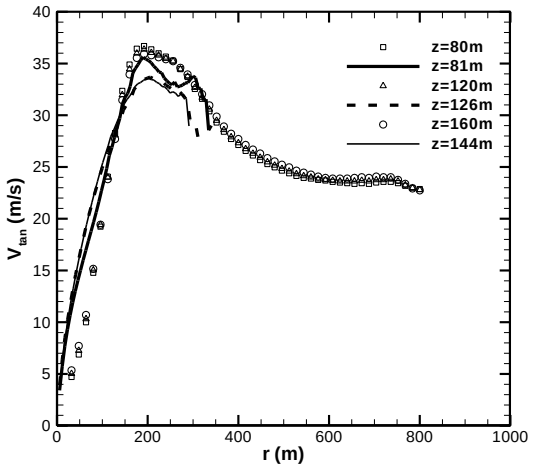
z=80m
z=81m
z=120m
z=126m
z=160m
z=144m
V tan (m/s)
r (m)

h)

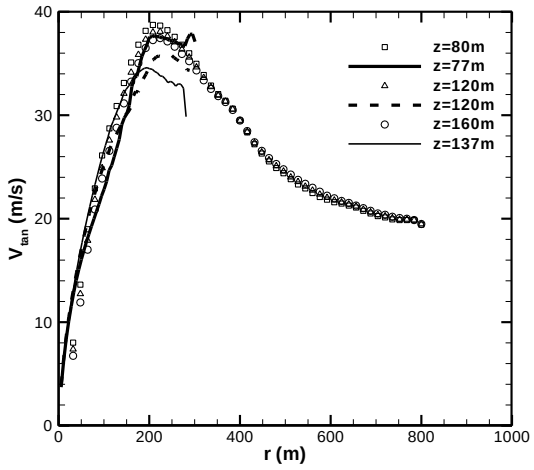

i)

Figure 6-7: Comparison between simulated (lines) and full-scale (symbols) tangential velocity profiles at various heights for nine radar volumes after applying the velocity and length scales; a) Clr v1: S=0.22, b) Hp v2: S=0.57, c) Hp v1: S=0.22, d) GC v1: S=0.73, e) GC v2: S=0.35, f) GC v3: S=0.96, g) Stc v1: S=0.73, h) Sp v1: S=1.14 and i) Sp v2: S=1.29.

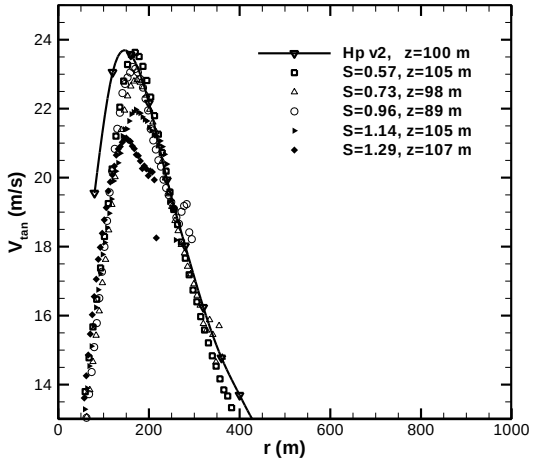

Figure 6-8: Tangential velocities of the experimental simulations at various swirl ratios compared with that of Hp v2.

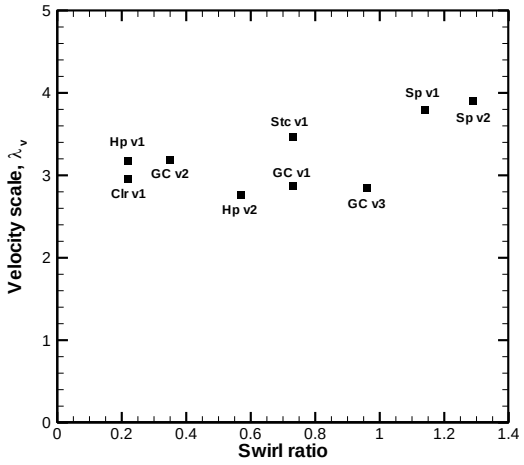

Figure 6-9: Velocity scales of the simulation as a function of swirl ratio.

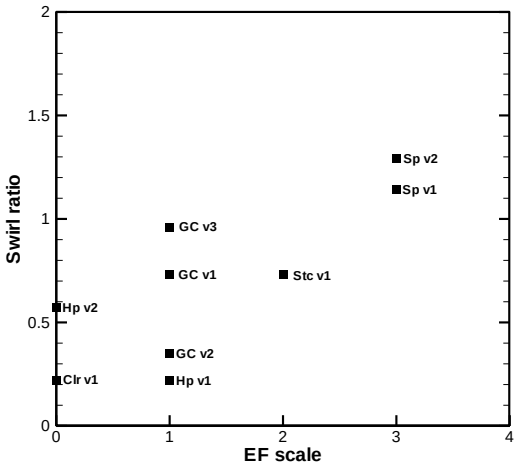

Figure 6-10: Potential relationship between swirl ratio and EF-Scale.

6.7 Conclusions

For the first time, a dataset of velocity fields of real tornadoes was analyzed to investigate the relationship between laboratory simulations of tornado-like vortices and real

tornadoes. This full-scale dataset consists of single-Doppler radar data of tornadoes with intensities varied between EF0 and EF3 based on the maximum tangential velocity. Data were collected by DOWs during VORTEX and ROTATE projects and analyzed by the GBVTD method to reconstruct the three-dimensional axisymmetric wind field structure of the tornadoes.

In an attempt to determine the velocity and length scale ratios of the simulations, the full-scale data were compared with experimental results of tornado-like vortices. These simulations were conducted in a 1/11 scaled replica of the WindEEE Dome at Western University and the results were provided by Refan and Hangan [13]. It was observed that for a given volume of full-scale data, the two length scales, one based on the core radius (r_c) and the other one based on the height corresponding the maximum tangential velocity (z_{max}), generally converge towards one value at a certain swirl ratio. Based on this, the geometric scaling of the experiments was determined and the swirl ratio of the real tornado was identified. Further investigations confirmed that the swirl ratio suggested by the convergence point also matches the flow pattern of the real tornado.

Based on the comparison of tangential velocity profiles at various heights presented here, the tornado-like vortices simulated in MWD with swirl ratios ranging from 0.12 to 1.29 appear to be representatives of EF0 to EF3 rated tornadoes in nature. In addition, it was concluded that the average length scale of the simulation in MWD for mid-range EF1 to low-end EF3 rated tornadoes with fully turbulent flow characteristics is 1550. This conclusion can be extended to higher intensity tornadoes once the GBVTD analysis results for high-end EF3 to EF5 tornadoes are available.

References

[1] Ward, N. B., 1972, "The Exploration of Certain Features of Tornado Dynamics using a Laboratory Model," Journal of Atmospheric Sciences, **29**pp. 1194.

[2] Jischke, M. C., and Parang, M., 1974, "Properties of Simulated Tornado-Like Vortices," J. Atmos. Sci., **31**pp. 506.

[3] Church, C. R., Snow, J. T., Baker, G. L., 1979, "Characteristics of Tornado-Like Vortices as a Function of Swirl Ratio: A Laboratory Investigation," Journal of Atmospheric Sciences, **36**pp. 1175.

[4] Baker, G. L., and Church, C. R., 1979, "Measurements of Core Radii and Peak Velocities in Modeled Atmospheric Vortices," Journal of Atmospheric Sciences, **36**pp. 2413-2424.

[5] Nolan, D. S., 2012, "On the use of Doppler-Radar-Derived Wind Fields to Diagnose the Secondary Circulation of Tornadoes," Journal of Atmospheric Sciences, Preliminary Accepted Version.

[6] Mishra, A. R., Jamesa, D. L., and Letchford, C. W., 2008, "Physical Simulation of a Single-Celled Tornado-Like Vortex, Part A: Flow Field Characterization," J. Wind Eng. Ind. Aerodyn., **96**pp. 1243.

[7] Haan Jr, F. L., Sarkar, P. P., and Gallus, W. A., 2008, "Design, Construction and Performance of a Large Tornado Simulator for Wind Engineering Applications," Engineering Structures, **30**pp. 1146.

[8] Wurman, J., and Alexander, C. R., 2005, "The 30 may 1998 Spencer, South Dakota, Storm. Part II: Comparison of Observed Damage and Radar-Derived Winds in the Tornadoes," Monthly Weather Review, **133**(1) pp. 97-119.

[9] Lee, W. C., and Wurman, J., 2005, "Diagnosed Three-Dimensional Axisymmetric Structure of the Mulhall Tornado on 3 may 1999," American Meteorological Society, **62**pp. 2373-2393.

[10] Kuai, L., Haan, F. L., Gallus, W. A., 2008, "CFD Simulations of the Flow Field of a Laboratory-Simulated Tornado for Parameter Sensitivity Studies and Comparison with Field Measurements," Wind and Structures, **11**(2) pp. 1-22.

[11] Zhang, W., and Sarkar, P. P., 2012, "Near-Ground Tornado-Like Vortex Structure Resolved by Particle Image Velocimetry (PIV)," Exp. Fluids, **52**pp. 479-493.

[12] Hangan, H., and Kim, J., 2008, "Swirl Ratio Effects on Tornado Vortices in Relation to the Fujita Scale," Wind and Structures, **11**(4) pp. 291.

[13] Refan, M., and Hangan, H., 2014, "Qualitative and Quantitative Characterization of the Tornado-Like Flow Field in a New Model Scale Wind Dome," Unpublished Results.

[14] Lee, W. C., Jou, J. D., Chang, P. L., 1999, "Tropical Cyclone Kinematic Structure Retrieved from Single-Doppler Radar Observations. Part I: Interpretation of Doppler Velocity Patterns and the GBVTD Technique," Monthly Weather Review, **127**pp. 2419-2439.

[15] Kosiba, K., and Wurman, J., 2010, "The Three-Dimensional Axisymmetric Wind Field Structure of the Spencer, South Dakota, 1998 Tornado," Journal of Atmospheric Sciences, **67**pp. 3074-3083.

[16] Wakimoto, R. M., Atkins, N. T., and Wurman, J., 2011, "The LaGrange Tornado during VORTEX2. Part1: Photogrammetric Analysis of the Tornado Combined with Single-Doppler Radar Data," Monthly Weather Review, **139**pp. 2233-2258.

[17] Wakimoto, R. M., Stauffer, P., Lee, W. C., 2012, "Finescale Structure of the LaGrange, Wyoming Tornado during VORTEX2: GBVTD and Photogrammetric Analyses," Monthly Weather Review, **140**pp. 3397-3418.

[18] Refan, M., Kosiba, K., Wurman, J., 2014, "Three-Dimensional Axisymmetric Wind Field Structure of Five Tornado Events," Unpublished Results, .

[19] Wood, V. T., and Brown, R. A., 1992, "Effects of Radar Proximity on Single-Doppler Velocity Signatures of Axisymmetric Rotation and Divergence," Monthly Weather Review, **120**(12) pp. 2798-2807.

[20] Storm Events Database , Www.Ncdc.Noaa.Gov/stormevents/, Aug 2013.

[21] Davies-Jones, R. R., Trapp, J., and Bluestein, H. B., 2001, "Tornadoes and Tornadic Storms," Meteorological Monographs, (50) pp. 167.

[22] Davies-Jones, R. P., 1973, "The Dependence of Core Radius on Swirl Ratio in a Tornado Simulator," Journal of Atmospheric Sciences, **30**pp. 1427.

[23] Durst, C. S., 1960, "Wind Speed Over Short Periods of Time," Meteorological Magazine, **89**pp. 181-187.

Chapter 7

7 Concluding remarks

A recently designed and built three-dimensional wind testing facility, the Model WindEEE Dome (MWD) at Western University was introduced. A comprehensive experimental investigation was conducted in this facility to determine its capability to simulate tornado vortices. Flow visualizations methods, surface static pressure measurements and a PIV system were utilized to study the vortex flow field qualitatively and quantitatively.

The flow visualization demonstrated the capability of MWD to produce tornado like vortices exhibiting the main features of every type of vortex as a function of swirl ratio. A laminar single-celled core at very low swirl ratios, a vortex breakdown bubble and a drowned vortex jump at moderate swirl ratios, and a two-celled turbulent vortex at high swirl ratios were captured in this simulator. The static pressure distribution on the floor surface of the chamber has shown close similarity to the analytical modified Rankin vortex model for single-celled vortex flows. Also, instantaneous pressure deficits provided evidence to the presence of subvortices in the flow.

The two-dimensional velocity field, tangential and radial velocity components, was measured using Planar PIV technique at eight horizontal planes above the surface, for eight swirl ratios and at three radial Reynolds number. The velocity field has been analyzed and it showed flow characteristics for each type of vortex as a function of swirl ratio, confirming the flow visualization and the surface pressure investigations.

Afterwards, the three-dimensional axisymmetric wind fields for nine volumes of single-Doppler radar data were reconstructed using the state-of-the-art GBVTD method. The radial profiles of the tangential velocity obtained from the simulated tornado vortices were compared with that of the full-scale to determine the scaling ratios of the simulation. Based on the scaling analysis it was shown that a relation can be derived

between the swirl ratio, a tornado-like vortex simulation parameter, and the Fujita Scale, the real tornado forensic parameter.

7.1 Discussion summary and conclusions

The qualitative and quantitative study of tornado-like vortices in MWD demonstrated the ability of this simulator in producing a wide range of tornado-like vortices. The aspect ratio, the flow rate and the swirl ratio can be controlled independently in this simulator. The effect of the radial Reynolds number on the core size and on the swirl ratio of the transition was investigated and it was concluded that for $Re_r \geq 6.7\times10^4$, the flow characteristics are nearly independent of the radial Reynolds number.

Changing the angle of vanes at the inflow resulted in producing tornado-like vortices with swirl ratios ranging from 0.12 to 1.29. The swirl ratio effect on the simulated vortex structure was visually assessed using helium bubbles and dry ice. The flow visualizations confirmed a laminar single-celled vortex at S=0.12, a vortex breakdown bubble formation at S=0.35, a touch down at S=0.57 and a fully turbulent two-celled vortex at S=0.96 or higher. In addition, the vertical structure of the vortex well matched with that of previously simulated vortices in Tornado Vortex Chambers (TVCs).

The surface static pressure measurements showed a minimum pressure at the central region of the vortex. Due to the wandering of the vortex at low swirl ratios, the minimum pressure deficit was captured at radial distances away from the geometric centre of the simulator. As the swirl ratio increased and the flow became turbulent at S=0.57, the vortex wandering over the surface decreased and the minimum pressures relocated to the center of the simulator. A comparison was made between the surface pressure deficit estimated by the modified Rankine vortex model and measured in MWD. It was noted that the performance of this analytical model improved as the swirl ratio and the radial distance from the center of the vortex increased. The variation of the time-dependent maximum pressure deficit with swirl ratio was in good agreement with previous experimental and numerical studies of tornado-like flows. The most striking observation

in the pressure tests, which distinguishes this flow from the straight atmospheric boundary layer flows, was the very large values of peak surface static pressure deficits. The largest pressure deficit value was captured at S=0.73 which is associated with the transitions in the flow from laminar to turbulent characteristics. The instantaneous pressure deficit fields confirmed that the flow consists of two sub-vortices for S>0.57 which is consistent with the flow visualization results.

The mean velocity field of the tornado-like vortex was measured using PIV. The radial profiles of the normalized tangential velocities (averaged over time and azimuth) were investigated over eight heights and for various swirl ratios. As the swirl increased, the tangential velocity dependency on height which was first observed in the outer core region, penetrated to the inner rotational core of the vortex. The modified Rankine vortex model estimation of radial profiles of tangential velocities matched the experimental data well, except for the heights close to the surface. This observation emphasizes the fact that idealized profiles such as Rankine vortex model are not applicable in the surface layer.

The near surface radial velocity (averaged over time and azimuth) values increased as the rotation in the flow intensified. In addition, the maximum radial velocity was located very close to the surface. As the flow reached the centerline, the radial velocity decreased as it turned into the axial velocity in the core region.

In the axial investigation of the flow, intensified radial velocities as well as local maxima in the tangential velocities were detected in the near-surface flow. These local maxima, along with the significantly large localized static pressure deficits, are unique characteristics of tornado-like vortices that are believed to be accountable for the damage to structures and buildings.

Nine volumes of radar data collected during five tornado events were analyzed using the GBVTD method to determine the wind field of the full-scale tornado events as well as the vertical structure of the vortex, i.e. one-celled, two-celled, etc. When analyzed, the full-scale dataset consisted of wind fields with the overall maximum tangential velocities

ranging from 36.3 m/s to 62 m/s and various vortex structures spanning from a weak single-celled vortex to a very strong two-celled vortex. Full-scale tangential velocity profiles were found to be less dependent on the height when compared with MWD experimental data, particularly in the core region. On the other hand, similar to the trend observed for the MWD experimental data, the tangential velocity profiles of the full-scale data were most accurately estimated by the modified Rankine vortex at higher elevations. The axial distribution of the maximum tangential velocities for each volume showed that for vortices that were estimated to be at or before the transition from a laminar to a turbulent flow, the peak tangential velocity was located at higher elevations. This trend was also observed at very low swirl ratios in the experimental data obtained from PIV measurements in MWD. For the first time, the swirl ratio of field data was related to the forensic EF-Scale which resulted in an agreement between the estimated swirl ratios and the vortex intensity and structure.

The experimental results of tornado-like vortices were compared with the full-scale data to determine velocity and length scale ratios of the simulations. Two measurable characteristic lengths in real tornadoes namely, the radius (r_c) and the height (z_{max}) corresponding to the overall maximum tangential velocity were used to define two length scales ratios. For a given volume of full-scale data, these two length scales were calculated using experimental data at various swirl ratios and it was observed that the two length scales mostly converge towards one value at a certain swirl ratio. The vertical structure of the simulated vortex at the swirl ratio of convergence was compared with that of the full-scale data which resulted in a good agreement. Therefore, it was assumed that the convergence point provides the geometric scaling of the simulation as well as the swirl ratio of the full-scale data. The tangential velocity profiles of the simulated tornado-like vortex were then scaled up using the length and velocity scales determined for each case and were compared with the full-scale measurements to further investigate the accuracy of the proposed method in identifying the scaling ratios. This exercise resulted in a good match between the simulated and real tornado data. Therefore, it was concluded that tornado-like vortices simulated in MWD with swirl ratios ranging from 0.12 to 1.29

are representative of EF0 to EF3 rated tornadoes in nature. The length scale distribution over the swirl ratios suggested two regions in the flow for simulation purposes; before touch-down in which there is a clear variability in the length scale with swirl and after the touch-down of the breakdown bubble in which the length scale may be considered quasi constant. As results, an average length scale of 1550 was approximated for simulating mid-range EF1 to low-end EF3 rated tornadoes with fully turbulent flow characteristics in MWD.

7.2 Contributions

The original contributions from this study to the scientific knowledge are as follows

- Commissioning a new wind facility, the Model WindEEE Dome, and characterizing the tornado-like flows in this simulator. This simulator can be used in the future to characterize the turbulent velocity field of tornado vortices as well as to investigate the effect of roughness and translation on the flow field.

- Detailed experimental data of tornado-like vortices for a wide range of swirl ratios and at various heights. This extended experimental data will serve as a benchmark for numerical simulations of tornado-like vortices.

- Detailed information on the wind field of nine volumes of full-scale tornado data. For the first time, a large dataset of full-scale tangential velocity profiles along with a thorough description of each vortex structure are provided. This dataset will serve as a benchmark for laboratory simulations of tornado-like vortices.

- For the first time, the length and velocity scales of simulations were determined and the swirl ratio of full-scale tornadoes was estimated. This provides the opportunity to properly model different structures and buildings in tornadic winds and measure the wind loads.

7.3 Future recommendations

The following recommendations can be made to complement and extend the current study

- Tornado-like vortices are complex and three-dimensional. Volumetric measurements of the flow can provide helpful insight towards the three-dimensional structure of the flow.
- A time-resolved PIV measurement is highly recommended in order to first characterize the turbulent wind field of tornado-like vortices and second, to allow for more realistic comparison between the simulation and full-scale data.
- The effect of roughness on the velocity field as well as the wind field of a translating tornado needs to be investigated.
- The length scale of simulations in MWD for higher intensity tornadoes needs to be determined once experimental data for higher swirl ratios and GBVTD analysis results for high-end EF3 to EF5 tornadoes are available.

Appendices

Appendix A: Fujita Scale derivation

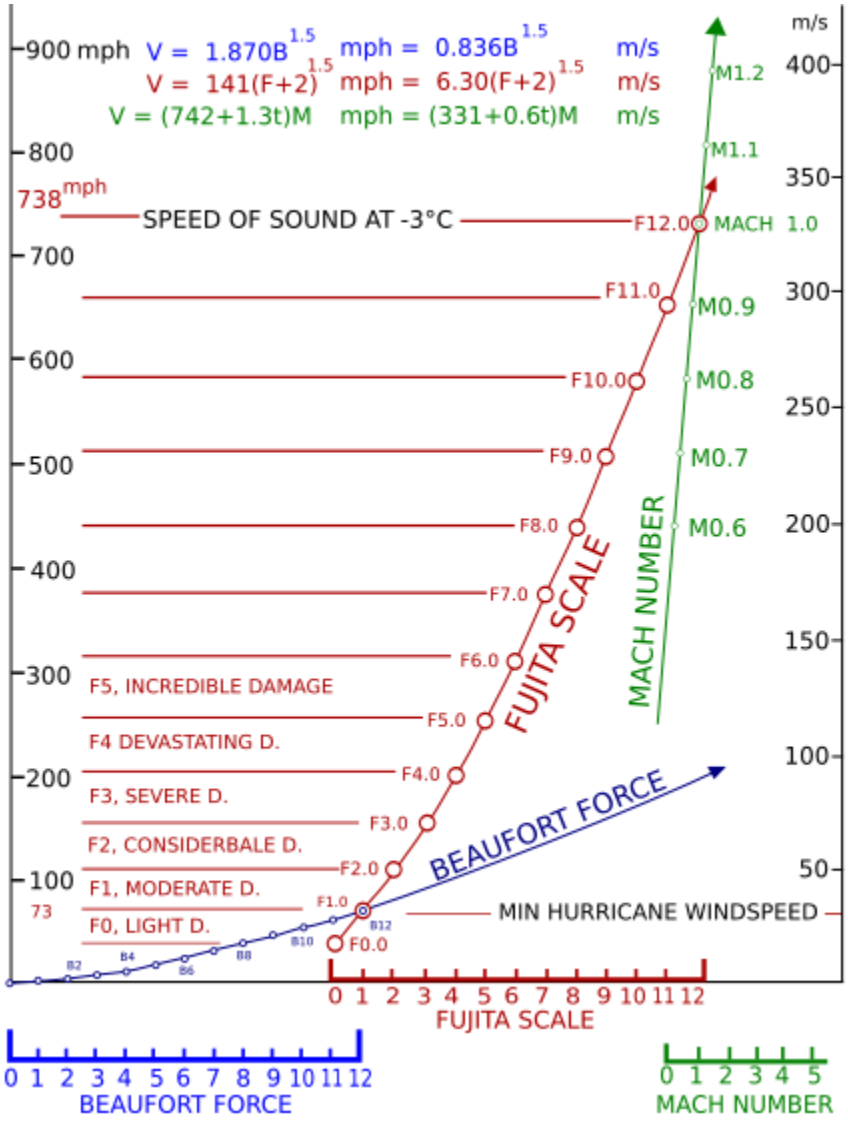

Source [1]

Appendix B: Damage Indicators and Degree of Damage

The following tables present the Damage Indicators (DI) used to assess the severity of a tornado and the Degree of Damage (DOD) for one- and two-family residence.

Damage Indicators for EF Scale

DI No.	Damage indicator (DI)
1	Small Barns or Farm Outbuildings (SBO)
2	One- or Two-Family Residences (FR12)
3	Manufactured Home – Single Wide (MHSW)
4	Manufactured Home – Double Wide (MHDW)
5	Apartments, Condos, Townhouses [3 stories or less] (ACT)
6	Motel (M)
7	Masonry Apartment or Motel Building (MAM)
8	Small Retail Building [Fast Food Restaurants] (SRB)
9	Small Professional Building [Doctor's Office, Branch Banks] (SPB)
10	Strip Mall (SM)
11	Large Shopping Mall (LSM)
12	Large, Isolated Retail Building [K-Mart, Wal-Mart] (LIRB)
13	Automobile Showroom (ASR)
14	Automobile Service Building (ASB)
15	Elementary School [Single Story; Interior or Exterior Hallways] (ES)
16	Junior or Senior High School (JHSH)
17	Low-Rise Building [1-4 Stories] (LRB)
18	Mid-Rise Building [5-20 Stories] (MRB)
19	High-Rise Building [More than 20 Stories] (HRB)
20	Institutional Building [Hospital, Government or University Building] (IB)
21	Metal Building System (MBS)
22	Service Station Canopy (SSC)
23	Warehouse Building [Tilt-up Walls or Heavy-Timber Construction](WHB)
24	Transmission Line Towers (TLT)
25	Free-Standing Towers (FST)
26	Free-Standing Light Poles, Luminary Poles, Flag Poles (FSP)
27	Trees: Hardwood (TH)
28	Trees: Softwood (TS)

DOD*	Damage description	EXP	LB	UB
1	Threshold of visible damage	65	53	80
2	Loss of roof covering material (<20%), gutters and/or awning; loss of vinyl or metal siding	79	63	97
3	Broken glass in doors and windows	96	79	114
4	Uplift of roof deck and loss of significant roof covering material (>20%); collapse of chimney; garage doors collapse inward or outward; failure of porch or carport	97	81	116
5	Entire house shifts off foundation	121	103	141
6	Large sections of roof structure removed; most walls remain standing	122	104	142
7	Top floor exterior walls collapsed	132	113	153
8	Most interior walls of top story collapsed	148	128	173
9	Most walls collapsed in bottom floor, except small interior rooms	152	127	178
10	Total destruction of entire building	170	142	198

- EXP: expected wind speed in mph
- LB: lower bound wind speed in mph
- ECP: higher bound wind speed in mph

Source [2]

Appendix C: Pressure test error calculation

Table 1 presents the thermal stability and the accuracy of pressure scanners used in experiments. The surface pressures measured in the current experiments are smaller than 35kPa. As a result, the total thermal shift for one degree F temperature change can be calculated as

$$B_r = \sqrt{(0.25^2 + 0.04^2)} = 0.253\%$$

However, the temperature change during experiments was less than 1F. Knowing that the accuracy of pressure scanners is S_r=0.2%, the total error ($E_{95,S}$) in measurements associated with the pressure sensors can be determined

$$E_{95,s} = \pm\sqrt{(B_r^2 + t_{95}S_r^2)} = 0.473\%$$

Where t_{95} is the 95th percentile point for two-tailed Student's distribution and is equal to 2 for current tests.

The error related to the data acquisition system can be calculated using Table 2. The maximum voltage output for the reference pressure was 2.912V. Therefore, the error of the pressure system is approximated as

$$E_s = \pm\sqrt{(0.473^2 + 0.08^2)} = \pm 0.48\%$$

The error associated with the tubing system response was corrected and was estimated to be E_{tu}=1%. Also, the repeatability error of 0.39% was calculated for measurements using Table 3. At the end, the overall uncertainty in pressure measurements can be estimated as

$$E_T = \sqrt{E_s^2 + E_{tu}^2 + E_r^2} = 1.17\%$$

Table 1: Accuracy and thermal stability of pressure scanners (worst case scenarios).

Scanner range	Accuracy (± %F.S)	Thermal zero shift (± %F.S /F)	Thermal span shift (± %F.S /F)
<35kPa	0.2	0.25	0.04
≥35kPa	0.15	0.05	0.02

Table 2: DAP 4400a resolution and accuracy specifications.

Voltage range	-5 to 5 volts
Resolution	2.4mV
Accuracy	±2.4mV

Table 3: multiple readings of reference pressure

Reference pressure readings (V)	2.8835	2.8925	2.8933	2.8883	2.9027	2.9114	2.9121

Appendix D: PIV error calculation

The total error of PIV is the sum of errors originating from seeding particles diameter and density, out of plane motion of the particles, velocity gradient, dynamic range, peak locking and Adaptive Gaussian Window interpolation [3]. Graphs provided by Cowen and Monismith [3] are used to obtain the mean and RMS errors of various sources of error and then calculate the total error. Cowen and Monismith define the RMS error, which is caused by random noise during imaging process, as the random uncertainty in locating both the correlation peak and particle image.

The error due to particle size is provided in Fig. 5a in [3]. Di-Ethyl-Hexyl-Sebacate (C26H50O4) particles with an average diameter of 1 μm were used as seeding particles. 1 μm diameter is equivalent to 0.00998 pixels. The smallest particle diameter in Fig. 5a is 1 pixel. Therefore, the total error due to particle diameter calculated based on 1 pixel diameter as follows

$$\varepsilon_p=(-0.03)+0.095=0.065 \text{ pixels}$$

To better estimate the error associated with a 0.00998 pixel diameter particle, Fig. 13 in Prasad *et al.* [4] was used. This figure shows the bias and peak locking errors of a particle with 0.00998 pixels diameter is 43% larger when compared to the error associated with a 1 pixel diameter particle. In the study of Prasad *et al.* [2], the center of mass cross-correlation procedure is susceptible to peak locking. However, three-point Gaussian estimation which has a reduced peak locking error was used for current work. As a result, additional error in particle diameter was estimated to be 30% which means

$$\varepsilon_p=0.065\times1.3=0.0845 \text{ pixels}$$

The mean and RMS errors due to velocity gradients were estimated using Fig. 5e in [3]. The average tangential and radial velocity gradients ($\partial V_{tan}/\partial r$ and $\partial V_{rad}/\partial r$, respectively) for each experimental run were calculated. The maximum tangential velocity gradient of 49.156s^{-1} and the maximum radial velocity gradient of 20.776 s^{-1} were obtained at S=1.29

and S=0.96, respectively. The error corresponding to velocity gradients can be approximated as follows

$$\varepsilon_{g,Vtan}=(-0.005)+0.02=0.015 \text{ pixels}$$

$$\varepsilon_{g,Vrad}=(-0.002)+0.015=0.013 \text{ pixels}$$

Fig. 5f in [3] was used to calculate the error associated with Adaptive Gaussian Window (AGW) interpolation. This figure shows AGW averaging error as a function of dynamic range. For 8-bit CCD cameras, the dynamic range varies between 100 and 150 counts. Therefore, the AGW averaging error is approximated to be

$$\varepsilon_{AGW}=0.08 \text{ pixels}$$

The error related to the out of plane motion of particles can be estimated using the in plane largest particle displacement. The PIV measurements were performed on horizontal planes and therefore, the out of plane particle velocity is expected to be smaller than the maximum in plane velocities. The maximum instantaneous velocity of 9.93 m/s or 9.91 pixels was captured at a horizontal plane 4 cm above the surface and at S=1.29. Since the laser sheet thickness was approximately 2 mm (equivalent to 19.96 pixels), the out of plane motion error is negligible in this work.

The total error for each velocity component is calculated by adding the previously calculated errors:

$$\varepsilon_{T,\ Vtan}=0.179 \text{ pixels}$$

$$\varepsilon_{T,\ Vrad}=0.177 \text{ pixels}$$

Therefore, the total error of measurement for the tangential velocity measurement is 0.18 m/s or 1.8% and for the radial velocity is 0.162 m/s or 7.2%.

Appendix E: The Ground-Based Velocity Track Display (GBVTD) Geometry and Symbols

The following figure shows the geometrical relationship between an atmospheric vortex and a ground-based Doppler radar. See Lee *et al.* [5] for the definition of each symbol.

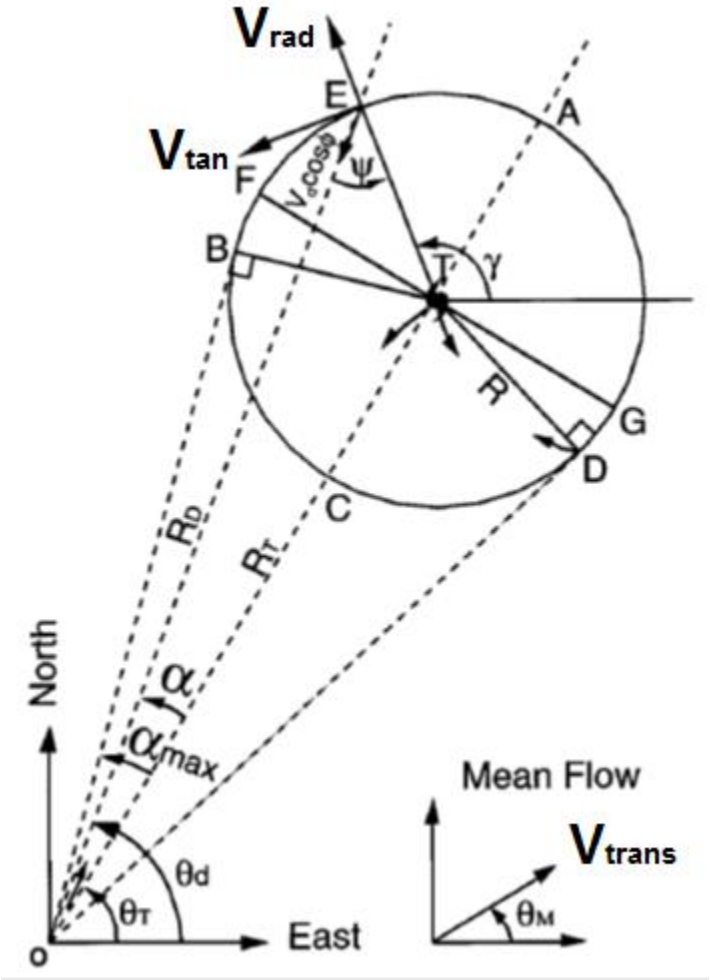

Source [5]

References

[1] Fujita, T.T., 1971, "Proposed characterization of tornadoes and hurricanes by area and intensity," Satellite Mesometeorology Research Program Research Paper, Department of Geophysical Sciences, 91, University of Chicago.

[2] Wind Science and Engineering Centre, 2004, "A Recommendation for an Enhanced Fujita scale (EF-Scale)," Texas Tech University, 79409-1023, .

[3] Cowen, E. A., Monismith, S. G., Cowen, E. A., 1997, "A Hybrid Digital Particle Tracking Velocimetry Technique," Experiments in Fluids, **22**(3) pp. 199-211.

[4] Prasad, A. K., Adrian, R. J., Landreth, C. C., 1992, "Effect of Resolution on the Speed and Accuracy of Particle Image Velocimetry Interrogation," Experiments in Fluids, **13**(2-3) pp. 105-116.

[5] Lee, W. C., Jou, J. D., Chang, P. L., 1999, "Tropical Cyclone Kinematic Structure Retrieved from Single-Doppler Radar Observations. Part I: Interpretation of Doppler Velocity Patterns and the GBVTD Technique," Monthly Weather Review, **127**pp. 2419-2439.

Curriculum Vitae

Name:	Maryam Refan
Post-secondary Education and Degrees:	University of Tehran Tehran, Iran 2002-2006 B.Sc. The University of Western Ontario London, Ontario, Canada 2007-2009 M.E.Sc.
Honours and Awards:	Alexander Graham Bell Canada Graduate Scholarship D (NSERC CGS D) 2012-2014 MITACS Accelerate Internship Program 2011 Graduate Thesis Research Fund 2008
Related Work Experience	Teaching Assistant The University of Western Ontario 2007-2013

Publications:

Journal Articles:

M. Refan, H. Hangan and J. Wurman, Reproducing tornadoes in laboratory using proper scaling, Submitted to the Journal of Wind Engineering and Industrial Aerodynamics, 2013.

M. Refan and H. Hangan, Aerodynamic performance of a small horizontal axis wind turbine, Journal of Solar (and Wind) Energy Engineering, 2012, Vol. 134-021013-1.

Book Chapter:

M. Refan and H. Hangan, Small-Scale Wind Power – Design, Analysis, and Economic Impacts, Chapter 5: Design of Horizontal-axis Wind Turbines, Momentum Press, Under publication, 2014.

Refereed Conferences:
M. Refan, H. Hangan and K. Siddiqui, Particle Image Velocimetry Measurement of Tornado-like Flow Field in Model WindEEE Dome, Proceedings of the ASME 2014 4th Joint US-European Fluids Engineering Division Summer Meeting, Accepted, August 2014.

M. Refan, H. Hangan and K. Siddiqui, Particle Image Velocimetry Measurement of Tornado-like Vortices Compared with Doppler Radar Data, The International Symposium on Applications of Laser Techniques to Fluid Mechanics, Accepted, July 2014.

Dissertation:
M. Refan, Aerodynamic performance of a small horizontal axis wind turbine, M.E.Sc Thesis, The University of Western Ontario, London, 2009.

Conference Papers:
M. Refan, H. Hangan and J. Wurman, Reproducing tornadoes in laboratory using proper scaling, The 12th Americas Conference on Wind Engineering (12ACWE), Seattle, Washington, USA, June 2013, Nominated for review for possible inclusion in the special issue of the Journal of Wind Engineering and Industrial Aerodynamics.

M. Refan and H. Hangan, The 19 May 2012 tornadoes, 3rd American Association for Wind Engineering Workshop, Hyannis, Massachusetts, USA, August 12 - 14, 2012.

M. Refan and H. Hangan, Developing similarity analysis for laboratory simulated and field tornadoes, 1000 Island Fluid Mechanics Meeting, Gananoque, April 2011.

M. Refan and H. Hangan, Qualitative assessment of tornadic flows in Model WindEEE Dome, 1000 Island Fluid Mechanics Meeting, Gananoque, April 2011.

M. Refan and H. Hangan, Experimental and theoretical study on the aerodynamic performance of a small horizontal axis wind turbine, ASME Power Conference, Chicago, July 2010.

M. Refan and H. Hangan, Wind tunnel testing of a small HAWT; Experiment vs. BEM theory, 1000 Island Fluid Mechanics Meeting, Gananoque, May 2009.

A. Adibfar and M. Refan, Air cooled condenser for dry countries, ASME Power Conference, Atlanta, May 2006.